## AC2 - SU 22


SU 21, 22, 33

## AC2 - SU 22


SU 21, 22, 34, 35

## AC2- SU 21 & SU 22

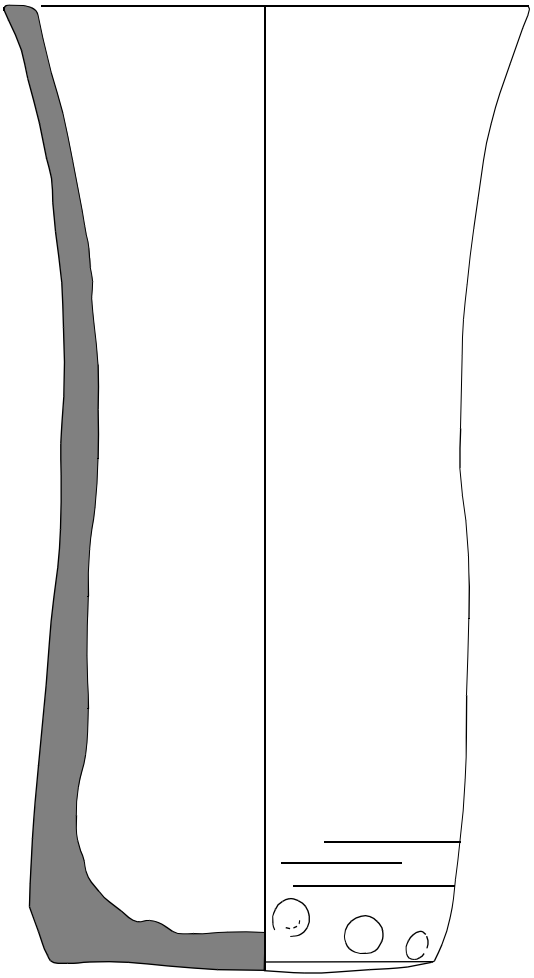

1

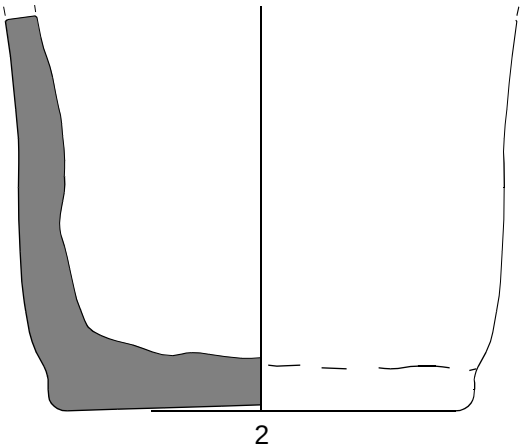

2

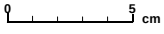

## AC2 - SU 23

**Definition:** Small pot in circulation floor

**Interpretation:**

**Observations:**

**Material:**

**Archaelogist:** Verònica Martínez

| | |
|---|---|
| *Composition* | |
| *Dimensions* | 32x20cm |
| *Formation* | human |
| *Potential* | 7cm |
| | |
| *Infill from (Stratum)* | 24 |
| _____ | |
| *Intersecting (Stratum)* | 20 |
| _____ | |

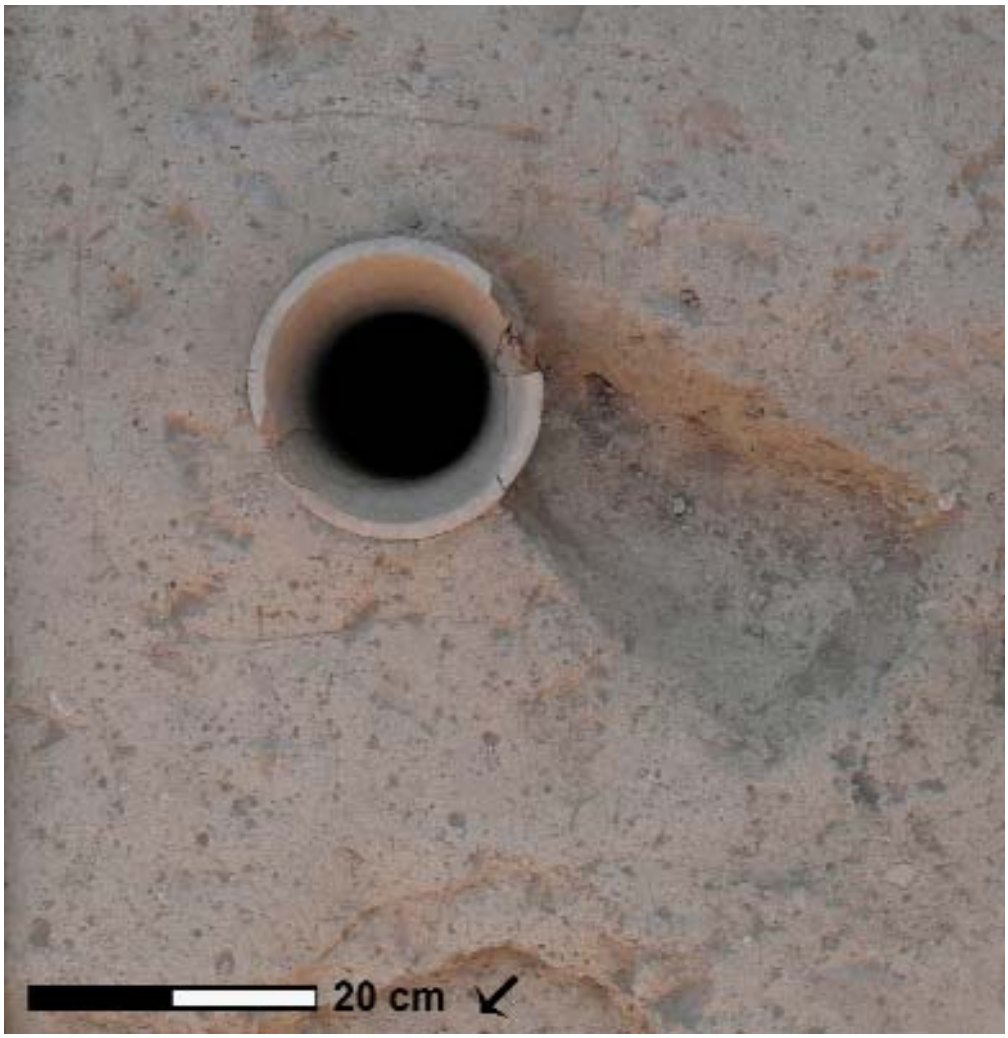


SU 23, 22, 20

## AC2 - SU 24

**Definition:** Infill of pit.

**Interpretation:** Infill of pit with household remains that may have been used in cooking.

**Observations:** Stratum formed largely of sand with pot sherds and some fauna remains. It fills in the negative SU 23 over SU 20.

**Material:** Slipware: 3 frag.
Common ware: 23 frags.
Bone: 7 frags. (45g)

**Archaelogist:** Verònica Martínez

| | |
|---|---|
| *Composition* | sand, pottery, fauna |
| *Dimensions* | 26x20cm |
| *Formation* | |
| *Potential* | 7 cm |
| | |
| *Covered by (Stratum)* | 17 |
| *Infill (Negative)* | 23 |


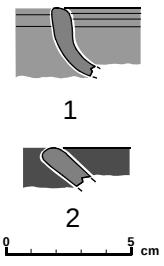

## AC2 - SU 25

**Definition:** Small pit in circulation floor.

**Interpretation:** Small pit to contain remains of household use in part of the circulation floor (SU 20), possibly designated for cooking purposes.

**Observations:** Negative level, measuring 32cm long and 24cm wide, with a depth of 8cm, made in SU 20 in the northeastern part of the sample trench, east of the pottery container SU 22. It is filled in by SU 26 and contains pottery sherds and bone.

**Material:**

**Archaelogist:** Verònica Martínez

| | |
|---|---|
| *Composition* | |
| *Dimensions* | 32x24cm |
| *Formation* | human |
| *Potential* | 8cm |
| | |
| *Infill from (Stratum)* | 26 |
| _____ | |
| *Intersecting (Stratum)* | 20 |
| _____ | |

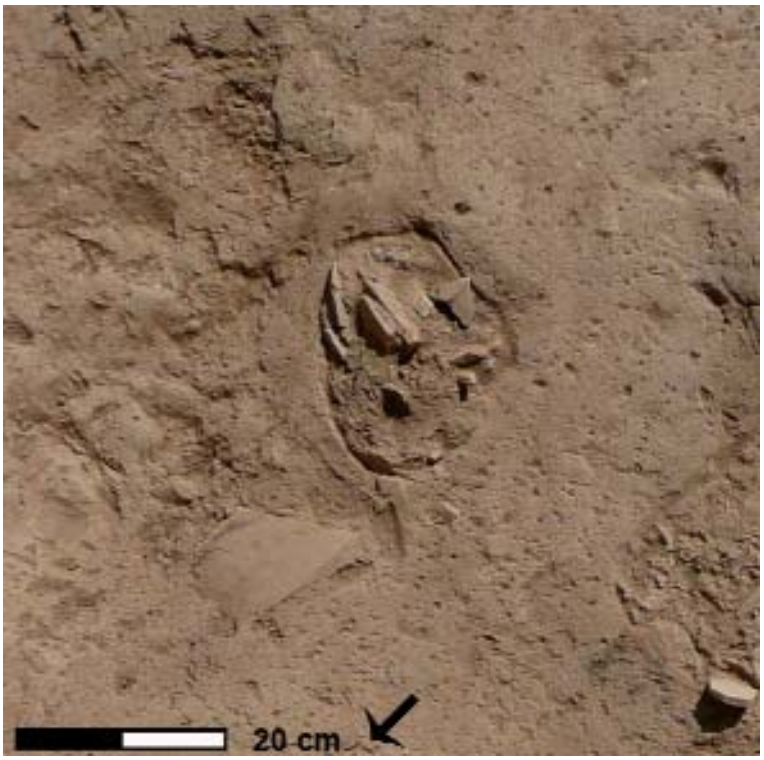


SU 25, 26, 20

## AC2 - SU 26

**Definition:** Infill of pit.

**Interpretation:** Infill of pit with household remains, possibly designated for cooking purposes.

**Observations:** Stratum largely formed by sand with pottery sherds and some fauna remains, filling the negative SU 25 in SU 20 and near the pottery container SU 22 and another set of small pits (SU 23 and 29).

**Material:**

**Archaeologist:** Verònica Martínez

| | |
|---|---|
| *Composition* | sand, pottery, fauna |
| *Dimensions* | 32x24cm |
| *Formation* | |
| *Potential* | 8cm |
| | |
| *Covered by (Stratum)* | 17 |
| _____ | |
| *Infill (Negative)* | 25 |
| _____ | |

## AC2 - SU 27

**Definition:** Small pit in circulation floor.

**Interpretation:** Small pit excavated possibly to build a hearth, as indicated by ash in the stratum of infill SU 28.

**Observations:** Negative level, measuring 66cm long and 40cm wide, with a depth of 21 cm, made in SU 20 in the central part of the sample trench and filled in by SU 28, a level of ash and pot sherds.

**Material:**

**Archaeologist:** Verònica Martínez

| | |
|---|---|
| *Composition* | |
| *Dimensions* | 66x40cm |
| *Formation* | human |
| *Potential* | 21cm |
| | |
| *Infill from (Stratum)* | 28 |
| _____ | |
| *Intersecting (Stratum)* | 20 |
| _____ | |

## AC2 - SU 27

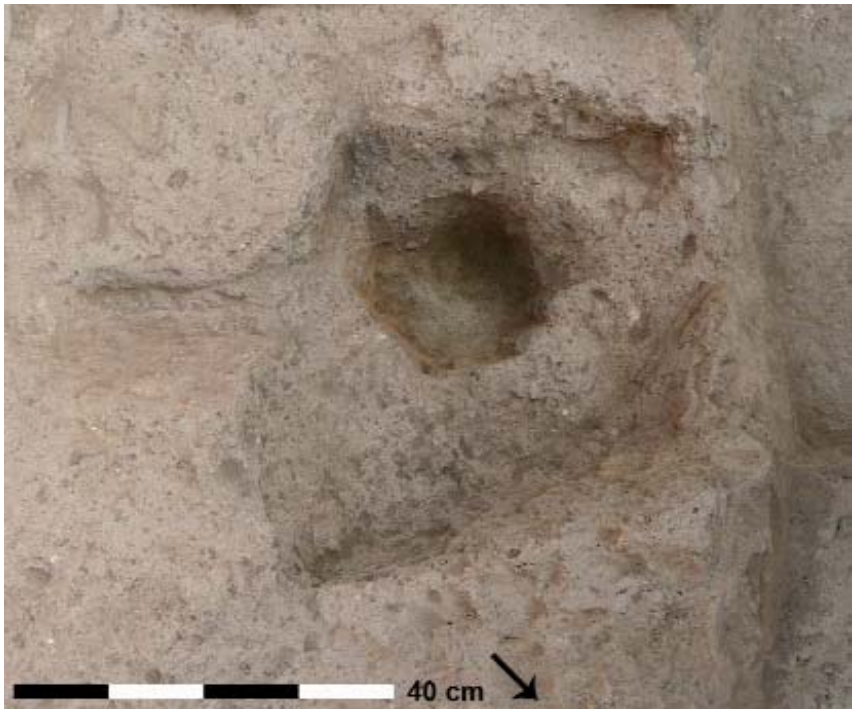


SU 27, 20

## AC2 - SU 28

**Definition:** Infill of pit with ash.

**Interpretation:** Ash and remains of pottery sherds and charcoal corresponding to remains of organic fuel and the floor of a possible hearth in the central part of the sample trench, of which remains the negative (SU 27) excavated in the floor of use SU 20.

**Observations:** Stratum of ash with pot sherds that fills in the negative SU 27 located over SU 20 in the central part of the sample trench.

**Material:** Slipware: 10 frags.
Common ware: 11 frags.
Bone: 9 frags. (50g.)

**Archaelogist:** Verònica Martínez

| | |
|---|---|
| *Composition* | ash, pottery |
| *Dimensions* | 66x40cm |
| *Formation* | human |
| *Potential* | 21cm |
| | |
| *Covered by (Stratum)* | 17 |
| _____ | |
| *Infill (Negative)* | 27 |
| _____ | |

## AC2 - SU 28

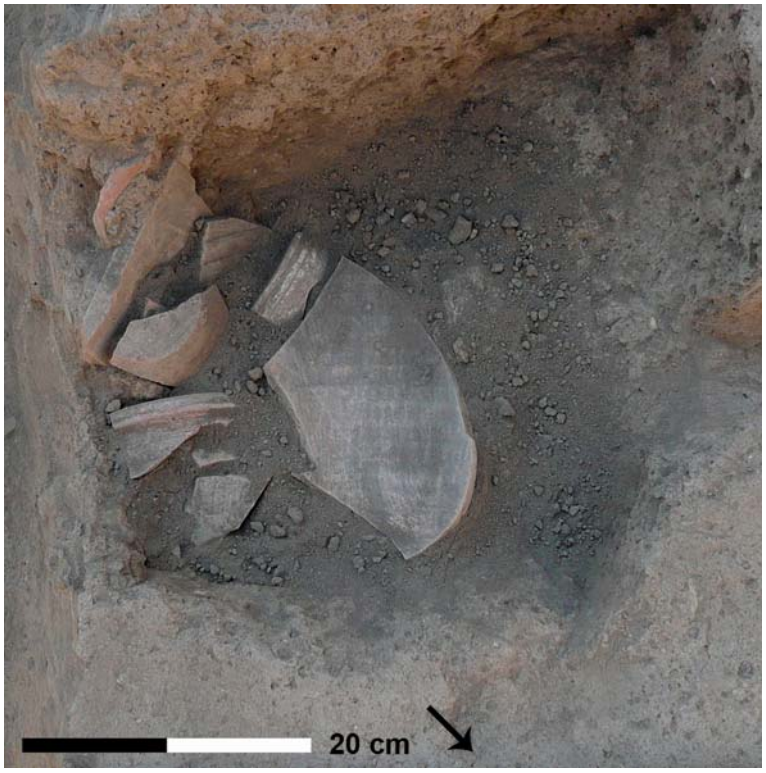


1

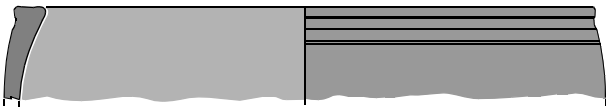

2

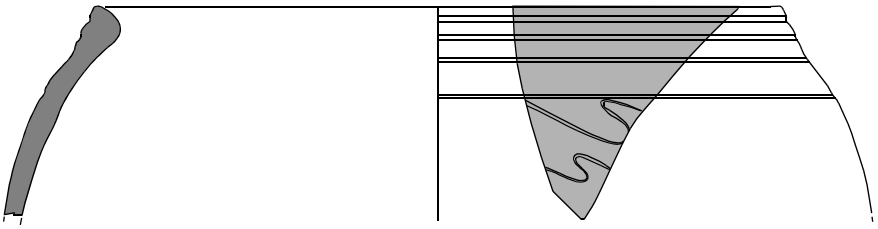

3

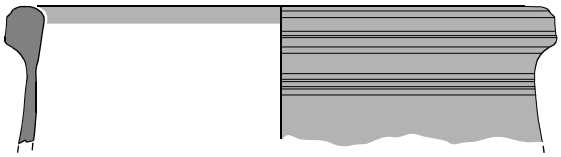

4

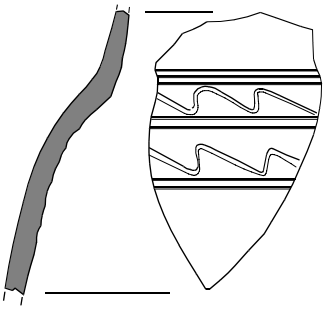

5

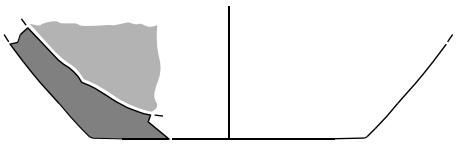

6

7

## AC2 - SU 29

**Definition:** Infill of pit.

**Interpretation:** Infill of pit possibly designated for domestic use related to the floor of circulation SU 20.

**Observations:** Stratum formed largely of sand with scarce pottery sherds of small sizes, filling the negative SU 29 over SU 20 to the north of the ceramic container SU 22 and a set of small pits (SU 23 and 29).

**Material:**

**Archaelogist:** Verònica Martínez

| | |
|---|---|
| *Composition* | |
| *Dimensions* | |
| *Formation* | human |
| *Potential* | |
| | |
| *Infill from (Stratum)* | 30 |
| _____ | |
| *Intersecting (Stratum)* | 20 |
| _____ | |

## AC2 - SU 30

**Definition:** Infill of pit.

**Interpretation:** Infill of pit.

**Observations:** Stratum with 11cm of potential formed largely by sand with scarce pottery sherds of small sizes, filling in negative SU 29.

**Material:** Slipware: 1 frags.
Common ware: 2 frags.

**Archaelogist:** Verònica Martínez

| | |
|---|---|
| *Composition* | sand, pottery |
| *Dimensions* | 32x26cm |
| *Formation* | |
| *Potential* | 11cm |
| | |
| *Covered by (Stratum)* | 17 |
| _____ | |
| *Infill (Negative)* | 29 |
| _____ | |

## AC2 - SU 30

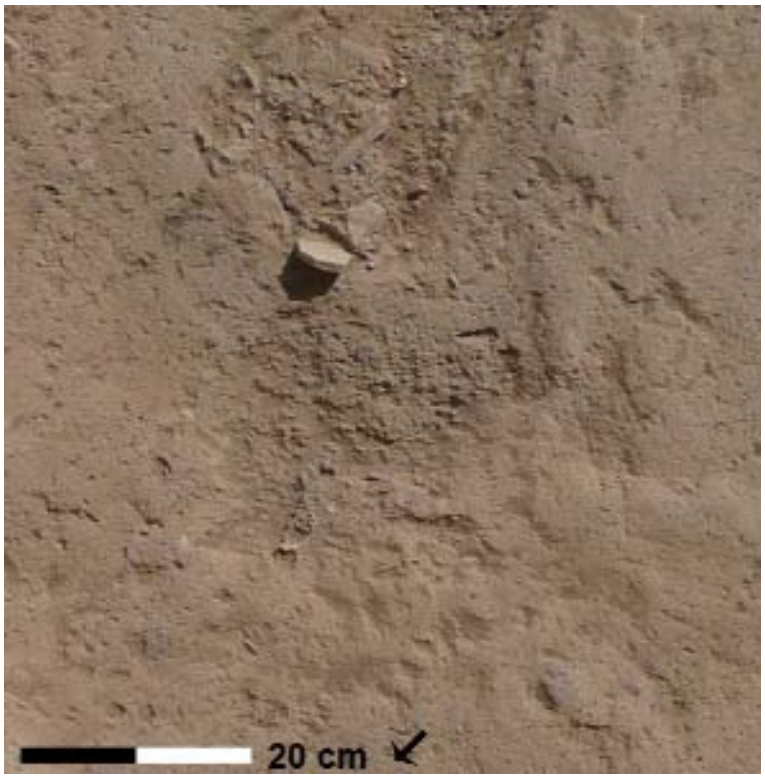


SU 30, 29,20

## AC2 - SU 31

**Definition:** Pit in floor of circulation.

**Interpretation:** Pit related to the floor of use and circulation SU 20. Its purpose is impossible to specify.

**Observations:** Negative level, measuring 1m long and 68cm wide, oval in shape, running north-south. The northern side has a depth of 30cm, while the southern side has a depth of 13cm. The bottom of the pit corresponds to a level of pebbles that forms the natural substrate (SU 34) of the sample trench on its western side. The level has been excavated in SU 20 in the southwestern side of the sample trench and is filled in by a level of sand with scarce pottery sherds (SU 32).

**Material:**

**Archaelogist:** Verònica Martínez

| | |
|---|---|
| *Composition* | |
| *Dimensions* | 1mx68cm |
| *Formation* | human |
| *Potential* | 30-13cm |
| | |
| *Infill from (Stratum)* | 32 |
| _____ | |
| *Intersecting (Stratum)* | 20 |
| _____ | |


SU 31, 20, 34

## AC2 - SU 32

**Definition:** Infill of pit.

**Interpretation:** Infill of pit with sand.

**Observations:** Stratum of sand, with some pottery sherds, filling in negative SU 31.

**Material:** Slipware: 4 frags.
Common ware: 8 frags.
Pottery coating: 1 frag.
Bone: 1 frag. (6g)

**Archaelogist:** Verònica Martínez

| | |
|---|---|
| *Composition* | sand, pottery |
| *Dimensions* | 1mx68cm |
| *Formation* | |
| *Potential* | 30-13cm |
| | |
| *Covered by (Stratum)* | 17 |
| _____ | |
| *Infill (Negative)* | 31 |
| _____ | |

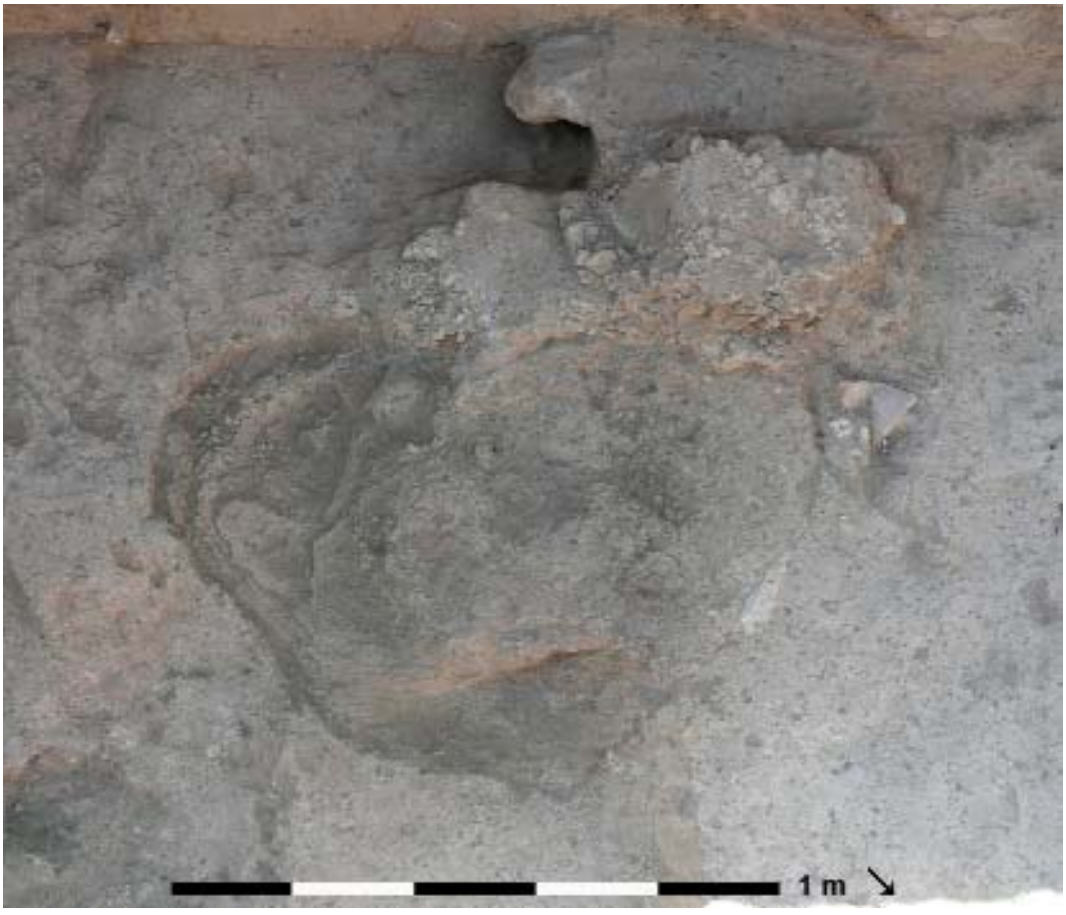


SU 32, 31, 20

## AC2 - SU 33

**Definition:** Level of silt and sandstone pebbles.

**Interpretation:** Level covering the non-uniform sandstone bedrock to level the area as a floor for household use, as shown by SU 20.

**Observations:** Stratum of silt and sandstone pebbles extending across the entire sample trench on the central side of the western extreme, with variable potential. Located below SU 20, it covers the sandstone bedrock SU 34. In the eastern extreme of the sample trench, the potential of SU 33 ranges from 2 to 10cm in width. Its thickness rises in the northwest extreme, reaching 38cm, covering the cuttings (SU 35 and 36) made in the sandstone bedrock. On the southwestern side, the thickness reaches 36cm. It contains pot sherds and fauna remains.

**Material:** Slipware: 49 frags.
Common ware: 164 frags.
Cooking ware: 3 frags.
Bone: 15 frags. (124g)
Stone construction material: 1frag.

**Archaelogist:** Verònica Martínez

| | |
|---|---|
| *Composition* | sand, sandstone pebbles, pottery, fauna |
| *Dimensions* | 19 sq m |
| *Formation* | human |
| *Potential* | variable |
| | |
| *Covered by (Stratum)* | 20 |
| *Se le asienta (Estructura)* | 22-21 |
| _____ | |
| *Covering (Stratum)* | 34 |
| _____ | |


SU 33, 34, 35, 22

## AC2- SU 33

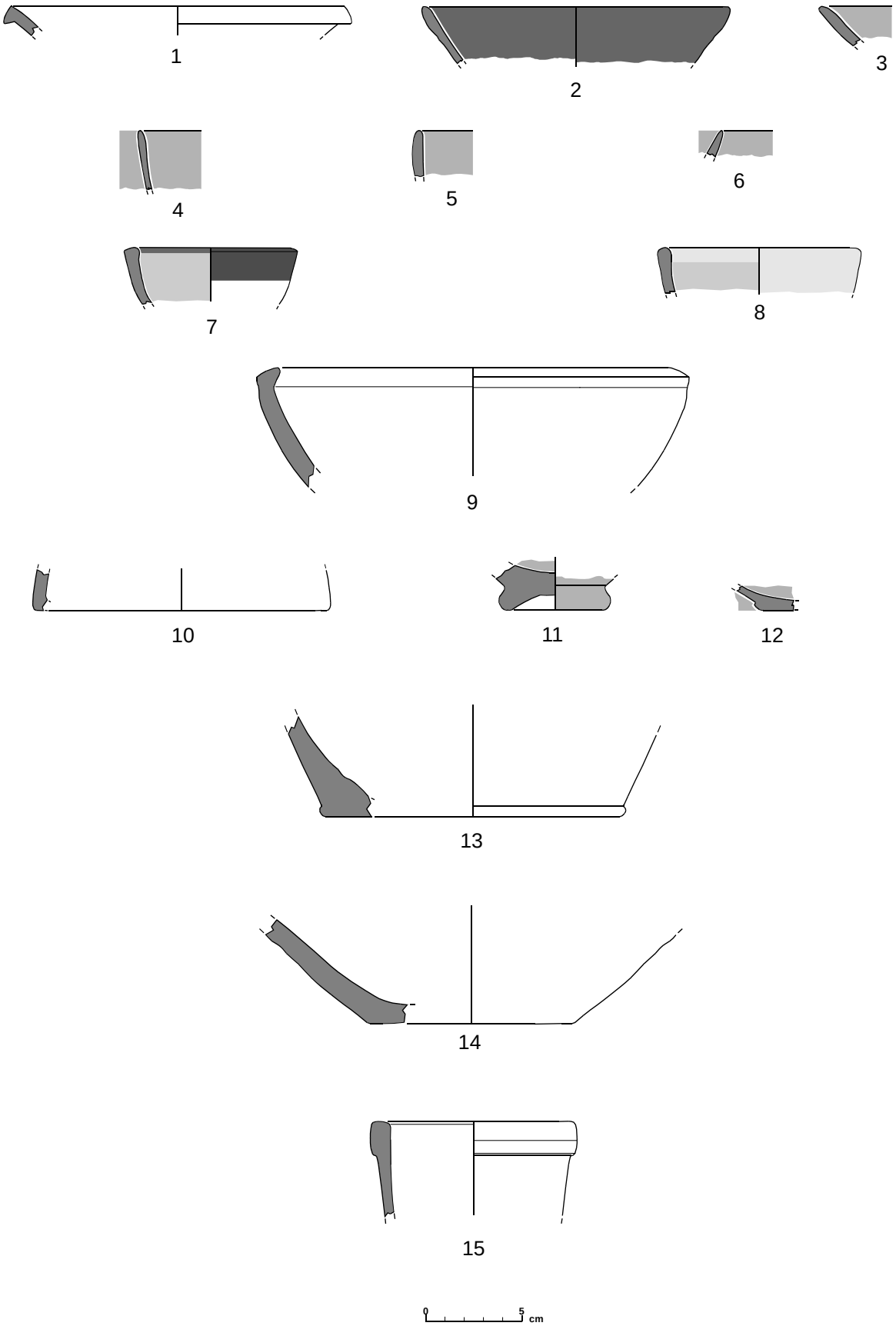

## AC2 - SU 34

**Definition:** Natural sandstone bedrock.

**Interpretation:** Natural substrate formed of bedrock with intercalations of siltstone and levels of pebbles.

**Observations:** Stratum of sandstone corresponding to the natural substrate of the excavation area, extending in a non-uniform manner across the length of the sample trench. Several levels of formation corresponding to different depositions of natural sediments can be seen. Sandstone predominates in the sample trench, but intercalations of levels of siltstone and nodules at some points of the surface can also be seen. Similarly, a level of small pebbles appears on the surface of the natural substrate on the western end of the sample trench. On the northern end of the sample trench, two cuttings on the natural substrate can be seen (SU 35 and 36).

**Material:**

**Archaeologist:** Verònica Martínez

| | |
|---|---|
| *Composition* | sandstone, siltstone, pebbles |
| *Dimensions* | 19 sq m |
| *Formation* | natural |
| *Potential* | |
| | |
| _____ | |
| *Covered by (Stratum)* | 33 |
| *Intersected by (Negative)* | 35-36 |
| _____ | |

## AC2 - SU 34


SU 34, southern stratigraphy


SU 34, 35, 36

## AC2 - SU 34


SU 34, 35

## AC2 - SU 35

**Definition:** Cutting of the natural substrate.

**Interpretation:** Cutting of the sandstone corresponding to the natural substrate that is only visible in a portion of the bottom of the sample trench and runs continuously toward the unexcavated area on the north side. Given that the cutting was filled in subsequently by a level of silt and sandstone pebbles from the bedrock itself, its original function is unknown.

**Observations:** Negative realised in the natural substrate on the north-central side of the sample trench.

**Material:**

**Archaelogist:** Verònica Martínez

| | |
|---|---|
| *Composition* | |
| *Dimensions* | 2x1.66m |
| *Formation* | human |
| *Potential* | 30cm |
| | |
| *Intersected by (Negative)* | 36 |
| _____ | |
| *Intersecting (Stratum)* | 34 |
| _____ | |


SU 35, 34

## AC2 - SU 35


SU 35, 34, 36

## AC2 - SU 36

**Definition:** Cutting of the natural substrate.

**Interpretation:** Cutting of the sandstone corresponding to the natural substrate. It is only visible in the north-western corner of the sample trench and runs continuously toward the unexcavated area. Given that the cutting was filled in subsequently by a level of silt and sandstone pebbles from the bedrock itself, its original function is unknown.

**Observations:** Negative realised in the natural substrate on the northwestern side of the sample trench, which in turn cuts negative SU 35. It measures 1.7m long and 30cm wide in the excavated area, but it continues toward the northwest.

**Material:**

**Archaelogist:** Verònica Martínez

| | |
|---|---|
| *Composition* | |
| *Dimensions* | 1.7m x 30cm |
| *Formation* | human |
| *Potential* | 25 cm |
| | |
| _____ | |
| *Intersecting (Stratum)* | 34 |
| *Intersecting (Negative)* | 35 |
| _____ | |


SU 36, 34, 35

# Geophysical Surveying

Victor Pinto

## Geophysical Surveying. Background information

The natural physical setting of the Termez region is defined by an arid climate (average precipitation of 148mm) with cold winters, influenced by its location in the interior of the vast Asian continent. This climate is associated with a steppe biome typical of flat, wide areas, but the vegetation cover is discontinuous and the substrate often appears completely devoid of vegetation. The geological substrate is composed of clastic rocks (sandstone), carbonates, and evaporites (anhydrite, salt) deposited between the Permian-Triassic and the Neogene in a sedimentary basin linked to the ancient peneplain of Central Asia. Carbonate, anhydrite and salt materials are involved in external morphogenetic processes (Ulmishek, 2004). The area under study occupies a zone inside a meander of the river Amu Darya, located on the broad surfaces of the piedmont (250-300m in height) rising in the northern foothills of the Hindu Kush in Afghanistan and the southern foothills of the Tien Shan range (Krebet). From a morphogenetic viewpoint, arid domains are characterised by processes tied to (I) abrupt changes in temperature (physical weathering); (ii) chemical processes arising from hydric deficit; (iii) wind action; (iv) surface erosion (water running downhill) and (v) gravity (slope processes, or processes of dune destabilisation when the slope of stability is surpassed). In the work area, morphogenetic processes, largely activated by a few principal agents, give rise to operative systems that are basically aeolic and fluvial in nature. The effects of weathering also come into play, in addition to the characteristics of complex polygenic, heterochronic terrain, such as surfaces of erosion and piedmonts, and a relatively significant effect of regional tectonic activity on the area.

This extreme climatology, together with the similar lithological composition of infill materials and materials constituting structures (sand, loess), gives rise to a low differential response in the principal physical parameters (i.e. electrical resistivity and dielectric permittivity) that are generally used in geophysical surveying applied to archaeology

Most of the geophysical survey systems used to detect archaeological remains are based on differentiating subsoil properties to delineate the position and condition of archaeological remains. In the present case, the surrounding environment and the type of remains hamper readings, because little physical or chemical difference exists between the sediments and the cultural environment under survey. The chief differences between sediments and archaeological structures are limited to granulometry and compaction, while factors such as humidity and conductivity show only very subtle differences. Another serious problem arises from the stratigraphy itself when it frequently and widely features a crust—basically limestone; extremely hard, resistant and resistive to electrical current—across the entire area of the excavation.

The initial hypotheses are the result of studies carried out in 2006 and 2007. The first season of surveying made use of magnetic gradiometry (FM-256) and georadar (GSSI SIR-3000) with a 400MHz antenna. Given the subtlety of the physical and chemical changes between the sediments and the built structures, it was necessary to test different systems that could, in theory, offer results and then verify their efficacy in practice.

Analysis of the data obtained revealed the total inefficacy of magnetic gradiometry in the description of urban areas or large elements. However, it was useful in locating combustion structures, which constitute the starting point of the archaeometric study planned in our project. Nonetheless, locating produ-

cer centres in archaeology does not entail knowledge of the sequence of their output. Chronological dating can only be achieved if the stratigraphy of consumption spaces is also available. Locating and effectively documenting stratigraphic sequences that reflect the circulation and consumption of ceramic products depend on the ability of establishing correct protocols for geophysical surveying and for sound geomorphological study, which will, in turn, determine the correct interpretation of the survey's results and, subsequently, the formative process of the archaeological site.

At first, the data obtained using georadar appeared to be useful in describing the site in question. Although a number of episodes of severe interference arose from the activities of the airport near the site, a large portion of the data could be processed using the GPR-Slice v.5 program to generate images of slices of the detected anomalies at different depths. The data filtering process yielded one of the keys for guiding the research in the 2007 season. Processing the data numerous times, we verified that the subtle variation in amplitude and frequency captured by the radar in the presence of a wall or simple sedimentary deposit of aeolic origin generated very low contrasts in the images. That hampered their interpretation. We also verified that the reading density applied in 2006 (50cmX2.5cm) generated a boundary in the interpolation (approximately 12cm per pixel), where theoretical archaeological structures become confused and complex and turn into statistical artefacts. By contrast, the schematisation that gave rise to large pixels (25-30cm) demanded less interpolation and was much more useful in the identification of structures. At the same time, a similar situation occurred with the numerical resolution of the readings (the different between the maximum and minimum values of detectable amplitude). It was verified that the original 16-bit data presented a dynamic range too wide to be represented in a graphic of only 256 colours. Converting the original data to 8-bits offered acceptable results in some of the grids, where it appeared possible to identify some interpretable structures clearly.

As a consequence, if the appropriate processing for surveys of adobe archaeological structures was related to spatial resolution and frequency, we proposed a new season of data collection applying the pertinent modifications arising from the previous year's data processing. In this case, we used a GSSI 5103 equipment model, with a 270MHz antenna. To take readings, we settled on a numerical resolution of 8-bits, a reading frequency of 40 sc/m (2.5cm), and a gap of 0.4m between radargrams, or slices. The survey focused on nine grids of varying sizes. In two of the grids, archaeological excavations were conducted and the results were compared with the results obtained from the georadar survey. The aim of the comparison of results was to validate or correct the results of the survey, based on the detailed description offered by the archaeology. The final result of the comparison of real data with data obtained by the sensors would feed into a survey strategy aimed at obtaining maximum performance from geophysical surveys in arid environments with adobe structures.

The results obtained in 2006 clearly showed the vulnerability of survey systems to external interferences when the anomalies to be described present low contrast. Another problem related to the antenna frequency became apparent when processing the information through a background filter to eliminate part of the background noise. At that point, the differences between any theoretical structures detected and sedimentary deposits dwindled to very subtle values. Therefore, any variation in the antenna's contact with the soil or any metallic element on the surface of the terrain generated anomalies dozens of times more often than subsoil structures. As a result, the maps and horizontal slices presented a large number of problems with contrast, because the elements of interest in the survey offered very low, fragmentary values. The strategy selected to correct the problem involved using a very low frequency antenna (GSSI 5103 model, with a 270MHz antenna). In this way, the aim was to obtain a less turbulent response, as medium and low-frequency antennas have much longer wavelengths. In other words, they are much less disturbed by small subsoil objects and generate more schematic images. In addition, the antenna used has a higher penetration and a lower sensitivity to the high-frequency interferences encountered during the 2006 season.

The changes to the reading parameters of the georadar system centred on three aspects:

a. Modification of the reading densities. The georadar survey results from 2006 revealed the importance of reading density on each survey axis in obtaining comprehensible results. As we had already set out the geological and built materials of the city of Termez, we limited our focus to sediments con-

tributed by the wind, built remains and any disintegration of them, and the geological based formed by sandstone. The vast similarity in the response obtained by georadar from these materials narrows the differences between sediment and built structures to a minimal part of the signal. In other words, the line of values that differentiated a structure from the sediment covering it or surrounding it was very subtle. Obviously, in this context, the separation between readings is crucial in obtaining a correct depiction. Figure 1 gives a schematic view of the change in resolution produced by modifying the spatial parameters for reading from a separation of 0.5m to 0.4m between radargrams (maintaining 0.2m of final resolution on the Y-axis) when defining an imaginary structure captured across its entirety. It is typical when conducting surveys with georadar to work in grids that reflect a disparity between the reading densities on one axis (direction of antenna's scanning) and the other (separation between radargrams, or slices). That does not create an obstacle to achieving good results if the contras is high between the structures being described and any irrelevant ones. If we increase the resolution on the X-axis (the separation between radargrams, or slices), we reduce the possibility of generating numerical artefacts when the results are interpolated, because we are reducing the disparity between the data obtained on each axis.

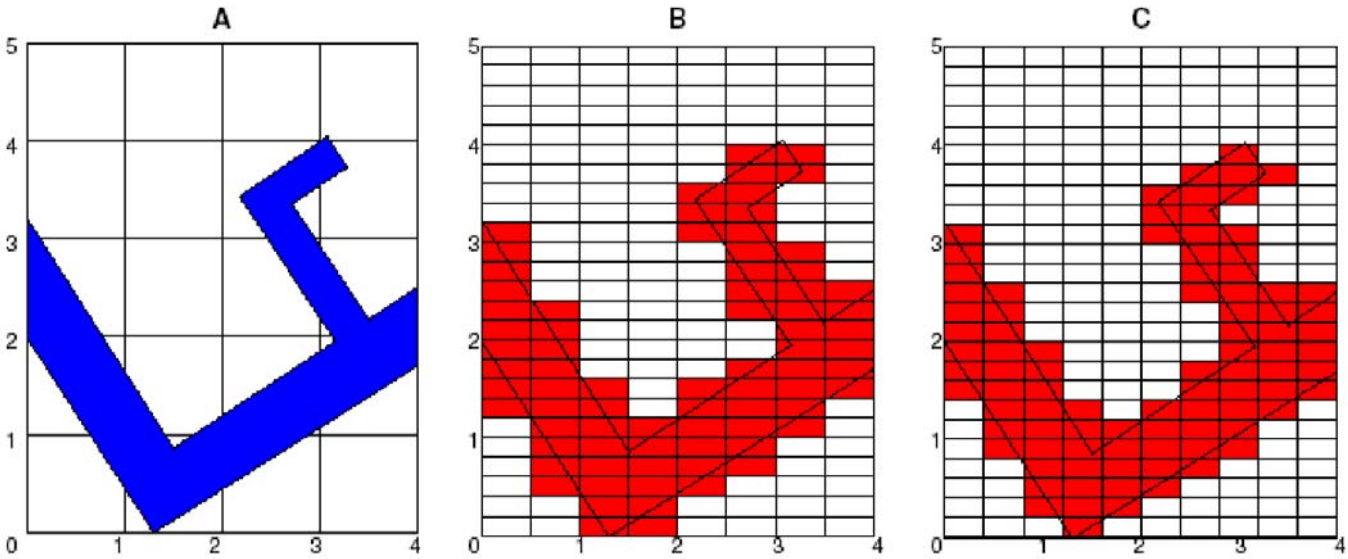


***Figure 1.*** The alias effect and spatial resolution of a survey. In an imaginary grid (A), an ideal anomaly created by a structure (in blue) is inscribed with geophysical properties that are differentiated from the sediment that covers it. B represents the ideal image that could be obtained from the structure using a final resolution of 0.5X0.2m. C shows the image based on a resolution of 0.4X0.2m.

Parameters for data acquisition. The adjustments made to the georadar system in order to acquire data respected the general criterion of modifying the signal obtained as little as possible. The goal was to achieve results that would permit the most open post-processing work possible. Therefore, only high-pass filters (90MHz) and low-pass filters (700MHz) were applied to the signal recorded by the georadar. As in the 2006 season, episodes of interference were detected during the fieldwork, causing some radargrams, or slices, to be unusable.

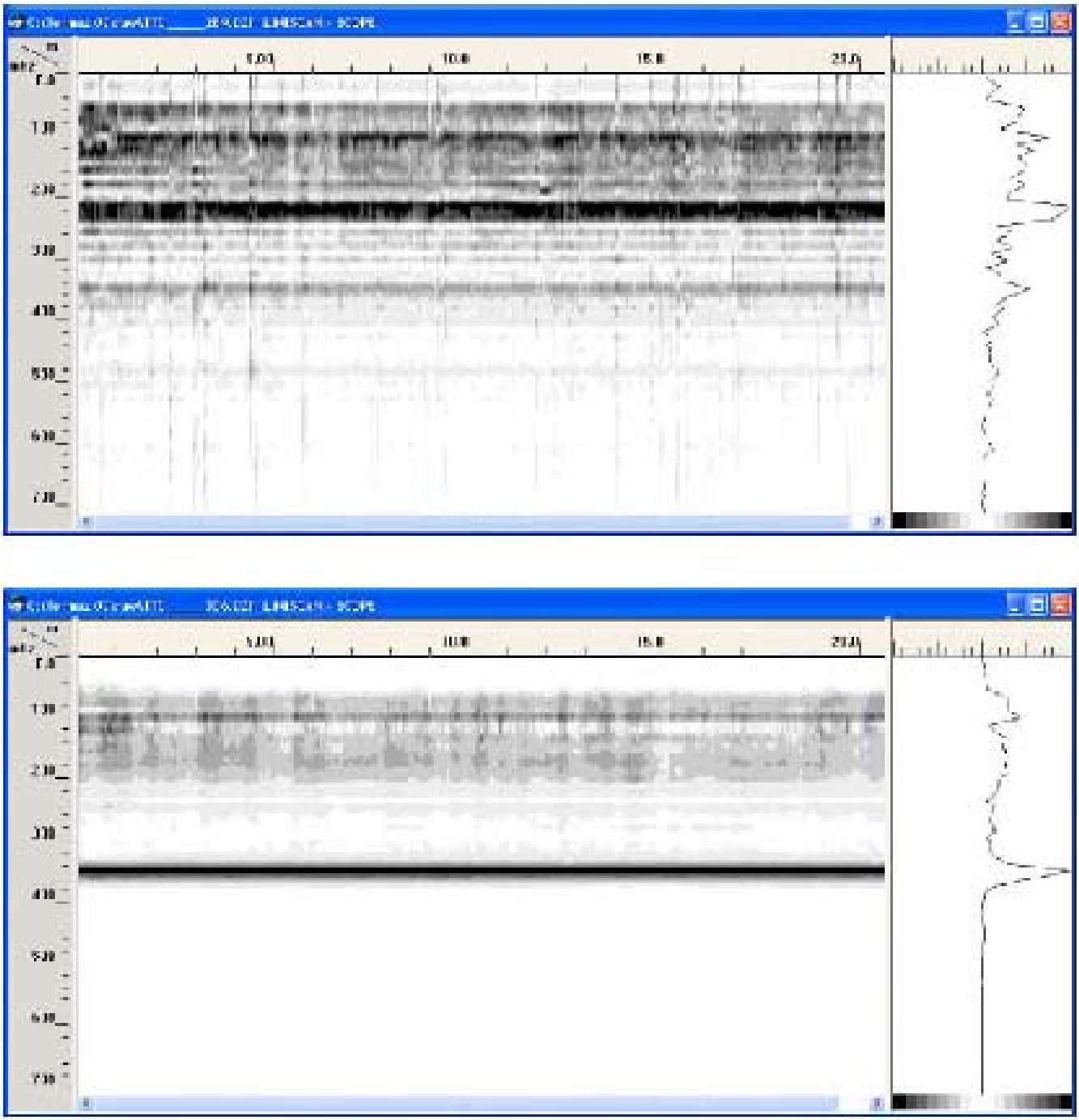

***Figure 2.*** Frequency spectra from radargrams 289 and 306 from grid L, obtained a few minutes apart. The spectrum of radargram 289 is very turbulent and discontinuous and a strong interference appears between 220 and 250 MHz.

c. The distribution of readings was maintained at 40 scans/metre (1 scan=2.5cm) and 512 samples per scan, with an exploration depth of 90 nanoseconds (Figure 3).

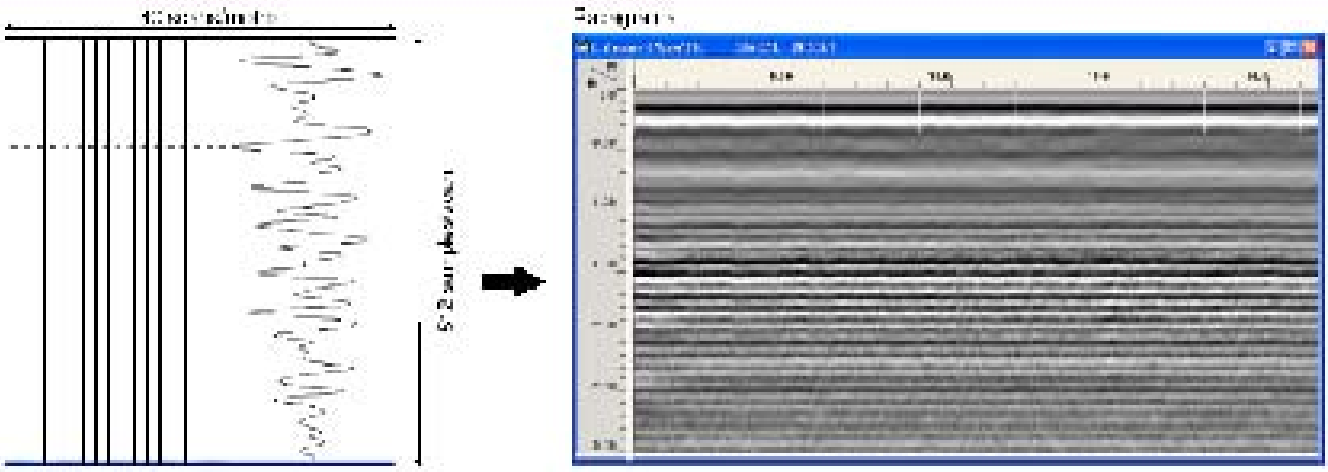

***Figure 3.*** The radargram is an expression of the response oscillations captured by the radar system. The reading parameters in use are indicated.

d. Lastly, given confirmation that it was essential to maintain maximum stability of the signal, the position of the cable was immobilised as much as possible between the antenna and the central unit to avoid any noise produced by the movement of the system (Figure 4).

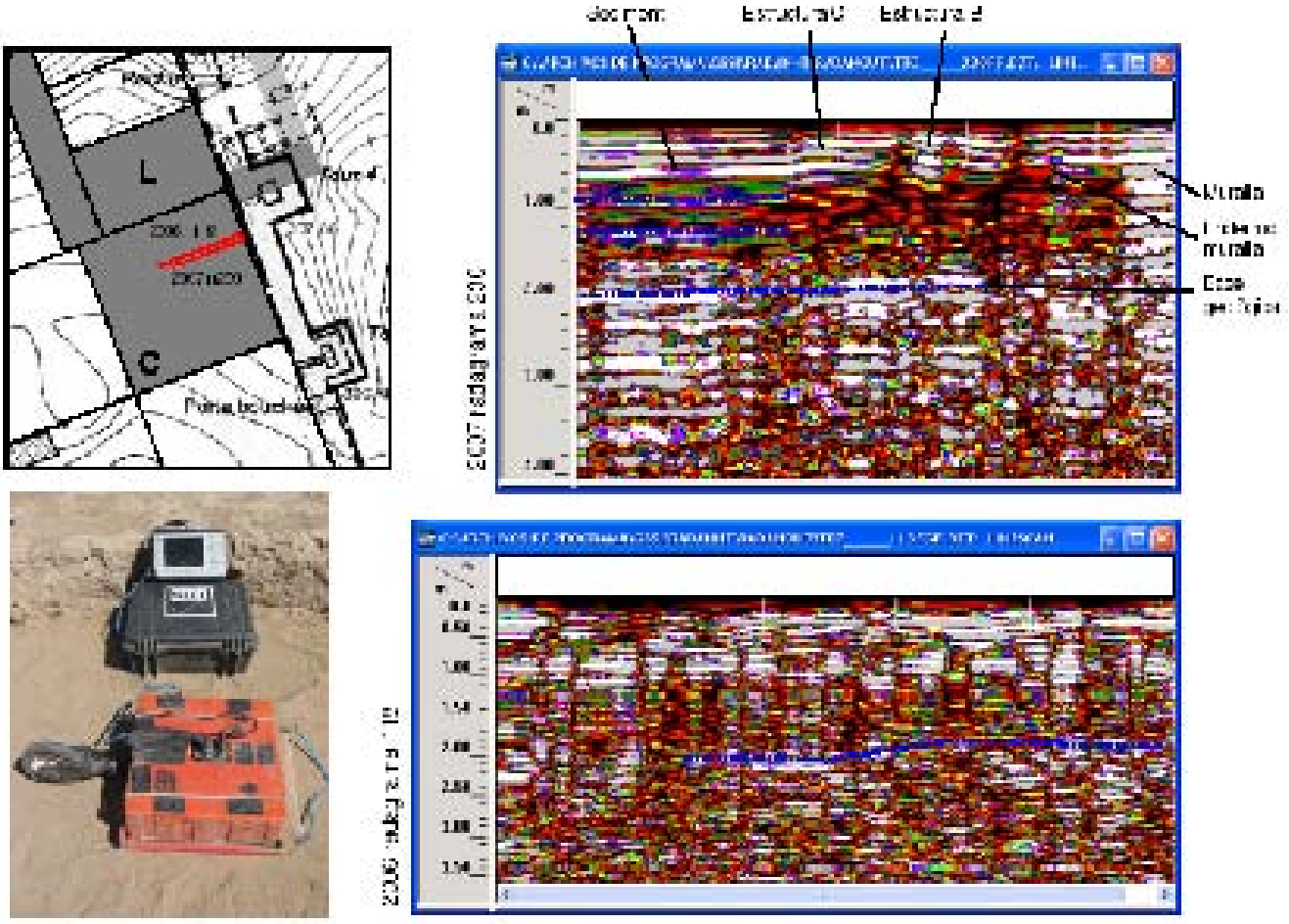

***Figure 4***. Differences between the data recorded in the 2007 season with a 270MHz antenna (above right) and the data from 2006 using a 400MHz antenna (below right). The radargrams correspond to positions near grid C (above left). Below left, the image given by the GSSI 5103 system with a 270MHz antenna and an immobilised signal cable.

The study and numerical processing of the data obtained on the hill of *Tchinguiz Tepe* up to that point, enabled the issue to be focused on two aspects: the spatial relationship between the data obtained and the low contrast between the subsoil elements being described. We have already described how corrections were applied to reading density when collecting data by using the lowest-frequency transducer or antenna (270MHz) and in our procedures in the field. Processing the signal and displaying the data visually is where the data obtained needs to be transformed into subsoil maps.

The technique used to display the data visually and analyse the results is called “time-slicing”, which involves interpolating the data recorded (radargrams) to generate three-dimensional data of the explored area that can then be viewed on any of the three axes. In this way, the entire work of analysis and signal processing aims to obtain layout images of any possible structures with the greatest definition possible. Thanks to the excavation undertaken in part of grid C, we were able to confirm that the best results, i.e. the results that correlated best with the excavated structures, were the results obtained from radargrams processed with a background filter. That gave rise to a new approach to take with the data obtained in 2006, which were reprocessed using the background filter to verify similarities and disparities in the results from the excavated area of grid C.

While processing the data, it was verified that the subtle variation in amplitude and frequency captured by the radar from a wall or simple infill, probably aeolic in origin, generates very low contrasts in the displays. This hampers their interpretation. It was also verified that the reading density applied (50cmX2.5 cm) creates a limit in the interpolation (approximately 12cm per pixel) where structures become more confused and complex and turn into statistical artefacts. By contrast, the schematisation that involving large pixels (25-30cm) demanded less interpolation and was much more useful in the identification of structures. Converting the original data to 8-bits gave results that were only acceptable in some grids. However, the result of applying these techniques in these conditions continues to be negative for good archaeological work.

**Applying low-frequency electromagnetic methods**

In conclusion, our experiences with georadar to data have yielded valuable information on some occasion, but most of the time it has failed to give good results and it has given results full of artefacts that did not correspond to any structure of archaeological interest. Low-frequency electromagnetic methods (with conduction currents predominating) should not, in principle, give results that are much better than high-frequency methods (with displacement currents predominating). This is because the signal (reflection) in georadar is highly marked by the contrast of dielectric permittivity between the two media, and in electromagnetic trial-pits, it is highly marked by the contrast of conductivity. Both parameters, dielectric permittivity and electrical conductivity, are extremely controlled in normal conditions by the content of water molecules present in materials. However, electromagnetic trial-pits offer the advantage of their greater speed of application and lower sensitivity to artefacts and attenuations of the signal.

## Electrical surveying

To work with the resistivity method, an electrical field is created between specific electrodes *A* and *B*, called emission electrodes. Through them, a continuous electrical current of intensity I is injected into the terrain. At another two points of the terrain, two measurement electrodes *M* and *N* are placed. Then using the corresponding measuring instrument, the differences in potential generated, $\Delta U$, are measured. The relative arrangement of electrodes *A*, *B*, *M* and *N*, which configure the four-electrode device, is determined by the type of geological problem in need of resolution.

Electrodes *A* and *B* create an electric field at point *M*, which is at a distance from them of $r_{AM}$ and $r_{BM}$, and has potentials $U_{MA}$ and $U_{MB}$, according to the expressions:

$$U_{hiA} = \frac{\rho I}{2\pi}\frac{1}{r_{Ahi}} \qquad U_{hiB} = -\frac{\rho I}{2\pi}\frac{1}{r_{Bhi}} \tag{1}$$

The total potential at point *M* is:

$$U_{hi} = U_{hiA} + U_{hiB} = \frac{\rho I}{2\pi}\frac{1}{r_{Ahi}} - \frac{\rho I}{2\pi}\frac{1}{r_{Bhi}} = \frac{\rho I}{2\pi}\left(\frac{1}{r_{Ahi}} - \frac{1}{r_{Bhi}}\right). \tag{2}$$

By analogy, the potential at point *N* is:

$$U_{hN} = U_{hA} + U_{hB} = \frac{\rho I}{2\pi}\frac{1}{r_{AhN}} - \frac{\rho I}{2\pi}\frac{1}{r_{BhN}} = \frac{\rho I}{2\pi}\left(\frac{1}{r_{AhN}} - \frac{1}{r_{BhN}}\right). \tag{3}$$

The difference in potential between points *M* and *N* will be:

$$\begin{aligned}\Delta U &= U_{hi} - U_{hN} = \frac{\rho I}{2\pi}\left(\frac{1}{r_{Ahi}} - \frac{1}{r_{Bhi}}\right) - \frac{\rho I}{2\pi}\left(\frac{1}{r_{AhN}} - \frac{1}{r_{BhN}}\right) \\ &= \frac{\rho I}{2\pi}\left(\frac{1}{r_{Ahi}} - \frac{1}{r_{Bhi}} - \frac{1}{r_{AhN}} + \frac{1}{r_{BhN}}\right).\end{aligned} \tag{4}$$

From here, we obtain the following expression for the resistivity $\rho$ of a homogeneous medium with a four-electrode device on its surface

$$\rho = K\frac{\Delta U}{I} \tag{5}$$

$$K = \frac{2\pi}{\frac{1}{r_{Ahi}} - \frac{1}{r_{Bhi}} - \frac{1}{r_{AhN}} + \frac{1}{r_{BhN}}} \tag{6}$$

Magnitude K is a function of the distribution of the four electrodes over the terrain and is called the device coefficient. According to expression (6), the device coefficient has dimensions of longitude

Expression (5), obtained in a homogeneous medium, can be applied to the interpretation of the results from measurements taken with a four-electrode device on the surface of a homogeneous terrain. However, in this case, the result of the calculation will be a certain arbitrary magnitude that expresses the dimensions of a resistivity. This arbitrary magnitude is called “apparent electrical resistivity” and is assigned $\rho\alpha$.

As a consequence, in the general case .

$$\rho_a = K\frac{\Delta U}{I} \qquad (7)$$

In the particular case of a homogeneous medium, the apparent resistivity is equal to the true resistivity, $\rho\alpha = \rho$. The trajectories of current flow in the terrain follow the route shown in Figure 5.

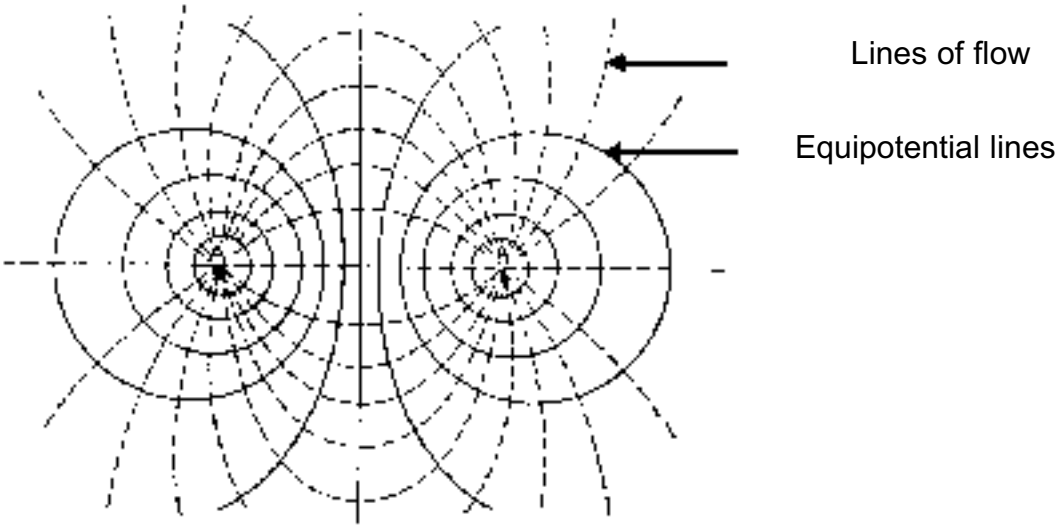


***Figure 5.*** *Equipotential lines and lines of flow in the horizontal plane of the surface of the terrain*

**Using the electrical tomography method for surveys**

The method of surveying using electrical tomography, also called 'automated array scanning’, is an extension of the vertical electrical sounding (VES) method involving automatic multiple VESs for different electrode configuration.

In this approach, we have a set of electrodes connected to a computer by a seismic cable. Using a control program, we direct the central unit to take measurements of apparent resistivity for pairs of consecutive electrodes until all the possible combinations of pairs have been measured. As in vertical electrical sounding, the many possible arrangements of electrodes include Wenner (in which the distance 'a' of inter-electrode separation is kept identical), Schlumberger (in which the electrodes with current are increasingly separated from the electrodes with potential), and dipole-dipole (in which the pairs of electrodes with current are separated from the electrodes with potential by a greater distance than they are separated from each other).

For this season, we selected the Wenner-Schlumberger method, which works as follows: a measure of apparent resistivity is taken between the 48 electrodes 1-48-24-25, 1-46-23-24, and so on until reaching 1-4-2-3. Then another measure is taken, starting with electrodes 2-47-24-25, 2-45-23-24 and so on through to 2-5-3-4. Measurement continues until reaching the last arrangement, which is 45-48-46-47.

By opening the distance between the electrodes with current and the electrodes with potential, we reach different levels of depth, obtaining its apparent resistivity at the mid-point of each set of electrodes. Bringing together all the different levels, we obtain the so-called “electrical pseudo-section”, which indicates the variations of vertical and lateral resistivity (Figure 6).

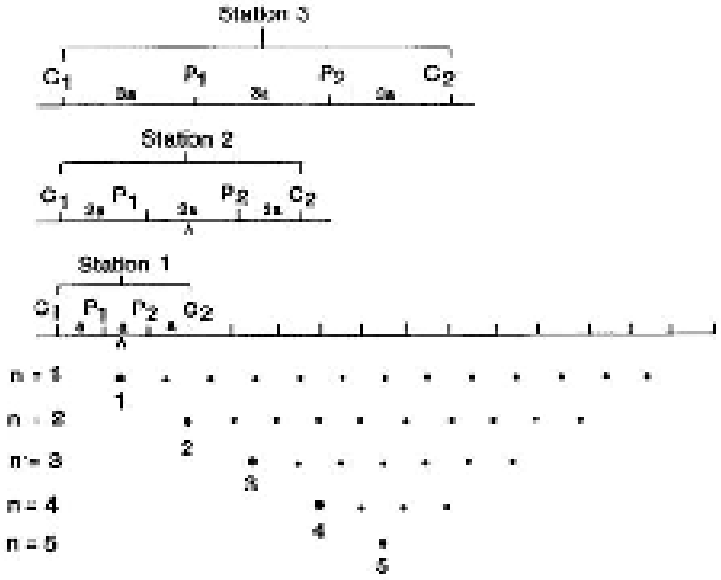


***Figure* 6.** Arrangement of measurements in the electrical tomography method.

The equipment used to acquire data during the season is a Syscal Switch Resistivity Meter, made by Iris Instruments (Orleáns, France). It has the following components: a central unit, 48 electrodes, a RS-232 computer connection cable and a seismic connection cable to the electrodes (Figure 7). The computer programs used to obtain the data are Electre II, which generates the sequence of slices, and Syscal, which downloads the information.

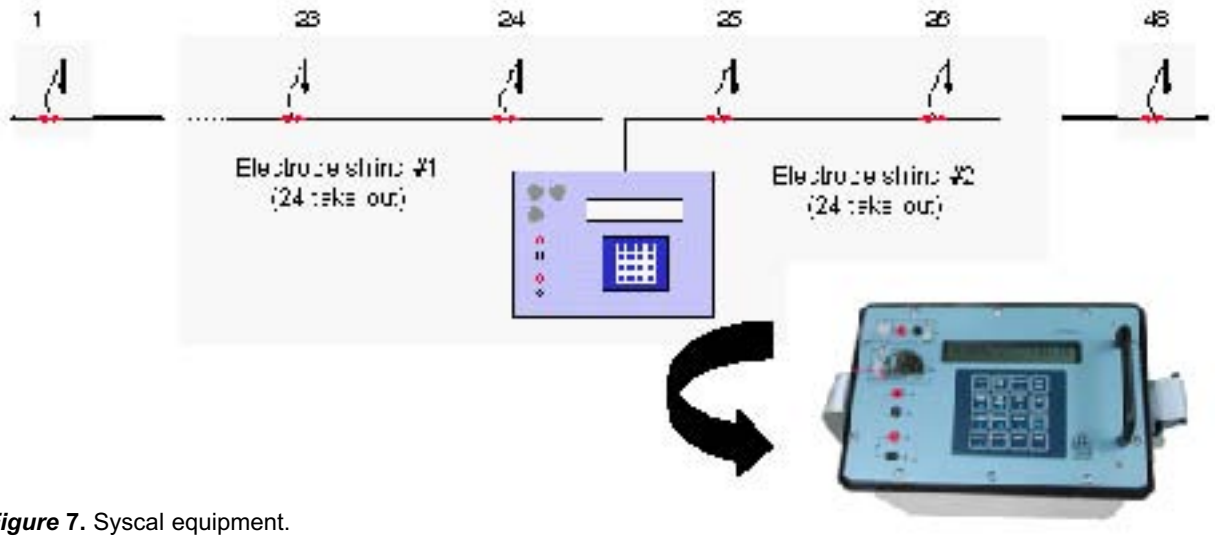


***Figure* 7.** Syscal equipment.

The equipment can take different kinds of measurements: Rho and Rho-IP. In the first case (Figure 8), we obtain the value of the apparent resistivity (Rho) based on squared pulses of energy, using the contrary sine pulse to eliminate the effect of the spontaneous polarisation of the electrode and the terrain.

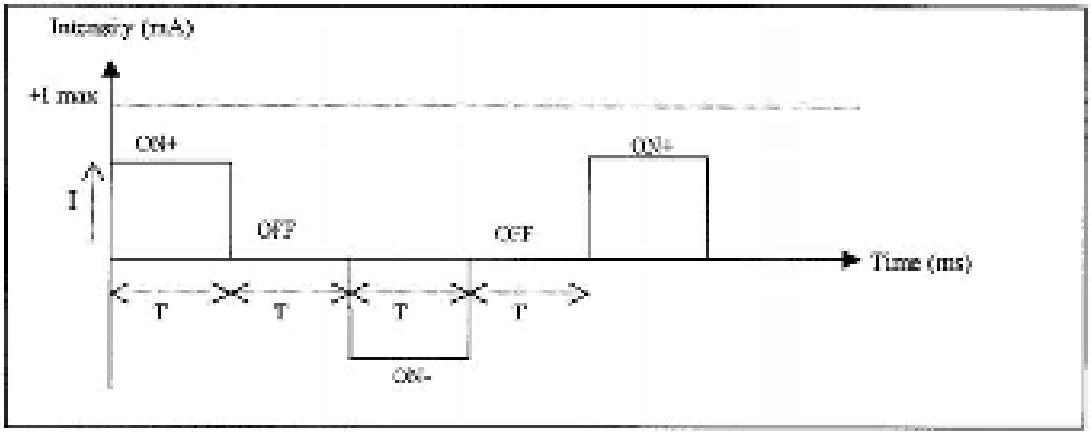


***Figure* 8.** Current pulse in resistivity mode.

In the Rho-IP mode, we inject the negative sine pulse to measure the induced polarisation of the terrain (Figure 9). Once the current to the ground has been cut, we measure four intervals of potential in order to calculate the decay curve of the polarisation. This mode is used in studies of induced polarisation.

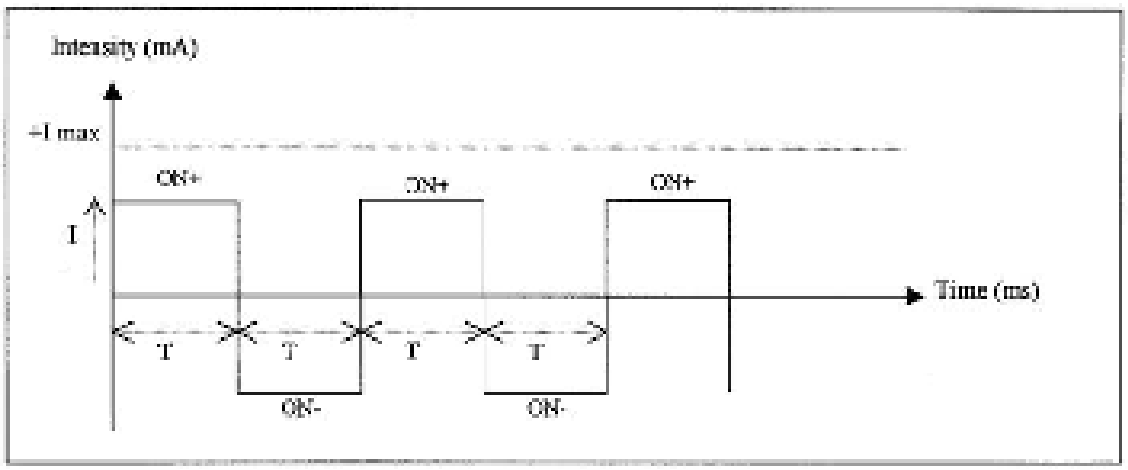


***Figure* 9.** Current pulse in Rho-IP mode.

The parameter measured by electrical tomography is the apparent resistivity of the terrain. As this resistivity is a function of the thickness of the layers and their real resistivity, it is necessary to process the field data to obtain the real resistivity.

This is carried out by means of an inversion procedure. Iteratively, we adjust a theoretical model and calculate its apparent resistivity. If the value diverges from the field curve beyond an estimated error, we calculate the model with new parameters until the theoretical model fits the field curve at the sought level of error.

This process was carried out using the RES2DINV program. Made by Geotomo Software of Malysia, it is an automated program that calculates two-dimensional (2-D) models of terrain resistivity based on

data obtained by electrical tomography equipment. With this program, we obtained the geoelectrical sections presented in this report.

To calculate apparent resistivity, the program uses a direct modelling sub-routine. To obtain inverse models of real resistivity, it uses a non-linear least-squares optimisation routine (deGroot- Hedlin and Constable, 1990 –*Geophysics*, 55, 1613-1624 -; Loke and Barker, 1996 –*Geophysical Prospecting*, 44, 131-152-). In its direct modelling, the program can use both the finite-difference method (if there is no topographical correction) and the finite-element method (if topographical correction is necessary).

La rutina de inversión se basa en el método de mínimos cuadrados constreñidos por suavización, de los autores citados. Puede utilizar la técnica de optimización quasi-Newton así como la habitual de Gauss-Newton.

To do this, the terrain is divided into rectangular blocks that can be equal or different in size. The number of blocks can be expanded beyond the number of measurements. The purpose of the program is to find which resistivity of the rectangular blocks will produce a pseudo-section of apparent resistivity that best fits the data obtained in the field. The difference between the two gives the root mean square (RMS) error obtained.

Different types of electrode devices can be used, including Wenner, Schlumberger, pole-pole, dipole-dipole, even non-linear configurations (electrodes distributed over the surface of the terrain in two dimensions).

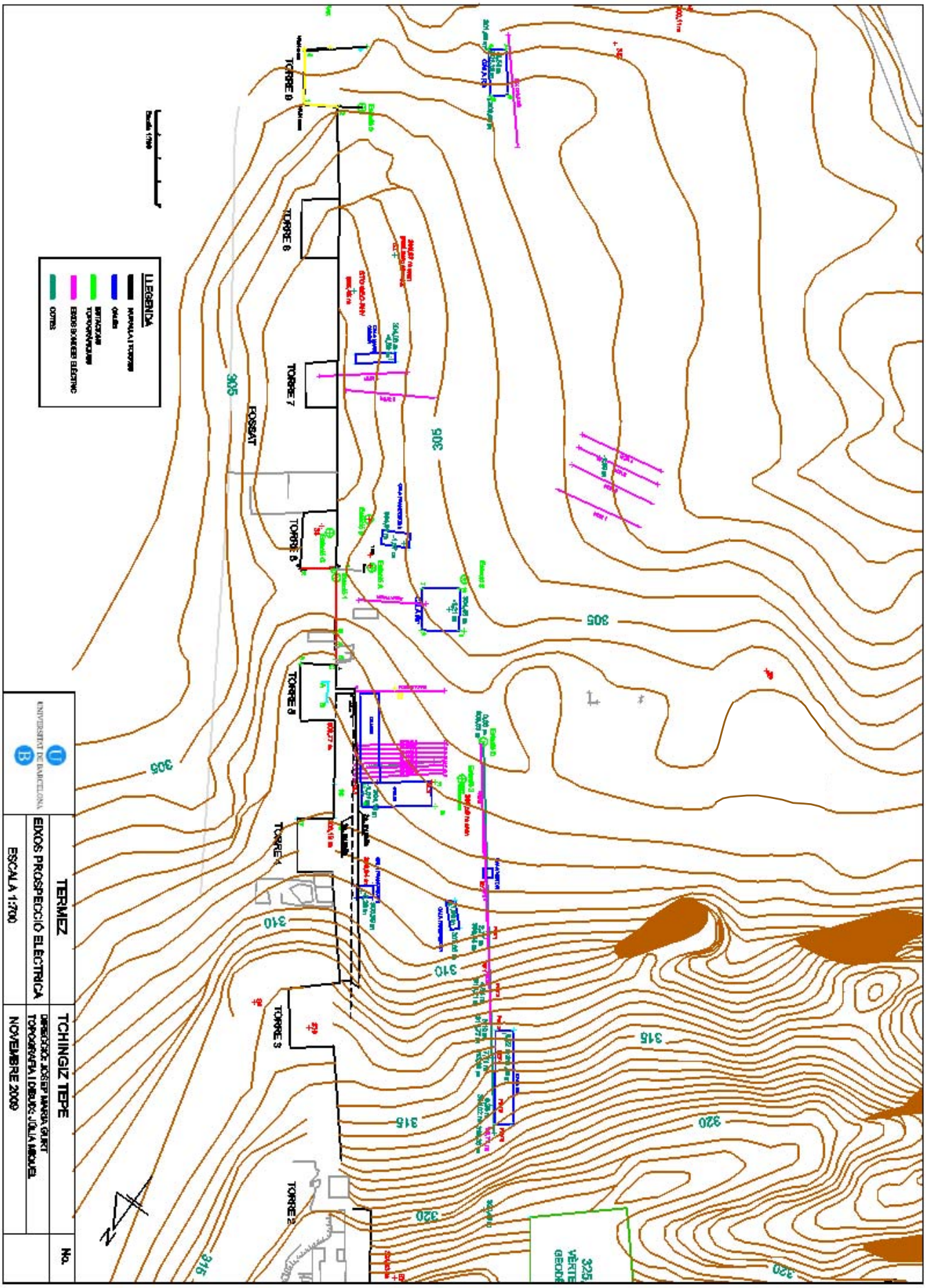
LLEGENDA
TORRE 9
TORRE 6
TORRE 7
TORRE 5
TORRE 8
TORRE 4
TORRE 3
TORRE 2
FOSSAT
305
310
315
320
325
TERMEZ
EIXOS PROSPECCIÓ ELÈCTRICA
ESCALA 1:700
NOVEMBRE 2009
TCHINGIZ TEPE
No.

### Results from the 2009 season

Below are set out the results of electrical tomography taken at the site in September 2009. The measures were taken using equipment made by Iris Instruments, the Syscal Pro Switch 48 model, serial number 10513-3161256421-189.

The conditions were extreme. The combination of a highly arid climate and a very hard, resistive crust on the surface together made the contact resistances between the electrodes and soil surface very high in some cases. Despite being sprinkled with water, they caused unacceptable noise errors. As a result, seven profiles have been eliminated. The presented profiles had mathematical inversion errors of between 8% and 24%, while optimal conditions typically give errors of 2-4%. Therefore, these results cannot be considered entirely reliable. However, most of the errors occurred in a very superficial area. In these circumstances, the electrical tomography in various tests conducted in situ was not able to differentiate precisely between fallen adobe bricks and solid adobe walls. There was simply not a sufficient contrast of electrical resistivity to differentiate them.

### RC Profiles

#### Situation

The eight parallel profiles taken in sample trench RC run perpendicular to the fortification wall and measure 19.2 metres in length. The real interval between electrodes was 0.4m. The device used was dipole-dipole; however, data were interpolated to 0.1m. The fortification is located to the left of the profiles. The area lies at the end of a rise to the foot of the primary fortress. The first profile, RC1, lies one metre from the sample trench (see diagram) and the remaining profiles have an equidistance of 1m from one another.

#### General characteristics

The profiles feature three types of facies. Two are highly resistive, while the third has low resistivity. One of the two highly resistive facies is a surface level of limestone crust with a thickness ranging from dozens of centimetres to almost one metre and presenting resistivity values of up to 700 ohm. This is the level responsible for the electrode contact problems aggravated by an extremely arid climate. The other highly resistive layer resembles a rocky sandstone substrate and is made of sandstone. Reworked at the time of the first urban development in the area, it gives rise to a very high variability of lateral morphology, especially starting with RC4. Between the two levels, the level of low resistivity (< 40 ohm) appears. It is made up of slope deposits which contain adobe remains that have come from the collapse of the principal fortress, which is located topographically just above, and loess, probably aeolic in nature, which is more resistive. In some places, the surface crust is totally or partially covered by loess and adobe remains and is therefore found beneath the surface. In the left-hand zone (touching the fortification), there is an area of some 2.5 metres where the limestone crust had already been removed during the excavation of another archaeological sample trench that was underway at the same time that these profiles were taken with electrical tomography.

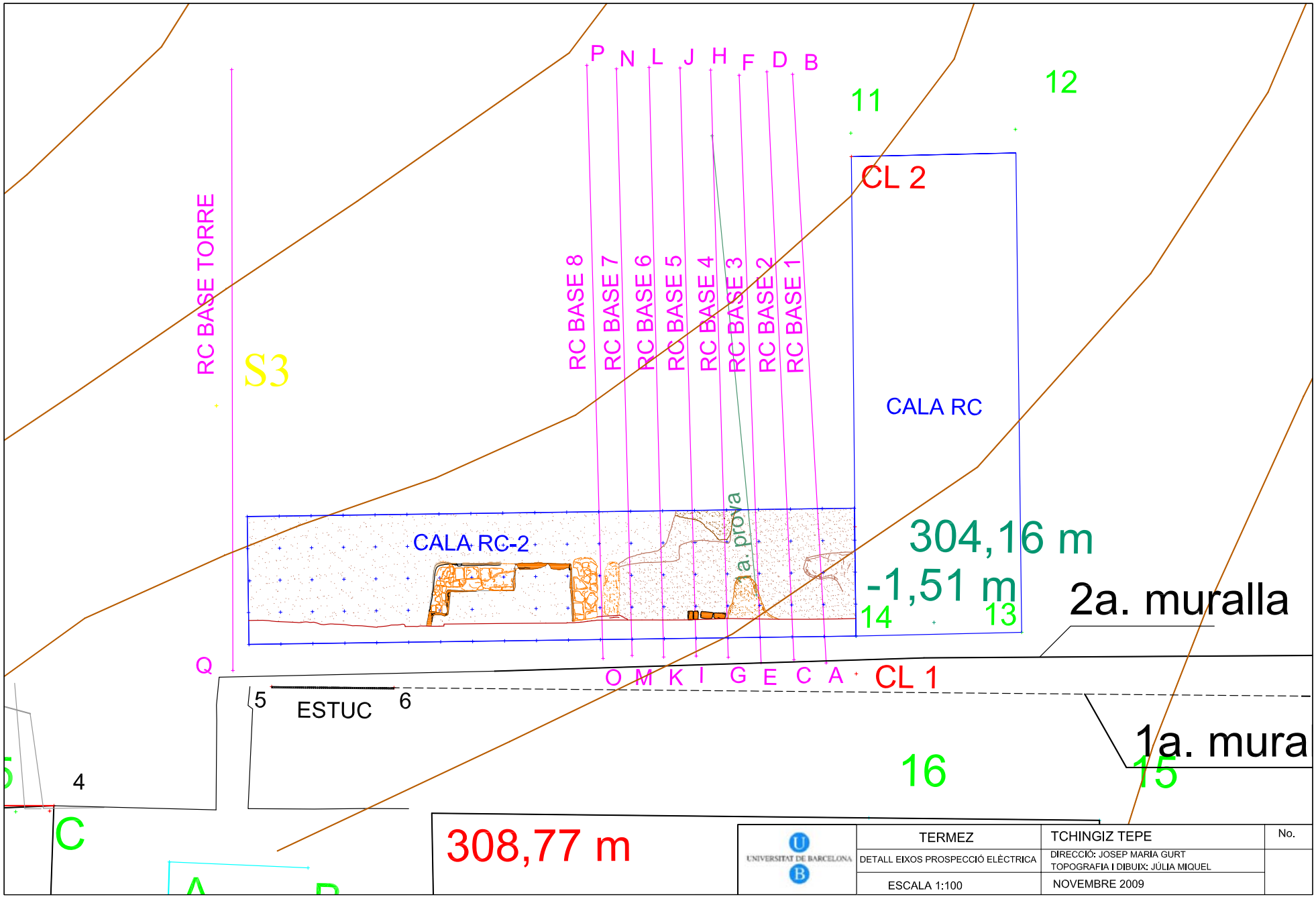
P N L J H F D B
11
12
CL 2
RC BASE TORRE
S3
RC BASE 8
RC BASE 7
RC BASE 6
RC BASE 5
RC BASE 4
RC BASE 3
RC BASE 2
RC BASE 1
CALA RC
CALA RC-2
1a. prova
304,16 m
-1,51 m
14
13
2a. muralla
Q
O M K I G E C A
CL 1
5
ESTUC
6
1a. mura
16
15
4
C
308,77 m
UNIVERSITAT DE BARCELONA
TERMEZ
TCHINGIZ TEPE
No.
DETALL EIXOS PROSPECCIÓ ELÈCTRICA
DIRECCIÓ: JOSEP MARIA GURT
TOPOGRAFIA I DIBUIX: JÚLIA MIQUEL
ESCALA 1:100
NOVEMBRE 2009

**Perfil RC1**

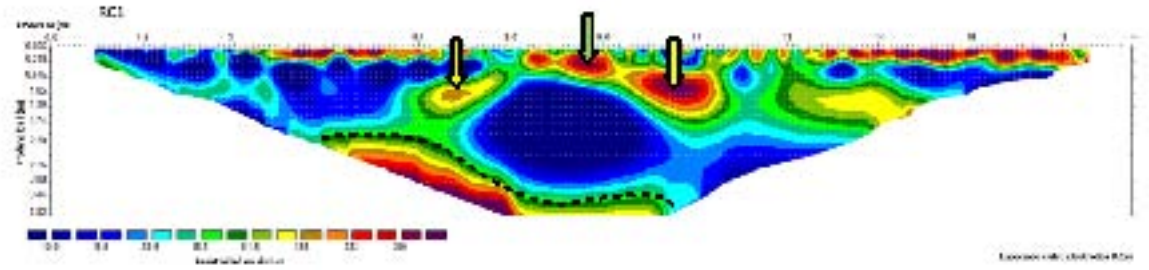

In this profile, three facies or levels can be very clearly observed. First, there is an upper highly resistive level, in which the effect of water used to reduce contact resistances is very pronounced, with local minimums. Below the resistive crust, intermediate levels present fallen adobe materials, intercalated with more resistive levels. The sample trenches excavated in the vicinity indicate that these levels have greater loess content, probably aeolic in origin. Similarly, all eight profiles feature intercalations at a distance from the fortification, as though a screen effect. For example, the most superficial intercalations, which are located between a horizontal position of 8m and 9.6m, are probably a crust of loess and adobe bricks, albeit partially covered. At a lower level starting at 2 metres of depth, lies the sandstone rocky sandstone substrate (marked with a broken line). This rocky sandstone substrate can clearly been observed to have undergone an artificial reworking, presumably to serve as a solid foundation on which to lay constructions made of adobe bricks. A green arrow indicates the partially covered limestone crust.

**Profile RC2**

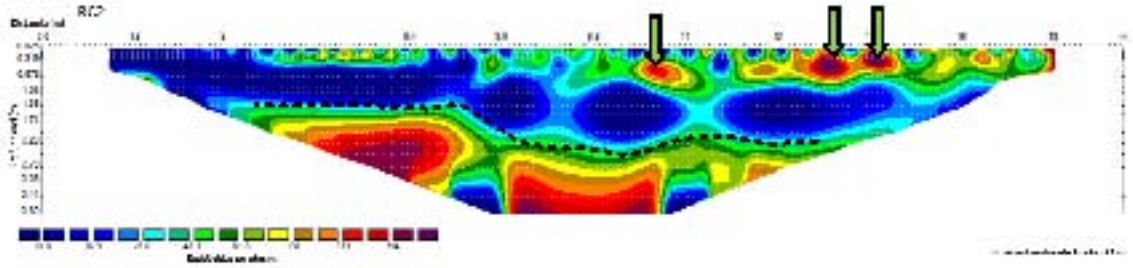

As in profile RC1, the most superficial level is a limestone crust. In this profile, it does not present total lateral continuity, but is covered by loess and adobe materials in places. At a depth of 1.5m, a resistive rocky sandstone substrate of sandstone appears (marked with a broken line). The least resistive intercalations (in blue) in the rocky sandstone substrate are considered errors resulting from the inversion process. A green arrow indicates the partially covered limestone crust.

**Profile RC3**

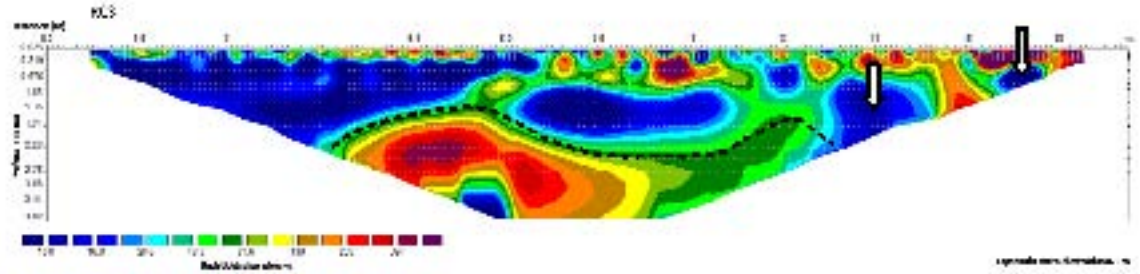

As in the previous profiles, the profile has the same structure. An upper resistive level is partially covered at times. Then there is an intermediate level of low resistivity and a more resistive rocky sandstone substrate. Structures such as the ones indicated by arrows contain conductive material at shallow depths, between resistive boundaries, and could point to the presence of a vertical adobe structure (wall). However, that cannot be stated with certainty. It could also be an infill of fallen adobe bricks in an irregular rocky sandstone substrate. Again, the small less-resistive intercalation (in blue) in the rocky sandstone substrate (marked with a broken line) is considered an error of the inversion process.

**Profile RC4**

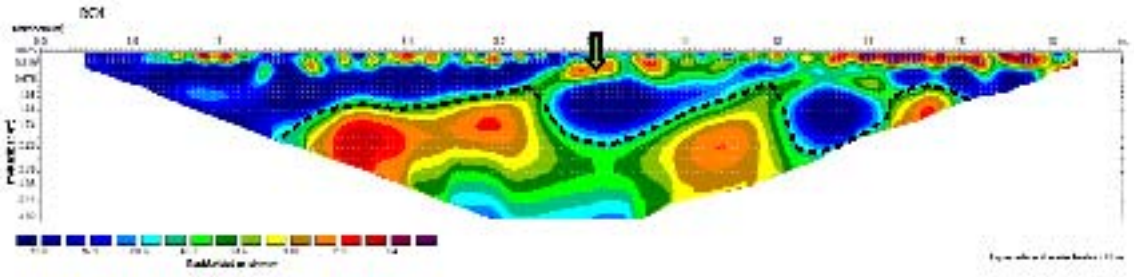

This profile, like the earlier ones, presents the same levels and materials. As a principal characteristic, we could highlight the lateral continuity of the disposition of the rocky sandstone substrate, which has irregularities that are filled in with adobe and loess. Over the position at 9.6m, an electrical continuity is observed between the surface materials and deepest materials. This must simply be due to the fact that the calcareous crust is partially covered by loess and adobe bricks, probably as a result of small topographical irregularities at the time of its formation. The measurement interval of 0.4m (real distance between electrodes) does not permit their total differentiation. Again the sandstone rocky sandstone substrate is highly worked (marked with a broken line). A green arrow indicates the partially covered limestone crust.

**Profile RC5**

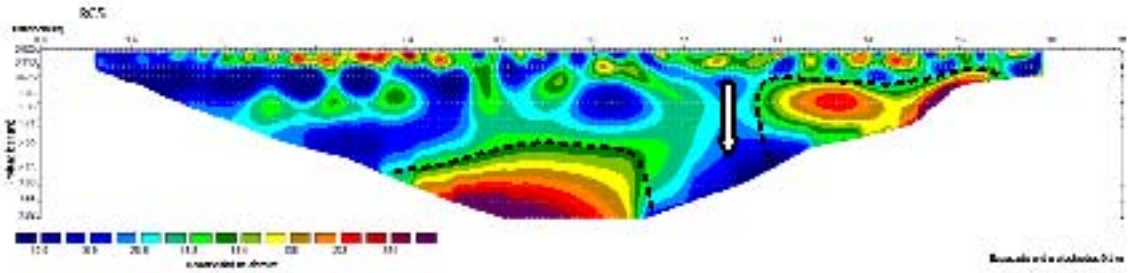

In this profile, the rocky sandstone substrate (marked with a broken line) is at a greater depth, increasing from a little more than 1m in the previous profile (equidistant at 1m) to more than 2m. In addition, a clear discontinuity is observed. It could be a passageway between sandstone walls, which is continuous in the three subsequent profiles RC6, RC7 and RC8, or it could be a (badly ruined) wall perpendicular to the profile and located parallel and 12m from the fortification wall. In previous profiles, there is some displacement of this structure rightward in the profile, resulting in a form that is oblique to the existing fortification. The archaeological interpretation must determine which, if either, of the two theories (passageway or wall) is more likely.

**Profile RC6**

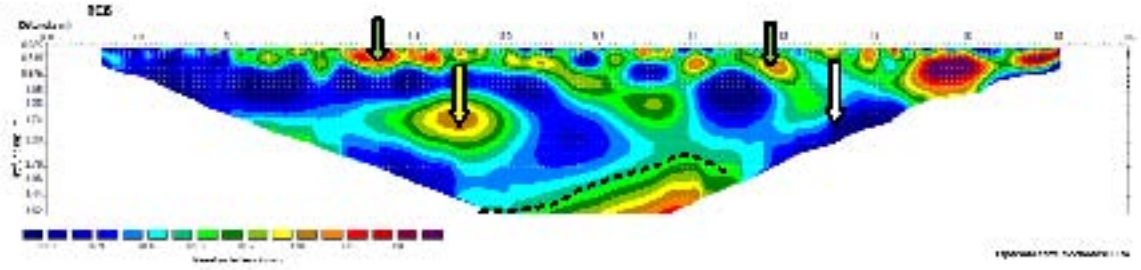

This profile features the same levels described above. There is a greater concentration of loess between the fallen adobe (yellow arrow) and the passageway or wall is displaced in a direction oblique to the fortification (following the length of the rocky sandstone substrate itself). Also, the depth of the rocky sandstone substrate is nearly 1m greater than in the previous profile. A green arrow indicates the partially covered limestone crust.

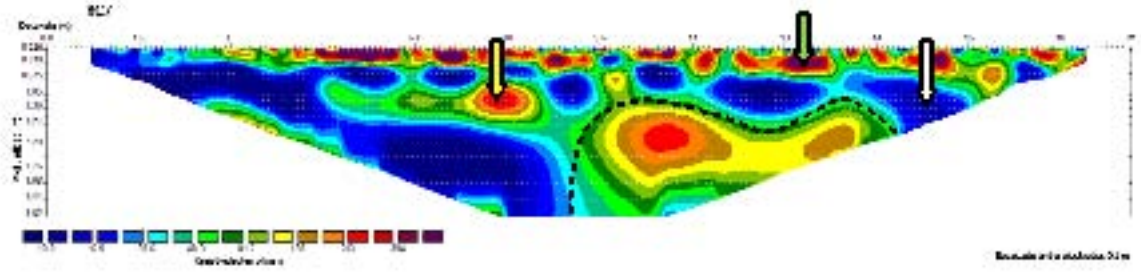

**Profile RC7**

This profile features the same levels described above. There is a greater concentration of loess between the fallen adobe (yellow arrow). The passageway or wall is displaced further to the right, following the variable morphology of the rocky sandstone substrate, which has continued to increase since RC4 (white arrow). A green arrow indicates the partially covered limestone crust.

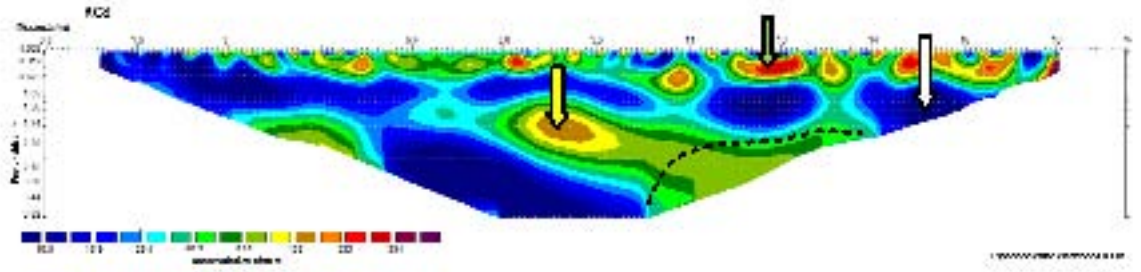

**Profile RC8**

In this profile, the rocky sandstone substrate has practically disappeared. That would indicate that this rocky sandstone substrate ends in a nearly vertical wall between this profile and the previous one. It would also seem to indicate that this zone contained a series of passageway structures, perhaps with adobe covering, that gave access to different structures of the fortification. Profile RC8 would be very close to a defensive tower and the empty space without any walls or structures would be the tower's antechamber. A green arrow indicates the partially covered limestone crust, while local accumulations of loess are indicated by a yellow arrow.

### Profile RCBASETORRE

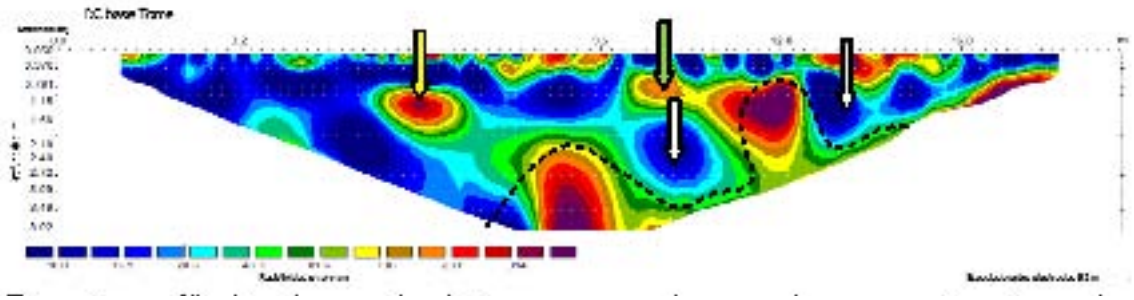

In this profile located at the foot of the tower, more “passageway” structures are observed in materials of the rocky sandstone substrate, probably covered by adobe walls. The structure is complex and permits entrance to the defensive tower. A green arrow indicates the partially covered limestone crust, while local accumulations of loess are indicated by a yellow arrow.

## RT Profiles

### Situation

Three partially overlapping profiles run parallel to the fortification. They are located at its foot and following the slope of the hill. RT1 lies on the slope itself, RT2 partially does, and RT3 lies on the flat section.

### General characteristics

The same three types of facies found in the previous profiles can be distinguished, but one important difference is the predominance of the level of low resistivity (in blue colours), which is made up of loess and adobe bricks fallen in the dismantling of the fortress on the hill. The rocky sandstone substrate is very reduced, certainly due to the fact that it is located at a depth greater than the depth reached by the electrical tomography profiles. In profile RT2, located in the topographical inflection zone , it is practically not visible.

### Profile RT1

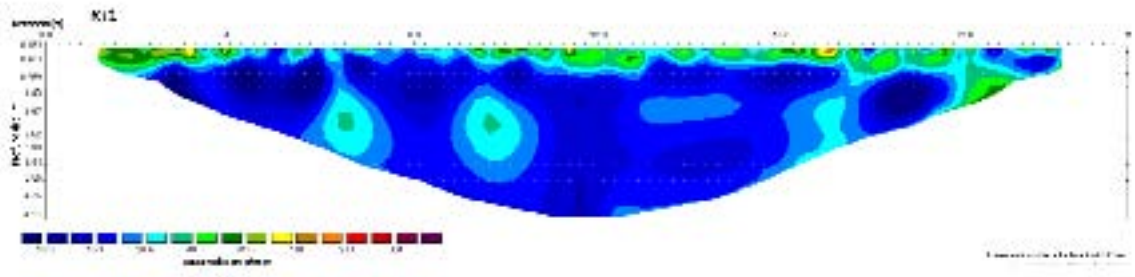

The limestone crust on the surface is very limited, the level of fallen adobe bricks on the slope reaches nearly 5 metres of potential. In this profile at the foot of the tower, passageway structures are observed again

### Profile RT2

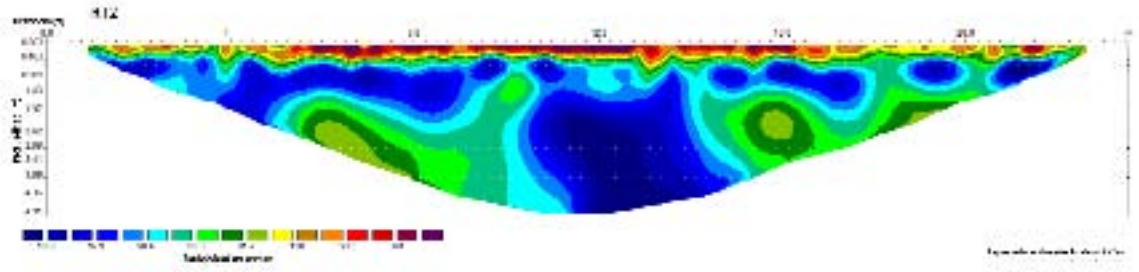

In this profile located in the inflection zone, the limestone crust on the surface is more extensive. Moderately more resistive levels (in green) correspond to levels of loess and arise from a sample trench excavated in the profile.

### Profile RT3

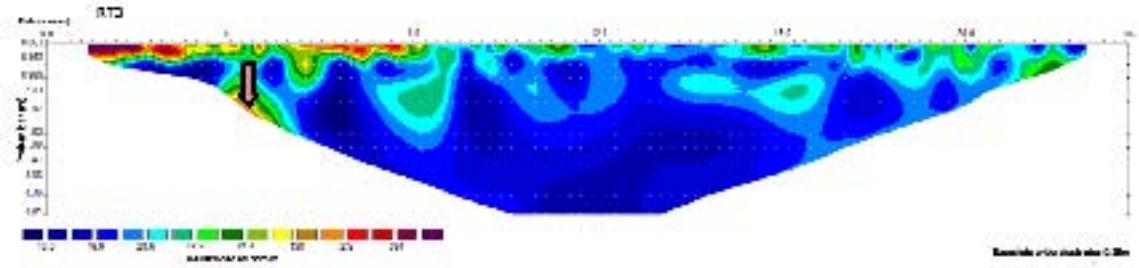

This profile presents basically the same characteristics as the previous one: a limestone crust and a strong pocket of adobe bricks and loess. We attribute the moderately more resistive values (marked with beige arrows) to inversion errors.

### AC2 Profiles

#### Situation

Three parallel profiles at an equidistance of 2 metres were obtained in a new survey zone situated within the military camp, in an area distant from *Tchinguiz Tepe*. The facies are similar, but there is no low resistivity facies of fallen adobe bricks in these profiles as there is in the RC and RT profiles. In a sample trench located hundreds of metres away but on the same topographical surface, the sandstone rocky sandstone substrate appears at approximately 3.5m of depth.

#### General characteristics

Four principal levels can be distinguished. The surface has a highly resistive limestone crust of the same type found in RC and AT profiles (yellow arrow). An intermediate level lies between 0.7m and 1m of depth, is resistive and has considerable lateral continuity (red arrow). The archaeological excavation has determined that this level is an extremely hard artificial soil. Beneath it, we found slightly less resistive materials, probably loess (green arrow), and lastly, at greater depth, there is the rocky sandstone substrate (broken line).

**Profile AC2- 1**

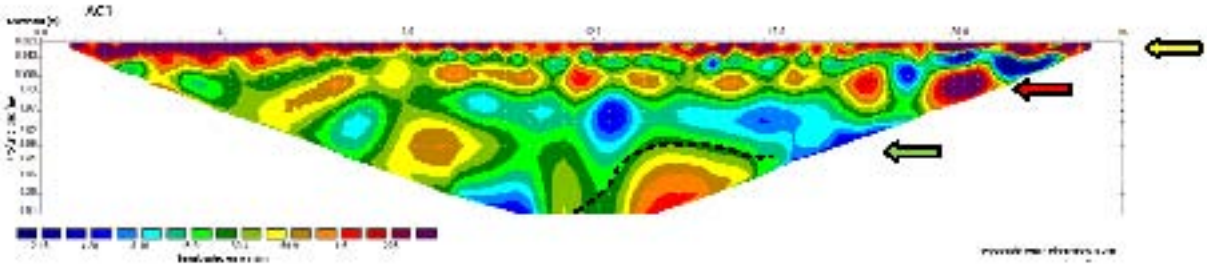

The four facies described above can be clearly observed (marked by arrows and a broken line). Earlier excavations identified the intermediate resistive level (red arrow) as an extremely hard artificial soil of a more modern period. No adobe wall structures have been found.

**Profile AC2- 2**

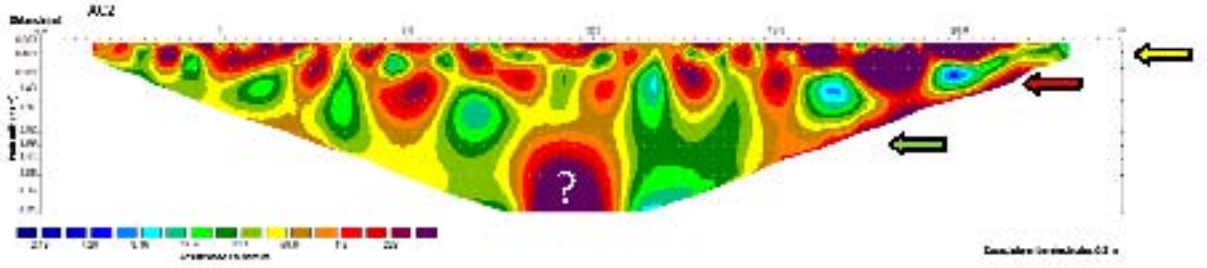


The surface crust is clearly visible, as is the resistive level or soil (red arrow). The third less resistive level is not very visible. It is highly masked by the previous two levels. Farther down, a highly resistive structure can be observed. It could be the rocky sandstone substrate, but the elevated errors present in the area mask the resistivity values obtained.

**Profile AC2- 3**

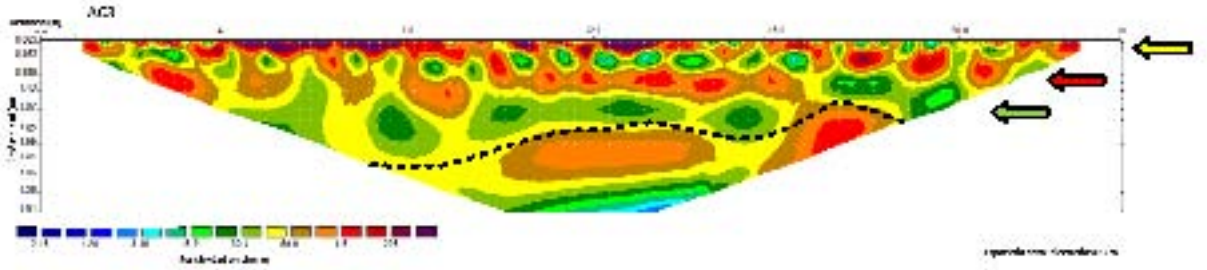

In this profile, the four characteristic levels can be observed well: crust, resistive soil, level of intermediate resistivity, and underlying rocky sandstone substrate. The boundaries are not very clear. Errors in the zone are high and the level of the signal is low as a result of the two very resistive superficial levels, which gives rise to indeterminate results.

# Report on Radiocarbon Dating -/1

**Joan S. Mestres i Torres, Anna Maria Rauret**

With the objective of determining their age, the University of Barcelona's Radiocarbon Dating Laboratory has received from Dr Anna Maria Rauret Dalmau and Dr Josep Maria Gurt Esparraguera of the Department of Prehistory, Ancient History and Archaeology of the University of Barcelona six samples of carbonaceous materials from *Tchinguiz Tepe*, in the ancient city of Termez (in the province of Surxondaryo, south Uzbekistan). The samples were given the following reference numbers for identification purposes based on their stratigraphic origin:

**Sector RC1**
**Sector RC2**
**Sector RC3**
**Sector RC4**
**Sector RC5**
**Sector RC6**

## ARCHAEOLOGICAL CONTEXT

*Tchinguiz Tepe* is a walled enclosure within the ancient city of Termez, whose function and chronology are both unknown. The RC sector corresponds to a stratigraphic record unearthed against the inner face of the wall that rises directly out of the surrounding rock substrate and which extends to the present day.

## 2. DESCRIPTION AND TREATMENT OF THE MATERIAL RECEIVED

- The first sample contained 23 amorphous charcoal fragments with surface soil attachments, with maximum measurement ranging from 6 to 21 mm including soil remains.

- The second sample contained 25 parallelepiped fragments of coal with maximum length ranging from 34 to 37 mm and minimum length from 10 to 21 mm, and many amorphous fragments whose maximum measurement was no greater than 12 mm.

- The third sample contained four parallelepiped fragments of coal with maximum length ranging from 175 and 16 mm and minimum length from 6 to 12 mm, together with three amorphous fragments whose maximum measurement was no greater than 8 mm.

- The fourth sample contained six parallelepiped fragments with maximum length ranging from 29 to 17 mm and minimum length from 4 to 19 mm, as well as many amorphous fragments whose maximum measurement diameter was no greater than 12 mm.

- The fifth sample contained just two fragments measuring 26´19´18 mm and 22´20´17 mm

- The sixth sample contained just four parallelepiped fragments with maximum length ranging from 12 to 25 mm and minimum length from 6 to 17 mm.

The surfaces of all the charcoal fragments were covered in soil. The quantity of material contained in each sample is recorded in column 2 of Table I

The material received for dating underwent a treatment that has two purposes: on the one hand, we sought to eliminate those components that were alien to the samples true nature or which had originated from external sources of contamination or from handling with chemical compounds of indeterminate age and, on the other, to conserve, as undisturbed as possible, the components representative of the age of the material to be dated.

The first sample was passed through a 0.5 mm sieve to separate charcoal from the soil and the smaller grain size fraction was rejected since it did not contain any charcoal. The remaining samples were treated directly. Where possible, the surfaces of the largest charcoal fragments were cleaned with a brush (medium hardness) so as to eliminate any dust; then, so as to be able to observe and to eliminate from them any possible intrusions of foreign materials, the largest charcoal fragments were fragmented along their natural fracture lines and the newly exposed surfaces were brushed clean. The amount of clean material from each of the samples is recorded in column 3 of Table I.

The clean materials were ground to a dust and then treated with 2M hydrochloric acid at 95°C for 18 hours so as to eliminate the carbonates from the percolating waters and/or from the soil and the acid soluble material fraction. In order to eliminate any humic acid originating from the soil plant matter, the insoluble residue resulting from the treatment with acid was suspended in water and was treated at room temperature with successive additions of 1M or 2M ammonia under pH measurement until the pH of the suspension was high enough to ensure the complete elimination of acidic substances. Finally, the residue resulting from this treatment was boiled with 0.4M hydrochloric acid in order to eliminate the carbonates originating from the atmosphere. In this way, we obtained residues of purified charcoal that were free of carbonates and humic acids, and hence suitable for dating. The quantities and percentage yields of purified charcoal are recorded in columns 4 and 5 of Table I.

| Reference for identification | Original material (g) | Clean charcoal (g) | Purified charcoal (g) | Yield (%) |
|---|---|---|---|---|
| **Sector RC1** | 10.196 | 8.361 | 6.642 | 79.44 |
| **Sector RC2** | 38.449 | 26.208 | 14.025 | 53.51 |
| **Sector RC3** | 6.042 | 5.659 | 3.610 | 63.80 |
| **Sector RC4** | 8.311 | 5.792 | 4.305 | 74.33 |
| **Sector RC5** | 4.090 | 3.625 | 1.986 | 54.79 |
| **Sector RC6** | 7.353 | 5.796 | 4.386 | 75.68 |

***Table I:*** Material received and treatment applied

## 3. PREPARATION OF THE $^{14}C$ CONTENT MEASUREMENT

As the content of radiocarbon in purified charcoal cannot be measured by direct radiometric techniques, the charcoal has to be transformed into a suitable chemical compound that allows its radioactivity to be measured by liquid scintillation.

An adequate amount of purified charcoal from the second sample and all the purified charcoal from the remaining samples were burnt in a combustion unit under high oxygen pressure. The carbon dioxide resulting from combustion, once purified and dried, was left for three weeks in order to allow the radioactive decay of possible $^{222}Rn$ accompanying it. Once this time had elapsed, we determined the $^{13}C$ isotopic abundance of the material by mass spectrometry in a small sample of carbon dioxide. Then the remaining carbon dioxide was reduced with lithium metal to lithium carbide, this was then hydrolysed to produce acetylene with water with low tritium content and, finally, the acetylene was catalytically converted into benzene (Mestres *et al.,* 1991).

## 4. RADIOMETRIC MEASURES

We proceeded to measure the radioactivity of the benzene resulting from the synthesis described above, and which contained the carbon present in the charcoal to be dated. When the amount of benzene was less than 5 ml, we diluted it gravimetrically with inactive benzene of analytical reagent grade to 5.2 ml. With this mixture, or, alternatively, directly with the benzene obtained from the synthesis, we prepared the solutions for measuring the activity, weighing out 5.000 ml into low-potassium glass vials together with appropriate amounts of the scintillators Bu-PBD and Bis-MSB in solid form, and having previously been weighed.

Oxalic acid II, supplied by the National Institute of Standards and Technology (USA), served as the reference substance for measurement of the initial activity. This was oxidised to carbon dioxide with a potassium permanganate solution and then transformed into benzene as described above for the samples (*loc. cit.*). The preparation of the solution for the initial measurement of activity was also conducted in the same manner as for the samples.

The background value for each vial was determined by measuring two reference blanks prepared in the same way as for the samples, but using inactive benzene for the measuring solution.

The samples, two standards of initial activity and two reference blanks for the background value were counted in a period of time that extended between 58 and 82 hours, divided into fifty-minute intervals, in a liquid scintillation counter (LKB Wallace 1217 Rackbeta). The efficiency of the measurement for each interval was determined using an efficiency calibration curve for quenching in terms of extinction. The calibration curve had been previously established from activity standards prepared in our laboratory (*loc. cit.*).

## 5. RESULTS AND DISCUSSION

The results of the $^{13}C$ isotope ($\delta^{13}C$) abundance measurements and the results of the counting and radioactivity measurement, together with their uncertainty expressed as one times the standard deviation (*loc. cit*), are shown in Table II. It can be seen that the value of $^{13}C$ isotope abundance measured, which for charcoal stands between -23 and -27‰ (Stuiver & Polach, 1977), was normal for all the samples.

| Sample | $\delta^{13}C$ (‰) | Amount of benzene measured (g) | Count estimate (cpm) | Back-ground (cpm) | Net count rate (cpm) | Count efficiency (%) | Normalised count estimate of benzene sample, $A_{SN}$ (cpm/g) | Normalised count estimate of standard benzene, $A_{0N}$ (cpm/g) |
|---|---|---|---|---|---|---|---|---|
| **RC2** | –24.623 | 3.9580 | 27.818±0.081 | 3.024±0.043 | 24.795±0.092 | 72.884±0.017 | 8.589±0.032 | 10.587±0.026 |
| **RC2** | –24.507 | 4.3974 | 30.298±0.094 | 3.027±0.043 | 27.271±0.104 | 72.840±0.030 | 8.506±0.033 | 10.587±0.026 |
| **RC3** | –25.011 | 2.0996 | 16.056±0.059 | 2.990±0.043 | 13.066±0.073 | 72.882±0.019 | 8.539±0.048 | 10.606±0.026 |
| **RC4** | –29.182 | 2.5920 | 18.982±0.072 | 3.005±0.043 | 15.977±0.083 | 72.9008±0.0084 | 8.526±0.044 | 10.606±0.026 |
| **RC5** | –25.695 | 0.7725 | 67.757±0.040 | 2.958±0.042 | 4.799±0.058 | 72.889±0.016 | 8.535±0.103 | 10.586±0.026 |
| **RC6** | –26.308 | 2.7767 | 20.038±0.076 | 2.955±0.042 | 17.083±0.087 | 72.894±0.013 | 8.462±0.043 | 10.586±0.026 |

***Table II:*** Results of the radio metric measurements

Calculation of the radiocarbon age is based on the experimental results shown in Table II, using the following equation:

$$R = \frac{T_{1/2}}{\ln 2} \times \ln \frac{A_{0N}}{A_{SN}} \qquad (T_{½} = 5568 \text{ years})$$

where $A_{0N}$ represents the initial activity and $A_{SN}$ represents the residual activity in the dated material corrected by isotopic fractionation of $^{14}C$.

Applying the above equation to the measurements obtained enables us to calculate the radiocarbon dates. The dating results (1) and date codes assigned by the Laboratory are listed below:

*Tchinguiz Tepe*

| | | | |
|---|---|---|---|
| **Sector RC1** | **UBAR-1043** | **1680 ± 35** | **BP** |
| **Sector RC2** | **UBAR-1044** | **1760 ± 35** | **BP** |
| **Sector RC3** | **UBAR-1045** | **1740 ± 50** | **BP** |
| **Sector RC4** | **UBAR-1046** | **1755 ± 45** | **BP** |
| **Sector RC5** | **UBAR-1047** | **1730 ± 100** | **BP** |
| **Sector RC6** | **UBAR-1048** | **1800 ± 45** | **BP** |

These results can only be reliably applied to the samples received.

At first sight what we observe is an inverse chronology in the layers between RC2 and RC5 inclusive, but below we show that, when taking the calibration curve into consideration, this inverted chronology can be more apparent than real.

## 6. CALIBRATION OF RADIOCARBON DATES

Radiocarbon dating is based on the fundamental supposition that the specific radiocarbon content present in the materials, which lends itself to be dated, has remained unchanged over time. However, this hypothesis is not strictly accurate, since there will have been fluctuations in this content. As such, the dates calculated on the basis of this hypothesis are conventional in nature, since they present deviations with respect to the dates expressed on the solar time scale and define what has come to be known as the radiocarbon time scale. Measuring the radiocarbon age of tree rings whose age has been previously ascertained using dendrochronological techniques, a curve has been drawn spanning the last 12,400 years (Reimer *et al.,* 2004), relating the conventional radiocarbon age to the age expressed on the solar time scale. This curve, known as the calibration curve, is not flat and does not establish a one-to-one relationship between the radiocarbon time scale and the solar time scale, but rather more than one solar date may correspond to each radiocarbon date.

Owing to the non-linear character and the complexity of the calibration curve, the probability distribution of the true calibrated date around the experimental calibrated date is not normal, as it is in the case of the probability distribution of the true radiocarbon date around the experimental radiocarbon date. The probability distribution of the true calibrated date is asymmetric and complex and it can present distinct modes around which one or more probability intervals can be defined. The sum of probability of the intervals is equal to a probability of 68.3% or 95.4% (Stuiver and Reimer, 1993). The two values are chosen by analogy to the probability distribution of the radiocarbon date and they correspond to the probability that the true radiocarbon date falls within an interval of time which, centring on the experimental radiocarbon date, has a width equivalent to one or two times the standard deviation, respectively.

Table III shows the results from calibrating the radiocarbon dates. The details contained in each column are as listed below:

Columns A and B: Material reference number and radiocarbon date code assigned by this Laboratory, respectively.

Column C: Radiocarbon date with uncertainty expressed in terms of standard deviation.

Column D: Experimental calibrated dates[2] corresponding to the intersection of the radiocarbon date with the calibration curve. They correspond to the maximum modes of the probability distribution of the true calibrated data.

Columns E and F: Calibrated date intervals centred on the modes of probability distribution for the true calibrated date corresponding to a total probability of 68.3% and the probability associated with each interval, respectively. In this set of intervals there is a probability of 68.3% that the true calibrated date will be found.

Columns G and H: Calibrated date intervals centred on the modes of distribution of probability of the true calibrated date corresponding to a total probability of 95.4% and the probability associated with each interval, respectively. In this set of intervals there is a probability of 95.4% that the true calibrated date will be found.

The appendix contains additional information on the calibration. Figure 1 shows the portion of the calibration curve involved in the calibration of the radiocarbon dates and it enables us to appreciate any incidents or possible distortions in the radiocarbon time scale in this particular time period; Figure 2 – an amplification of a detail contained in Figure 1 – illustrates the calculation of the experimental calibrated date as the intersection of the experimental radiocarbon data with the calibration curve. Figures 4 show the probability distribution of the true calibrated date and enable us to appreciate the intervals with the highest probability indicated in columns E and G in Table III. Finally, Figures 5 show the accumulated probability curves that enable us to calculate the probability that the true calibrated date lies in a time interval equivalent to the difference between the ordinates corresponding to the interval extremes;

| A | B | C | D | E | F | G | H |
|---|---|---|---|---|---|---|---|
| **RC1** | UBAR-1043 | 1680± 35 BP | cal AD 386 | cal AD 265–272<br>cal AD 335–412 | 4.6%<br>63.7% | cal AD 255–428 | 95.4% |
| **RC2** | UBAR-1044 | 1760± 35 BP | cal AD 254<br>cal AD 310 | cal AD 235–336 | 68.3% | cal AD 139–159<br>cal AD 165–195<br>cal AD 209–385 | 2.7%<br>4.7%<br>88.0% |
| **RC3** | UBAR-1045 | 1740± 50 BP | cal AD 259<br>cal AD 290<br>cal AD 321 | cal AD 240–350<br>cal AD 368–380 | 63.0%<br>5.3% | cal AD 139–159<br>cal AD 165–196<br>cal AD 209–411 | 2.2%<br>3.9%<br>89.2% |
| **RC4** | UBAR-1046 | 1755± 45 BP | cal AD 256<br>cal AD 302<br>cal AD 316 | cal AD 231–348<br>cal AD 369–378 | 65.4%<br>2.9% | cal AD 138–199<br>cal AD 206–395 | 10.6%<br>84.8% |
| **RC5** | UBAR-1047 | 1730±100 BP | cal AD 262<br>cal AD 279<br>cal AD 327 | cal AD 143–147<br>cal AD 171–193<br>cal AD 210–420 | 0.8%<br>4.3%<br>63.2% | cal AD 84–536 | 95.4% |
| **RC6** | UBAR-1048 | 1800± 45 BP | cal AD 236 | cal AD 136–255<br>cal AD 305–312 | 65.5%<br>2.8% | cal AD 87–105<br>cal AD 121–345 | 1.9%<br>93.4% |

***Table III:*** Calibration of radiocarbon dates

by way of example, Figure 5A shows the probability of the true calibrated date of the material from RC1 being from the fourth century AD, which was found to be 64.5%.

## 7. GENERAL DISCUSSION OF RESULTS

Given its own nature, radiocarbon dating establishes the date of the formation of the materials and not that of the archaeological events of which these materials form a part. The experimental date measured is an approach to a physical date (MESTRES, 2000, 2003, 2008), which in the case of carbon dating refers to the moment of the formation of the plant tissues that make up the plant material and which later give rise to the charcoal. In no case, however, does the physical date refer to the archaeological date that we wish to know, if by this we understand ascertaining when the plant materials were transformed into charcoal or when they were deposited in the archaeological structures or levels that we wish to date. For the physical date to correspond to the archaeological date, we must seek to fulfil the conditions of archaeological association and synchrony (*loc. cit.*).

A look at Figure 2 shows the reason for the apparent inverse chronology of the layer sequence. Indeed, between the radiocarbon dates 1717 BP and 1760 BP the calibration curve shows an inverse slope which is reflected in an inversion of their corresponding solar dates in the sense that the higher the radiocarbon dates, the more recent are the corresponding solar dates; thus, a radiocarbon date of 1717 BP corresponds to a solar date of 270 AD, while the higher radiocarbon date of 1760 BP corresponds to a more recent solar date of 310 AD. A further effect of the inverse slope is the correspondence of multiple solar dates to the radiocarbon dates affected by this anomaly (see column D in Table III and Figure 2). Table IV and Figure 3 show that for radiocarbon dates affected by this inverse chronology, from among the many experimental calibrated dates there is one for each radiocarbon date (shown in red in Table IV) that allows us to establish a chronological sequence that is coherent with the strati-

graphic sequence, apart from the date corresponding to RC5, which breaks the coherence because it gives experimental calibrated dates that are too young in relation to their stratigraphic position.

Two hypotheses might be forwarded to account for the break in the chronological coherence of the radiocarbon dating presented by layer RC5:

The high degree of uncertainty of the radiocarbon dating in question (UBAR-1047: 1730 ± 100) allows for marked differences between the experimental radiocarbon date and the true radiocarbon date (MESTRES, 2008); this together with the narrow time range of the stratigraphic sequence –120 years BP on the radiocarbon time scale and 151 years on the solar time scale – may be the cause of the anomalous nature of the date for RC5 (See footnote[1] ).

The dated material suffers from a lack of representativeness. As the radiocarbon date is too young, this lack of representativeness cannot be due to a defect in synchrony, but rather to a defect in the archaeological association. This suggests the intrusion in the stratum of a material that is younger than the formation of stratum itself.

| Identification | Dating code | Radiocarbon date | Experimental calibrated date |
|---|---|---|---|
| **Sector RC1** | UBAR-1043 | 1680 ± 35 | cal AD **387** |
| **Sector RC2** | UBAR-1044 | 1760 ± 35 | cal AD **310**, 255 |
| **Sector RC3** | UBAR-1045 | 1740 ± 50 | cal AD 321, **296**, 259 |
| **Sector RC4** | UBAR-1046 | 1755 ± 45 | cal AD 316, 302, **256** |
| **Sector RC5** | UBAR-1047 | 1730 ± 100 | cal AD 327, 279, **262** |
| **Sector RC6** | UBAR-1048 | 1800 ± 45 | cal AD **236** |

***Table IV:*** Establishment of the time sequence of the layers

**1.-**The chronological coherence of the stratigraphic sequence means that the true calibrated date of stratum RC5 must lie between that of RC4 (256 AD) and that of RC6 (236 AD). If forstratum UE=18 we accept the hypothetical intermediate calibrated date 246 AD, the discontinuous green line in Figure 3 shows that the corresponding radiocarbon date is 1772 BP. This also hypothetical radiocarbon date is statistically indistinguishable from the experimental radiocarbon date UBAR-1047: 1730 ± 100 BP

## NOTES AND BIBLIOGRAPHY

BP (before present): used to represent a date expressed on the radiocarbon time scale where present is defined as AD 1950. The date is always accompanied by the degree of uncertainty expressed as the standard deviation corresponding to the set of radiometric measurements.

cal AD (*anno domini*): used to represent a calibrated date, expressed in years after Christ, based on radiocarbon dating.

MESTRES, J.S. (2000): "La datació per Radiocarboni. Una visió actual" a *Tribuna d'Arqueologia 1997-1998,* pp. 195-239. Generalitat de Catalunya, Departament de Cultura. Barcelona.

MESTRES, J.S., 2003: "La química i la cronologia: La datació per radiocarboni". *Revista de la Societat Catalana de Química* 4, pp. 10-25

MESTRES, J.S., 2008: "El temps a la prehistòria i el seu estbliment a través de la datació per radiocarboni". *Cypsela* **17**, p. 11-21

MESTRES, J.S.; J.F. GARCÍA I G. RAURET, 1991: "The Radiocarbon Laboratory at the University of Barcelona". *Radiocarbon* **31**(1), p. 23-34.

REIMER, P.J, G.L. BAILLIE, E. BARD, A. BAYLISS, J.W. BECK, C.J.H. BERTRAND, P.G. BLACKWELL, C.E. BUCK, G.S. BURR, K.B. CUTLER, P.E. DAMON, R.L. EDWARDS, R.G. FAIRBANKS, M. FRIEDERICH, T.P. GUILDERSON, A.G. HOGG, K.A. HUGHEN, B. KROMER, G. MCCORMAC, S. MANNING, C.B. RAMSEY, R.W. REIMER, S. REMMELE, J.R. SOUTHON, M. STUIVER, S. TALAMO, F.W. TAYLOR, J. VAN DER PLICHT I C.E. WEYHENMEYER. 2004: "IntCal04 Terrestrial Radiocarbon Age Calibration 0–26 cal kyr BP". *Radiocarbon* **46**(3), pp. 1029-1058.

STUIVER, M. I H. POLACH, 1977: "Discussion: Reporting of $^{14}C$ Data". *Radiocarbon* **19**(3), p. 358

## APPENDIX

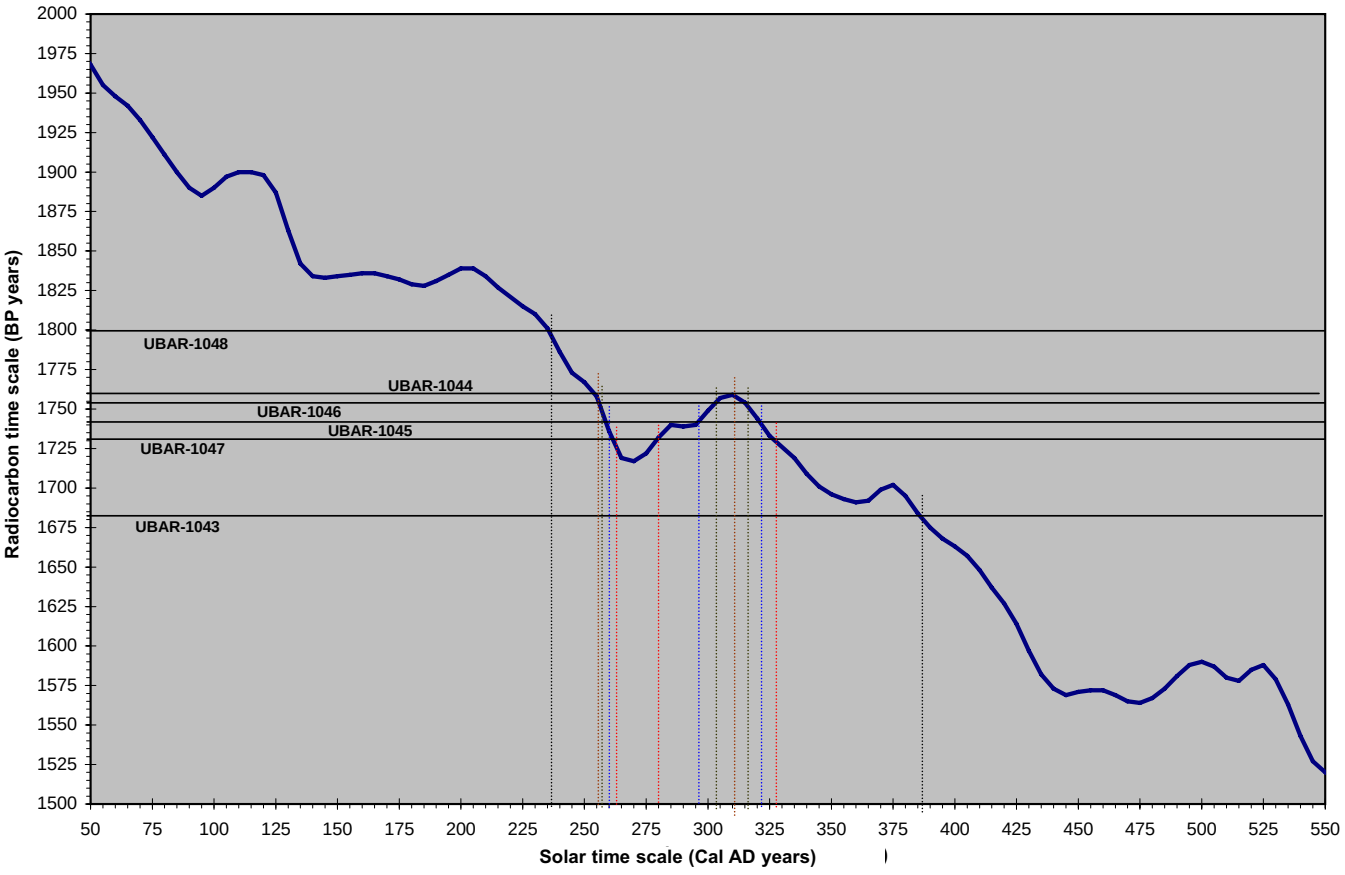


*Figura 1*

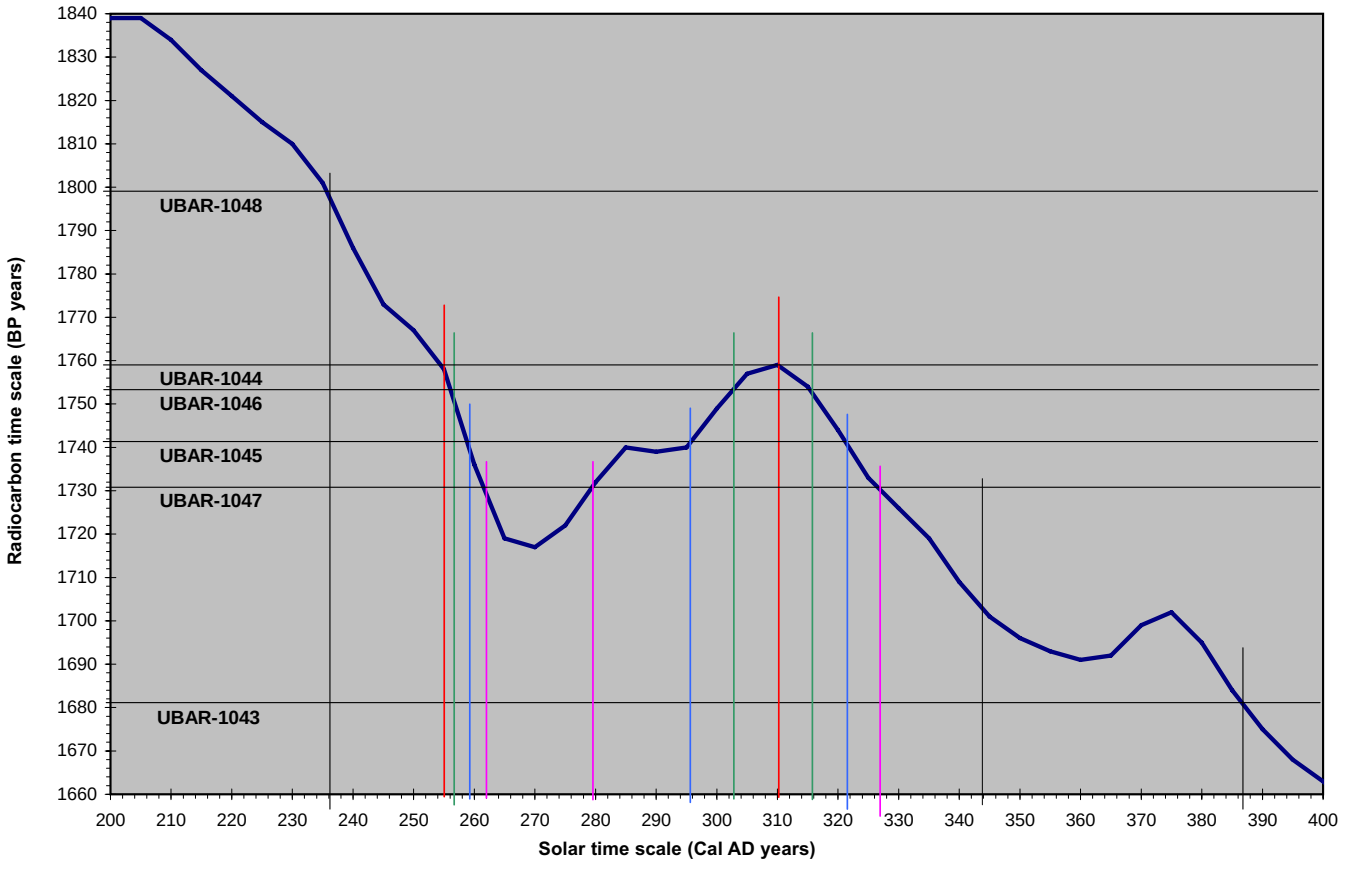


*Figura 2*

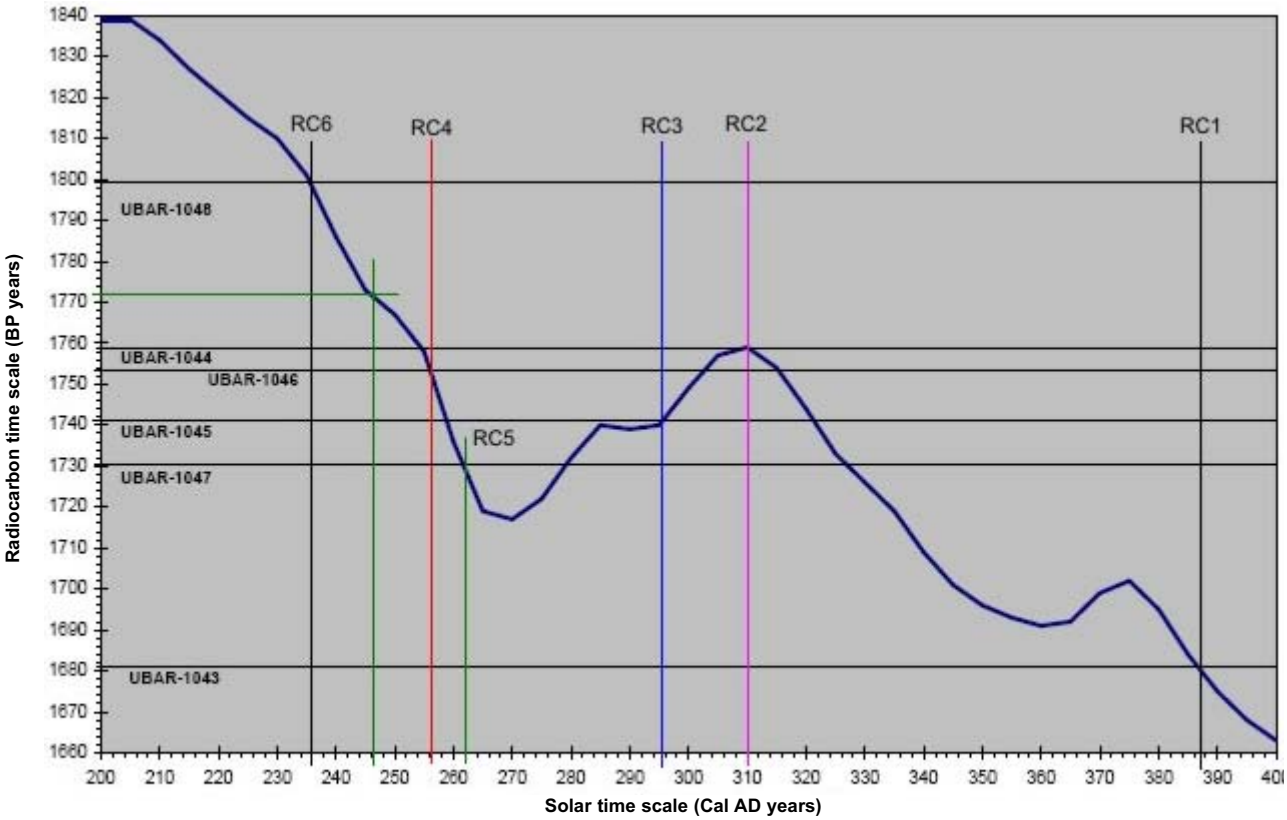


*Figure 3*

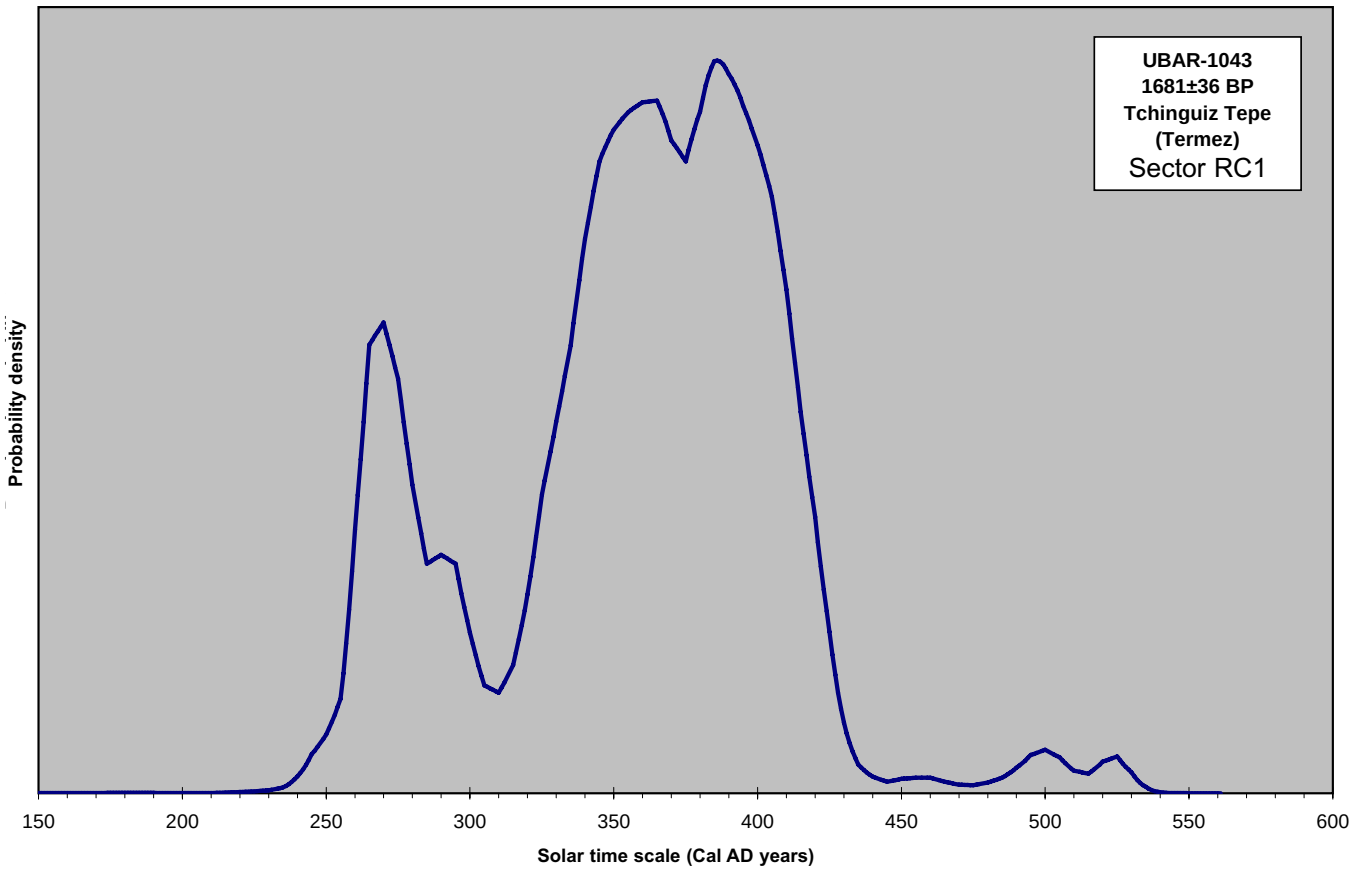


*Figure 4 A*

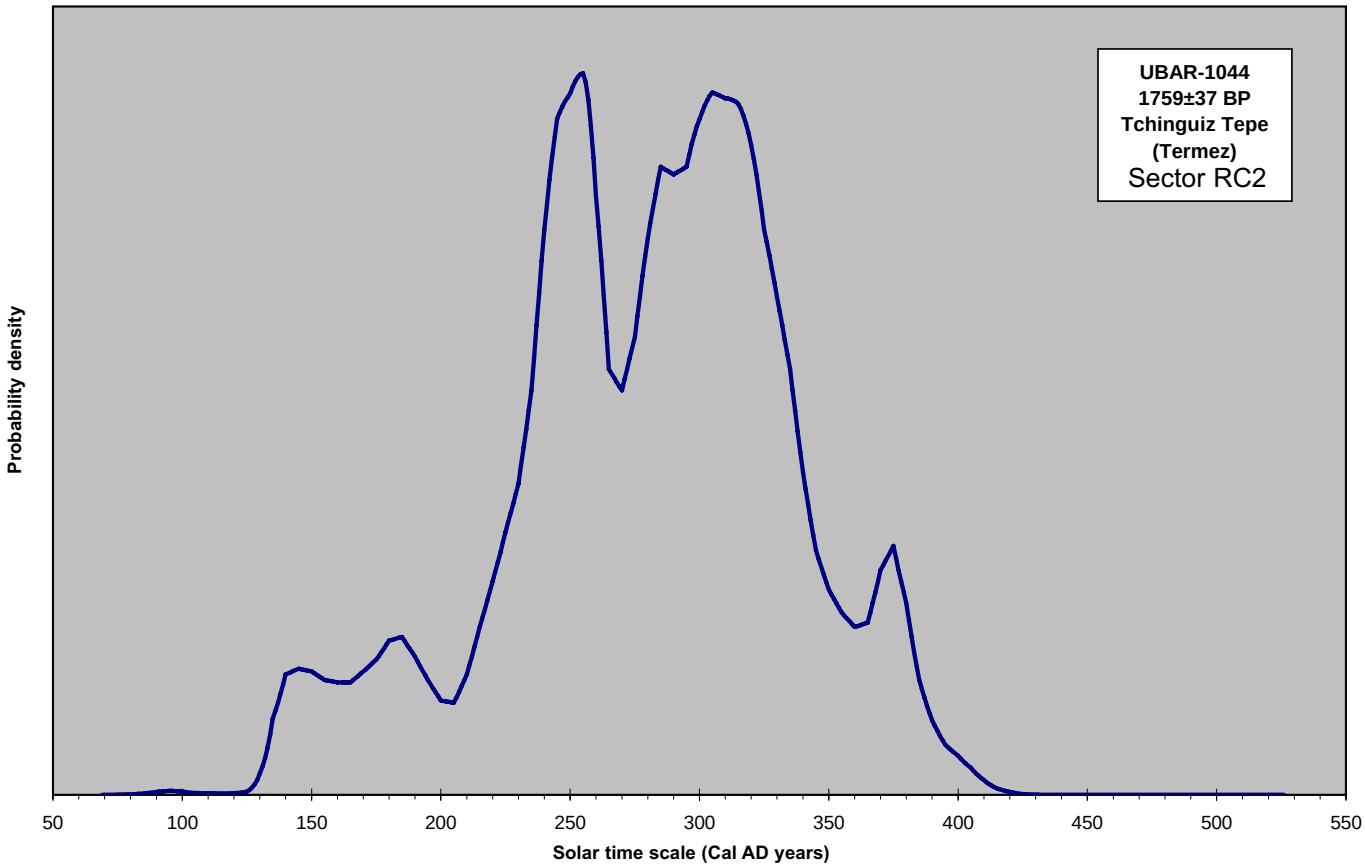


*Figure 4 B*

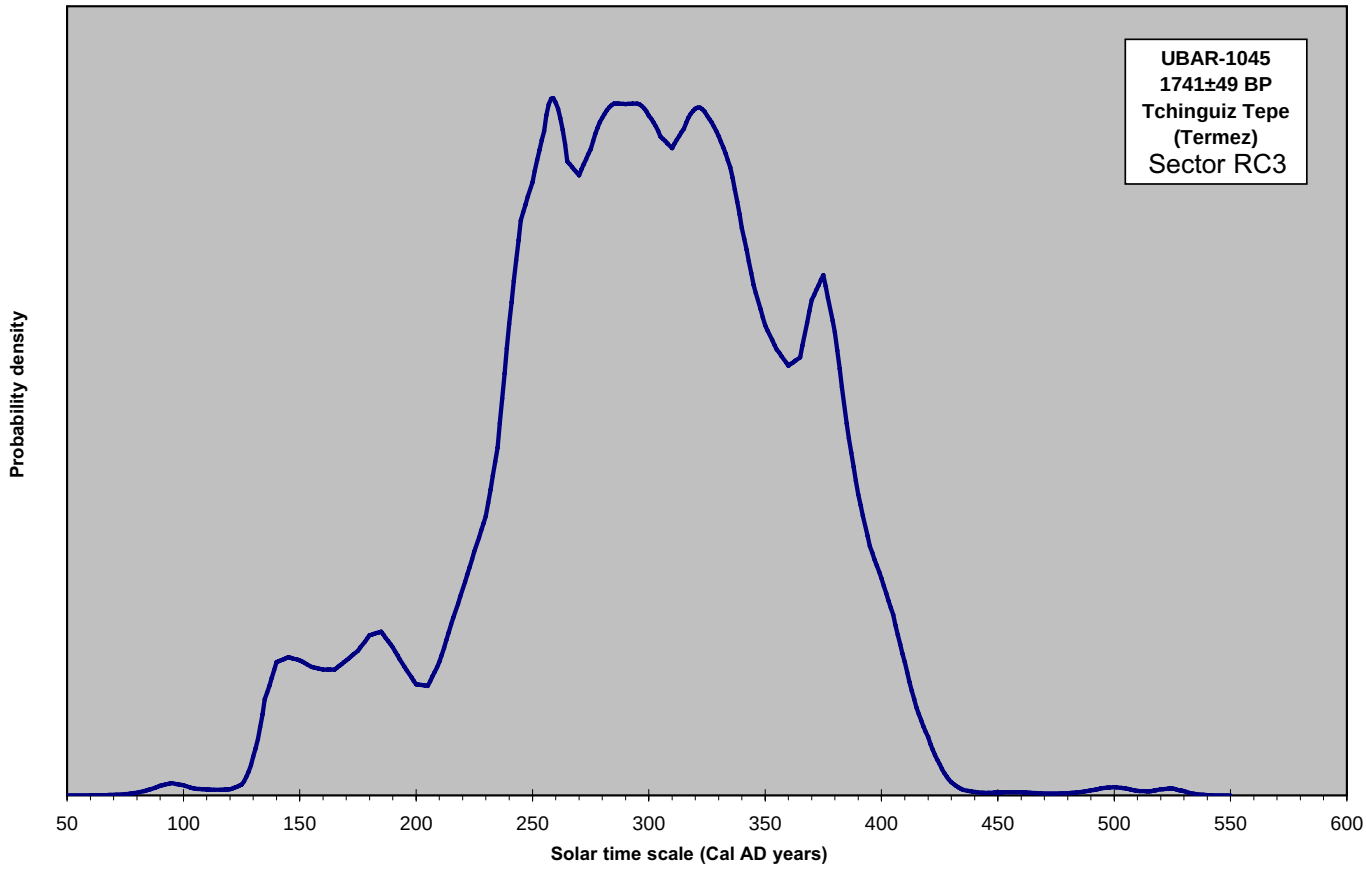


*Figure 4 C*

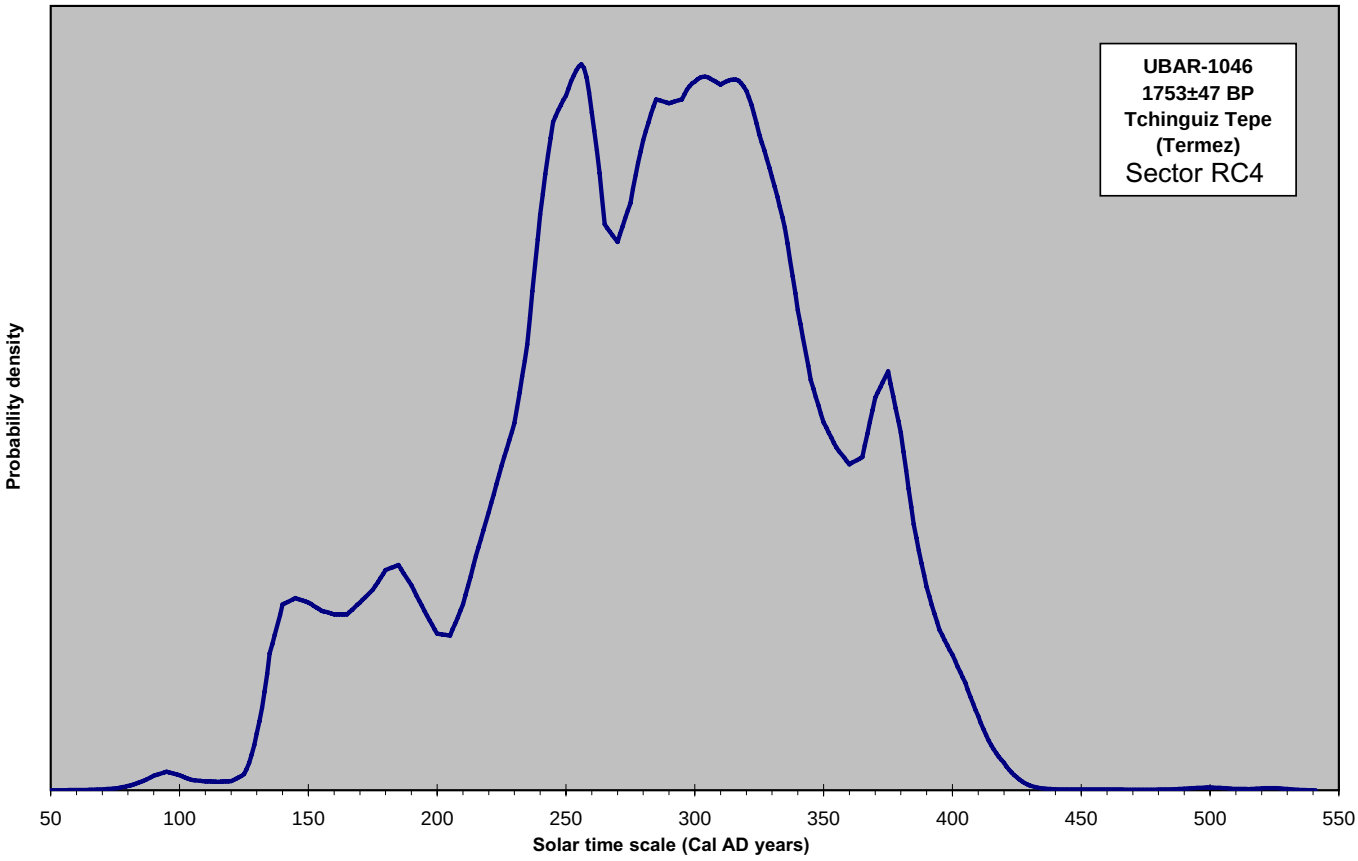


*Figure 4 D*

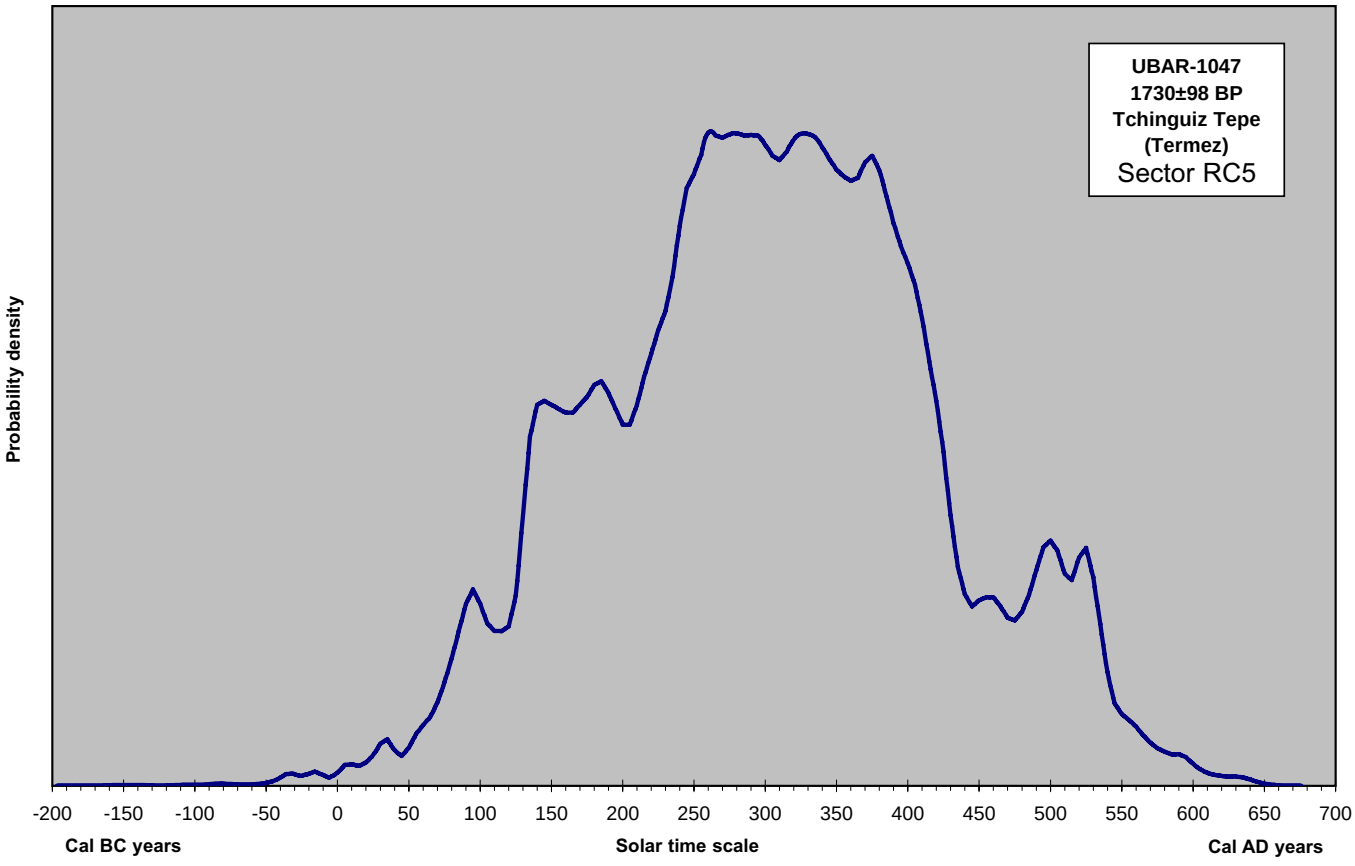


*Figure 4 E*

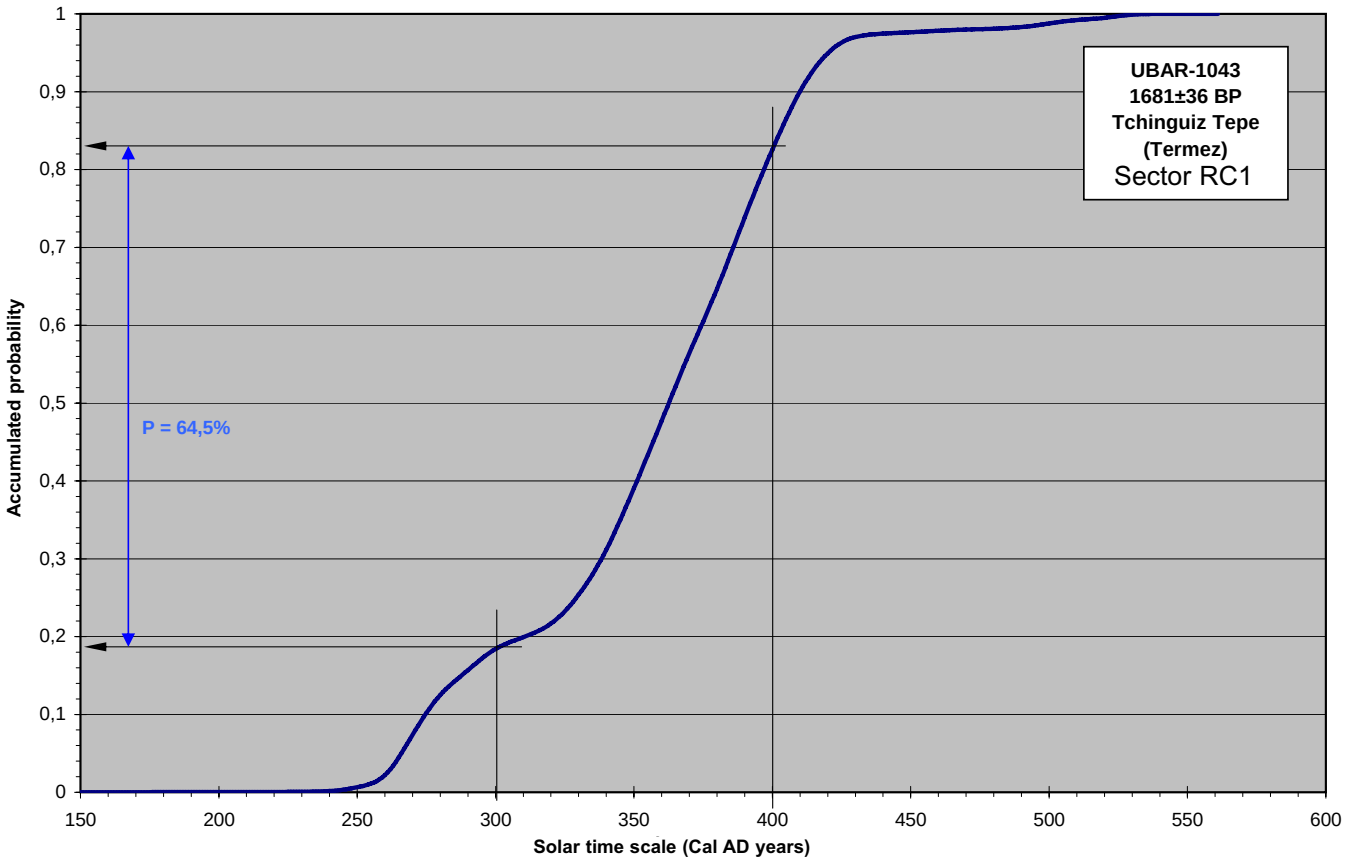


*Figure 5 A*

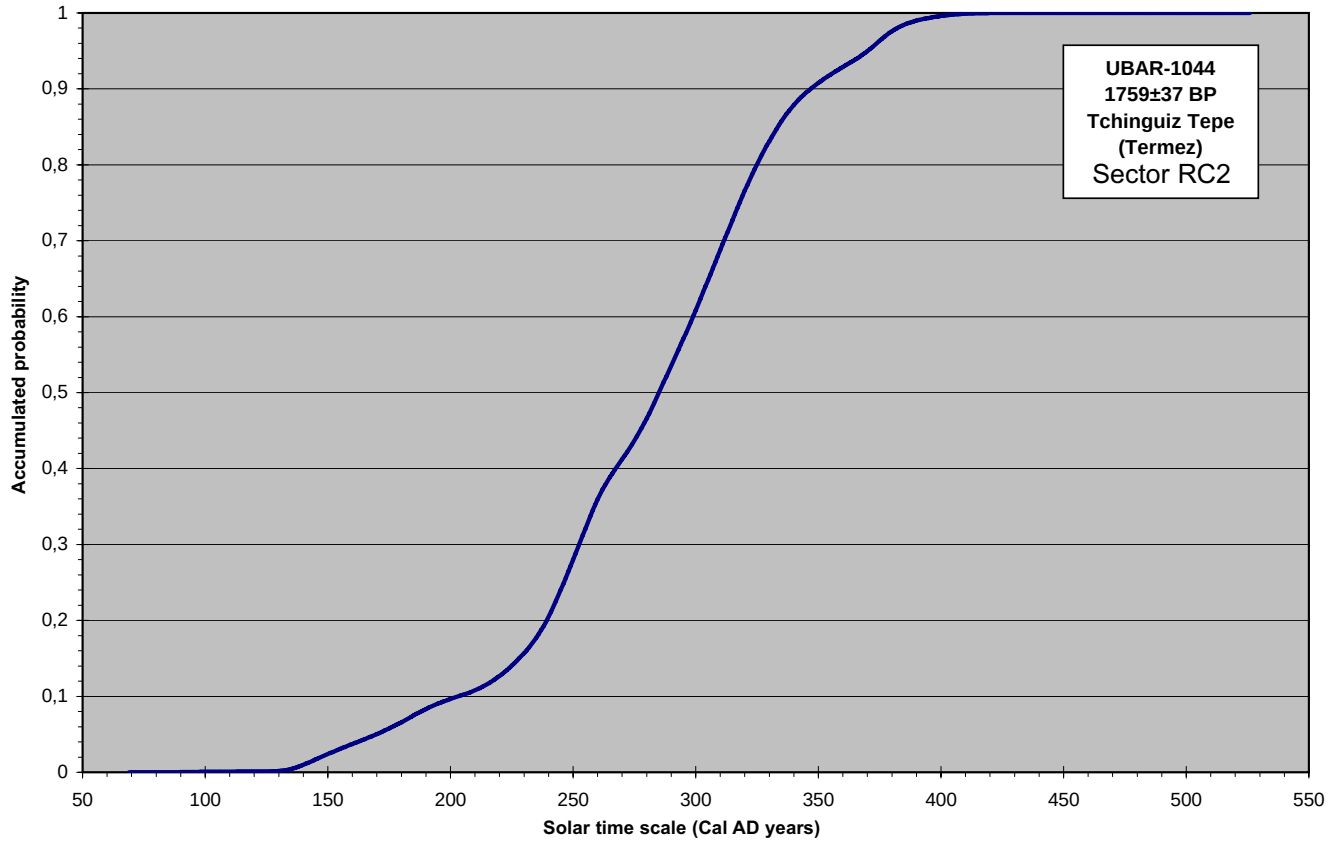


*Figure 5 B*

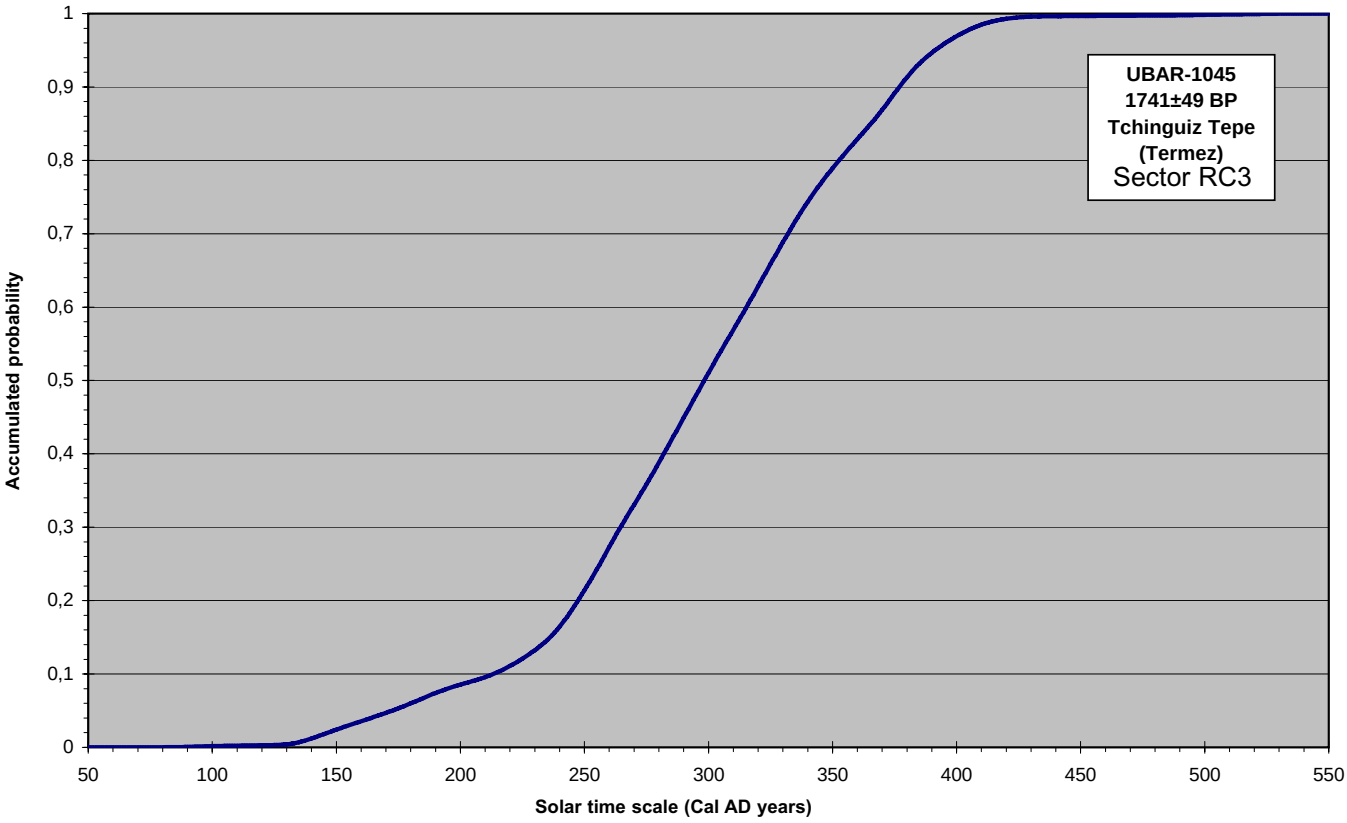


*Figure 5 C*

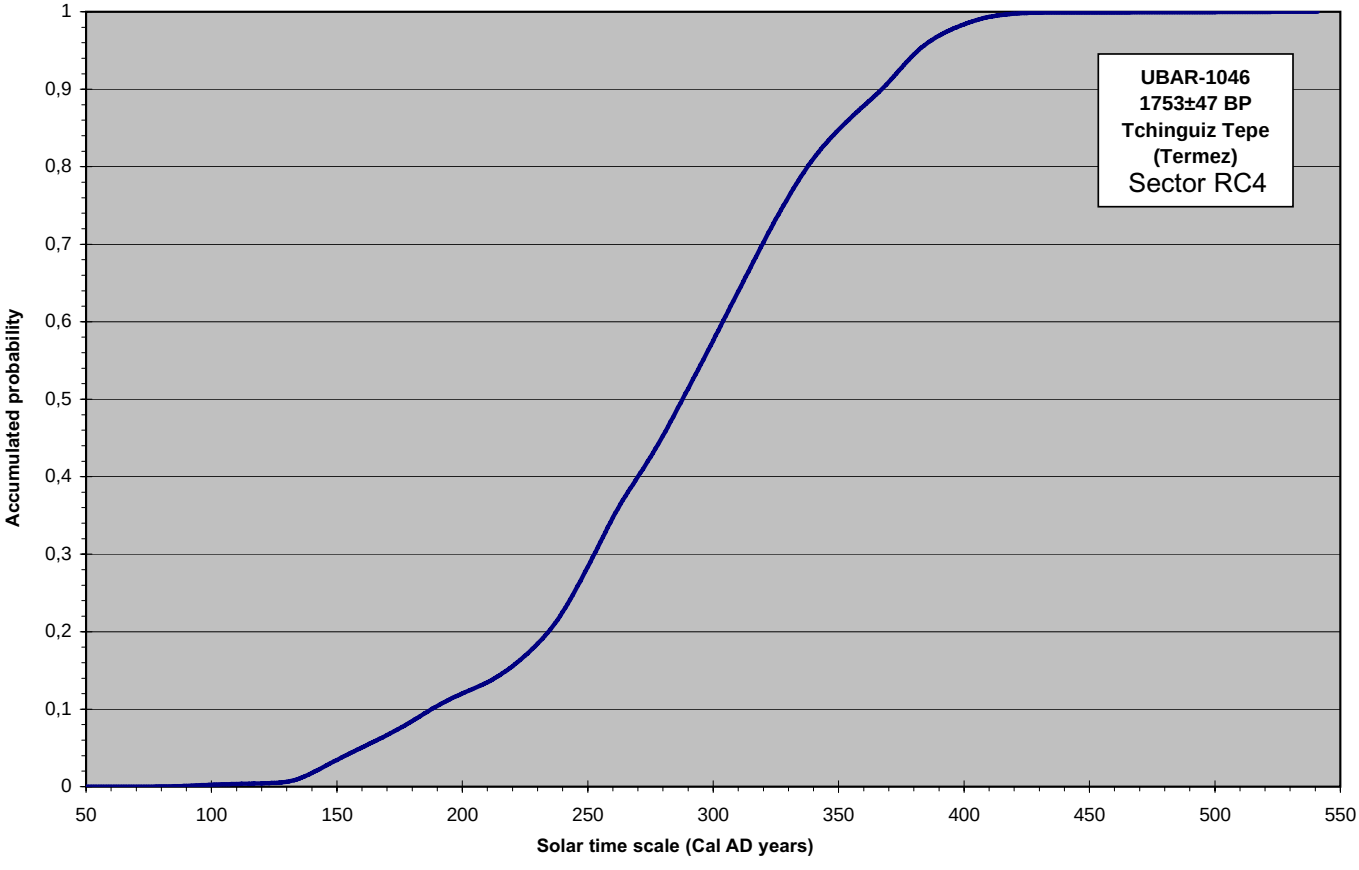


*Figure 5 D*

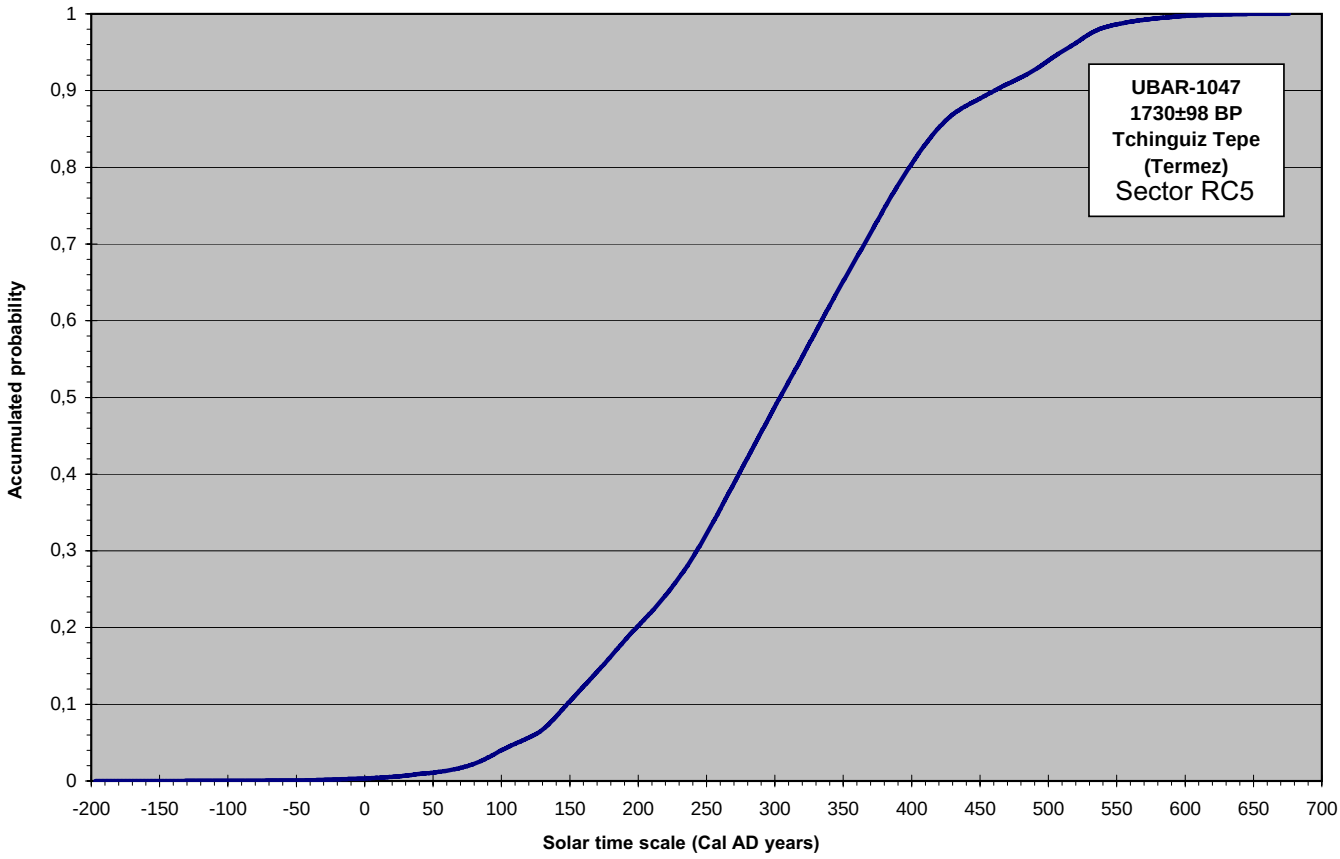
UBAR-1047
1730±98 BP
Tchinguiz Tepe
(Termez)
Sector RC5
Accumulated probability
Solar time scale (Cal AD years)
1
0,9
0,8
0,7
0,6
0,5
0,4
0,3
0,2
0,1
0
-200
-150
-100
-50
0
50
100
150
200
250
300
350
400
450
500
550
600
650
700

***Figure 5 E***

# Report on Radiocarbon Dating /2

**Joan S. Mestres i Torres, Anna Maria Rauret**

With the objective of determining their age, the University of Barcelona's Radiocarbon Dating Laboratory has received from Dr Anna Maria Rauret Dalmau and Dr Josep Maria Gurt Esparraguera of the Department of Prehistory, Ancient History and Archaeology of the University of Barcelona six samples of carbonaceous materials from *Tchinguiz Tepe*, in the ancient city of Termez (in the province of Surxondaryo, south Uzbekistan). The samples were given the following reference numbers for identification purposes based on their stratigraphic origin:

**Sector RF1**
**Sector RF2**
**Sector RF3**
**Sector RF4**
**Sector Wall/Tower 5**

## ARCHAEOLOGICAL CONTEXT

*Tchinguiz Tepe* is a walled enclosure within the ancient city of Termez, whose function and chronology are both unknown. The RF Sector corresponds to the excavation of an oven built for the manufacture of pottery near the RC Sector. Based on its position relative to known remains and despite its construction directly on bedrock, the oven must correspond by stratigraphy to the final period of settlement at *Tchinguiz Tepe*.

The Wall Sector corresponds to the excavation at tower 5 of the fortification. Dated material points to infilling in the circulation area within the tower after the abandonment of the enclosure and shortly before changes were undertaken on the tower.

## 2. DESCRIPTION AND TREATMENT OF THE MATERIAL RECEIVED

The first sample consisted of charcoal fragments covered in soil, with a maximum size of between 5 and 20 mm, accompanied by carbonaceous soil.

The second sample arrived in two jars labelled 1 and 2 and consisted of charcoal fragments, with a maximum size varying between 5 and 28 mm, accompanied by carbonaceous soil. The charcoal fragments were covered in soil and their surfaces showed radicles.

The third sample consisted of charcoal fragments covered in soil, with a maximum size of between 4 and 22 mm.

The fourth sample included fragments of charred little branches, reaching a maximum length of 186 mm and 3-4 mm in thickness.

The fifth sample contained 18 charcoal fragments covered in soil, ranging in size from 46×12×5 mm and 10×7×4 mm, accompanied by carbonaceous soil.

The quantity of material received for each sample is indicated in the second column of Table I.

The material received for dating underwent a treatment that has two purposes: on the one hand, we sought to eliminate those components that were alien to the samples' true nature or coming from external sources of contamination or from handling with chemical compounds of indeterminate age and, on the other, to conserve, as undisturbed as possible, the components representative of the age of the material to be dated.

In the samples with carbonaceous soil (1, 2 and 5), we first extracted the largest fragments of charcoal directly. Then we separated the remaining fragments using a sieve. The carbonaceous soil was discarded. Where possible, given the size of the charcoal fragments, their surfaces were cleaned by scrubbing with a bristle and the radicles were removed. Then, so as to be able to observe and to eliminate from them any possible intrusions of foreign materials, the largest charcoal fragments were fragmented along their natural fracture lines and the newly exposed surfaces were brushed clean. The amount of clean material from each of the samples is recorded in column 3 of Table I.

The clean materials were ground to a dust and then treated with 2M hydrochloric acid at 95°C for 18 hours so as to eliminate the carbonates from the percolating waters and/or from the soil and the acid soluble fraction. In order to eliminate any humic acid originating from the soil plant matter, the insoluble residue resulting from the treatment with acid was suspended in water and was treated at room temperature with successive additions of 1M or 2M ammonia under pH measurement until the pH of the suspension was high enough to ensure the complete elimination of acidic substances. Finally, the residue resulting from this treatment was boiled with 0.4M hydrochloric acid in order to eliminate the carbonates originating from the atmosphere. In this way, we obtained residues of purified charcoal that were free of carbonates and humic acids, and hence suitable for dating. The quantities and percentage yields of purified charcoal are recorded in columns 4 and 5 of Table I.

| Reference for identification | Original material (g) | Clean material (g) | Purified charcoal (g) | Yield (%) |
|---|---|---|---|---|
| **Sector RF1** | 3.9 | 3.2 | 1.3 | 41.2 |
| **Sector RF2** | 13.0 | 11.6 | 7.1 | 61.2 |
| **Sector RF3** | 6.5 | 5.7 | 4.0 | 69.9 |
| **Sector RF4** | 32.6 | 31.8 | 23.9 | 75.2 |
| **Sector Wall/Tower 5** | 14.2 | 10.0 | 8.0 | 80.0 |

***Table I:*** Material received and treatment applied

## 3. PREPARATION METHOD FOR MEASUREMENT OF RADIOACTIVITY: BENZENE SYNTHESIS

As the content of $^{14}C$ in charcoal purified with this procedure cannot be measured by direct radiometric techniques, the carbon in charcoal has to be transformed into a suitable chemical compound that allows its radioactivity to be measured by liquid scintillation. The description of the chemical procedure used to prepare this compound, benzene, appears below.

An adequate amount of purified charcoal from the fourth sample and all the purified charcoal from the remaining samples were burnt in a combustion unit under high oxygen pressure. The carbon dioxide resulting from combustion, once purified and dried, was left for three weeks in order to allow the radioactive decay of possible $^{222}Rn$ accompanying it. Once this time had elapsed, we determined the $^{13}C$ isotopic abundance of the material by mass spectrometry in a small sample of carbon dioxide. Then the remaining carbon dioxide was reduced with lithium metal to lithium carbide, this was then hydrolysed to produce acetylene with low tritium water and, finally, the acetylene was catalytically converted into benzene (MESTRES *et al.,* 1991).

## 4. RADIOMETRIC MEASURES

We proceeded to measure the radioactivity of the benzene resulting from the synthesis described above, and which contained the carbon present in the charcoal to be dated. When the amount of benzene was less than 5 ml, we diluted it gravimetrically with inactive benzene of analytical reagent grade to 5.2 ml. With this mixture, or, alternatively, with the benzene obtained directly from the synthesis, we prepared the solutions for measuring the activity, weighing out 5.000 ml into low-potassium glass vials together with appropriate amounts of the scintillators Bu-PBD and Bis-MSB in solid form, and having previously been weighed.

Oxalic acid II, supplied by the National Institute of Standards and Technology (USA), served as the reference substance for measurement of the initial activity. This was oxidised to carbon dioxide with a potassium permanganate solution and then transformed into benzene as described above for the samples (*loc. cit.*). The preparation of the solution for the initial measurement of activity was also conducted in the same manner as for the samples.

The background value for each vial was determined by measuring two reference blanks prepared in the same way as for the samples, but using inactive benzene for the measuring solution.

The samples, two standards of initial activity and two reference blanks for the background measurement value were counted in a period of time that extended between 58 and 82 hours, divided into fifty-minute intervals, in a liquid scintillation counter (LKB Wallace 1217 Rackbeta). The efficiency of the measurement for each interval was determined using a calibration curve of efficiency for quenching. The calibration curve had been previously established from activity standards prepared in our laboratory (*loc. cit.*).

## 5. RESULTS AND DISCUSSION

The results of the $^{13}C$ isotope abundance measurements ($\delta^{13}C$) and the results of the counting and radioactivity measurement, together with their uncertainty expressed as once the standard deviation (*loc. cit*), are shown in Table II. It can be seen that the value of $^{13}C$ isotope abundance measured, which for charcoal stands between -23 and -27‰ (STUIVER & POLACH, 1977), was normal for all the samples except the fourth, which was unusually high[1].

**1.-**Given the surprise caused by the atypical value found for $\delta$13C in the material RF/SU=26, we took another measurement of isotopic fractionation on a sample of purified charcoal and confirmed the atypical value. The unusually high value could be the result of an exotic plant species with a C4 photosynthetic cycle for the assimilation of atmospheric carbon dioxide, while the more typical photosynthetic cycle in the northern hemisphere is the C3 cycle.

Calculation of the radiocarbon age is based on the experimental results shown in Table II, using the following equation:

$$R = \frac{T_{1/2}}{\ln 2} \times \ln \frac{A_{0N}}{A_{SN}} \qquad (T_{1/2} = 5568 \text{ years})$$

where $A_{0N}$ represents the initial activity and $A_{SN}$ represents the residual activity in the dated material corrected by isotopic fractionation of $^{14}C$.

| Sample countrate | $\delta^{13}C$ (‰) | Amount of benzene measured (g) | Measured counrate (cpm) | Estimated background (cpm) | Net countrate (cpm) | Counting efficiency (%) | Normalised net countrate of sample benzene, $A_{SN}$ (cpm/g) | Normalised net of standard benzene, $A_{0N}$ (cpm/g) |
|---|---|---|---|---|---|---|---|---|
| **RF1** | –25,483 | 0,27302 | 4,678±0,023 | 2,973±0,044 | 1,705±0,050 | 72,879±0,020 | 8,58±025 | 10,592±0,028 |
| **RF2** | –25,076 | 4,3258 | 29,453±0,089 | 2,978±0,043 | 26,475±0,098 | 72,884±0,019 | 8,399±0,031 | 10,608±0,026 |
| **RF3** | –24,531 | 2,4237 | 17,780±0,076 | 2,970±0,044 | 14,810±0,088 | 72,871±0,023 | 8,378±0,050 | 10,592±0,028 |
| **RF4** | –11,558 | 4,3980 | 30,929±0,091 | 2,993±0,043 | 27,936±0,100 | 72,889±0,013 | 8,480±0,030 | 10,608±0,026 |
| **S. Muralla Tower 5** | –26,110 | 4,3980 | 30,163±0,090 | 3,008±0,043 | 27,155±0,099 | 72,9032±0,0060 | 8,488±0,031 | 10,608±0,026 |

***Table II:*** Results of the radiometric measurements

Applying the above equation to the measurements obtained enables us to calculate the radiocarbon dates. The dating results (1) and date codes assigned by the Laboratory are listed below:

– *Tchinguiz Tepe* –

| | | |
|---|---|---|
| **Sector RF1** | **UBAR-1053** | **1690 ± 230 BP** |
| **Sector RF2** | **UBAR-1054** | **1875 ± 35 BP** |
| **Sector RF3** | **UBAR-1055** | **1885 ± 50 BP** |
| **Sector RF4** | **UBAR-1056** | **1800 ± 35 BP** |
| **Sector Wall Tower 5** | **UBAR-1049** | **1790 ± 35 BP** |

These results can only be reliably applied to the samples received.

Given its own nature, radiocarbon dating establishes the date of the formation of the materials and not the date of the archaeological events of which these materials form a part. The experimental date measured is an approach to a physical date (MESTRES, 2000, 2003, 2008), which in the case of charcoal dating refers to the moment of the formation of the plant tissues that make up the plant material and which later give rise to the charcoal. In no case, however, does the physical date refer to the archaeological date that we wish to know, if by this we understand ascertaining when the plant materials were transformed into charcoal or when they were deposited in the archaeological structures or levels that we wish to date. For the physical date to correspond to the archaeological date, we must seek to fulfil the conditions of association and synchrony (*loc. cit.*).

With respect to the radiocarbon dates for the RF Sector, both the limited chronological extent of the stratigraphic sequence and the high level of uncertainty for the dating of RF1 make the four radiocarbon dates statistically indistinguishable. Nonetheless, building on the assumption that the experimental radiocarbon dates are not very different from the actual radiocarbon dates[2], the stratigraphic sequence has some chronological coherence. Lastly, the deepest stratum RF4 breaks the chronological coherence by yielding a more recent radiocarbon date. The cause of the rupture in the chronological coherence of the stratigraphic sequence could be attributable to a deficiency in the representativeness of the dated material from RF4. If we accept this hypothesis, the deficiency in the representativeness must be the result of a fault in archaeological association or synchrony. A problem with the synchrony is not admissible because the date is more recent than the date that would correspond to the stratigraphic position. As a result, we must accept that the cause of the chronological inversion lies in a fault of archaeological association caused by the intrusion of more recent material from higher strata.

An alternative paradigm for interpretation of the four radiocarbon dates from the RF Sector arises from the fact that the dates are statistically indistinguishable, that the anomalous date falls between the other dates and that the anomaly may be the result of an intrusion from the upper strata. In effect, the four radiocarbon dates could be interpreted as distinct experimental expressions of the same physical date or at least very close physical dates. In that case, the weighted average of the four dates would be a better expression of the shared physical date of the four dated materials and, therefore, of the chronology of the stratigraphic sequence from RF1 to RF3, if we accept the intrusion hypothesis and leave RF4 undated, or of the stratigraphic sequence from RF1 to RF4, if we reject the intrusion hypothesis. Following the alternative interpretation, the radiocarbon date of the stratigraphic sequence is:

**Sector RF UBAR-1053/1056 1840 ± 20 BP**

## 6. CALIBRATION OF RADIOCARBON DATES

Radiocarbon dating is based on the fundamental supposition that the specific radiocarbon content present in the materials, which lends itself to be dated, has remained unchanged over time. However, this hypothesis is not strictly accurate, since there have been fluctuations in this content. As such, the dates calculated on the basis of this hypothesis are conventional in nature, since they present deviations with respect to the dates expressed on the solar time scale and define what has come to be known as the radiocarbon time scale. Measuring the radiocarbon age of tree rings whose age has been previously ascertained using dendrochronological techniques, a curve has been drawn spanning the last 12,400 years (REIMER *et al.,* 2004), relating the conventional radiocarbon age to the age to the age expressed on the solar time scale. This curve, known as the calibration curve, is not flat and does not establish a one-to-one relationship between the radiocarbon time scale and the solar time scale, but rather more than one solar date may correspond to each radiocarbon date.

**1.-**This hypothesis is easy to accept for the three more precise radiocarbon dates, but it is riskier for the least precise date.

Owing to the non-linear character and the complexity of the calibration curve, the probability distribution of the true calibrated date around the experimental calibrated date is not normal, as it is in the case of the probability distribution of the true radiocarbon date around the experimental radiocarbon date. The probability distribution of the true calibrated date is asymmetric and complex and it can present distinct modes around which one or more probability intervals can be defined. The sum of probability of the intervals is equal to a probability of 68.3% or 95.4% (STUIVER AND REIMER, 1993). The two values are chosen by analogy to the probability distribution of the radiocarbon date and they correspond to the probability that the true radiocarbon date falls within an interval of time which, centring on the experimental radiocarbon date, has a semi-width equivalent to once or twice the standard deviation, respectively.

Table III shows the results from calibrating the radiocarbon dates. The details contained in each column are as listed below:

Columns A and B: Material reference number and radiocarbon date code assigned by this Laboratory, respectively.

Column C: Radiocarbon date with uncertainty expressed in terms of standard deviation.

Column D: Experimental calibrated dates[2] corresponding to the intersection of the radiocarbon date with the calibration curve. They correspond to the maximum modes of the probability distribution of the calibrated data.

Columns E and F: Calibrated date intervals centred on the modes of probability distribution for the true calibrated date corresponding to a total probability of 68.3% and the probability associated with each interval, respectively. In this set of intervals there is a probability of 68.3% that the true calibrated date will be found.

Columns G and H: Calibrated date intervals centred on the modes of distribution of probability of the true calibrated date corresponding to a total probability of 95.4% and the probability associated with each interval, respectively. In this set of intervals there is a probability of 95.4% that the true calibrated date will be found.

| A | B | C | D | E | F | G | H |
|---|---|---|---|---|---|---|---|
| **RF1** | UBAR-1053 | 1690±230 BP | cal AD 355<br>cal AD 366<br>cal AD 381 | cal AD 85–580 | 68.3% | cal BC 345–320<br>cal BC 205–AD 780<br>cal AD 790–810<br>cal AD 845–855 | 0.5%<br>94.4%<br>0.4%<br>0.1% |
| **RF2** | UBAR-1054 | 1875± 35 BP | cal AD 128 | cal AD 77–140<br>cal AD 150–170<br>cal AD 194–210 | 48.5%<br>11.0%<br>8.8% | cal AD 63–232 | 95.4% |
| **RF3** | UBAR-1055 | 1885± 50 BP | cal AD 126 | cal AD 68–175<br>cal AD 191–212 | 59.2%<br>9.1% | cal AD 5– 13<br>cal AD 16–244 | 0.7%<br>94.7% |
| **RF4** | UBAR-1056 | 1800± 35 BP | cal AD 236 | cal AD 138–197<br>cal AD 207–254 | 33.4%<br>34.4% | cal AD 129–263<br>cal AD 276–331 | 78.5%<br>16.9% |
| **Sector RF** | UBAR-1053/1056 | 1840± 20 BP | cal AD 135 | cal AD 131–178<br>cal AD 187-213 | 43.8%<br>24.5% | cal AD 90–101<br>cal AD 124–237 | 2.5%<br>92.9% |
| **S. Wall Tower 5** | UBAR-1049 | 1790±35 BP | cal AD 238 | cal AD 139–157<br>cal AD 166–195<br>cal AD 209–258<br>cal AD 299–319 | 7.9%<br>14.6%<br>34.8%<br>11.0% | cal AD 130–266<br>cal AD 271–336 | 71.8%<br>23.6% |

***Table Iii:*** Calibration of radiocarbon dates

The appendix contains additional information on the calibration. Figures 1 show the portions of the calibration curve involved in the calibration of the radiocarbon dates which enable us to appreciate any incidents or possible distortions in the radiocarbon time scale in this particular time period;. Figures 2 show the probability distribution of the true calibrated date and enable us to appreciate the intervals with the highest probability indicated in columns E and G in Table III. Finally, Figures 3 show the accumulated probability curves that enable us to calculate the probability that the true calibrated date lies in a time interval equivalent to the difference between the ordinates corresponding to the interval extremes.

## NOTES AND REFERENCES CITED

BP (before present): used to represent a date expressed on the radiocarbon time scale where present is defined as AD 1950. The date is always accompanied by the degree of uncertainty expressed as the standard deviation corresponding to the set of radiometric measurements.

cal BC (Before Christ): used to represent a calibrated date, expressed in years before Christ, based on radiocarbon dating.

cal AD (*anno domini*): used to represent a calibrated date, expressed in years after Christ, based on radiocarbon dating.

MESTRES, J.S. (2000): "La datació per Radiocarboni. Una visió actual" a *Tribuna d'Arqueologia 1997-1998,* pp. 195-239. Generalitat de Catalunya, Departament de Cultura. Barcelona.

MESTRES, J.S., 2003: "Laquímica i la cronologia: La datació per radiocarboni". *Revista de la Societat Catalana de Química* 4, pp. 10-25

MESTRES, J.S., 2008: "El temps a la prehistòria i el seu estbliment a través de la datació per radiocarboni". *Cypsela* **17**, p. 11-21

MESTRES, J.S.; J.F. GARCÍA I G. RAURET, 1991: "The Radiocarbon Laboratory at the University of Barcelona". *Radiocarbon* **31**(1), p. 23-34.

REIMER, P.J, G.L. BAILLIE, E. BARD, A. BAYLISS, J.W. BECK, C.J.H. BERTRAND, P.G. BLACKWELL, C.E. BUCK, G.S. BURR, K.B. CUTLER, P.E. DAMON, R.L. EDWARDS, R.G. FAIRBANKS, M. FRIEDERICH, T.P. GUILDERSON, A.G. HOGG, K.A. HUGHEN, B. KROMER, G. MCCORMAC, S. MANNING, C.B. RAMSEY, R.W. REIMER, S. REMMELE, J.R. SOUTHON, M. STUIVER, S. TALAMO, F.W. TAYLOR, J. VAN DER PLICHT I C.E. WEYHENMEYER. 2004: "IntCal04 Terrestrial Radiocarbon Age Calibration 0–26 cal kyr BP". *Radiocarbon* **46**(3), pp. 1029-1058.

STUIVER, M. I H. POLACH, 1977: "Discussion: Reporting of $^{14}C$ Data". *Radiocarbon* **19**(3), p. 358

## APPENDIX

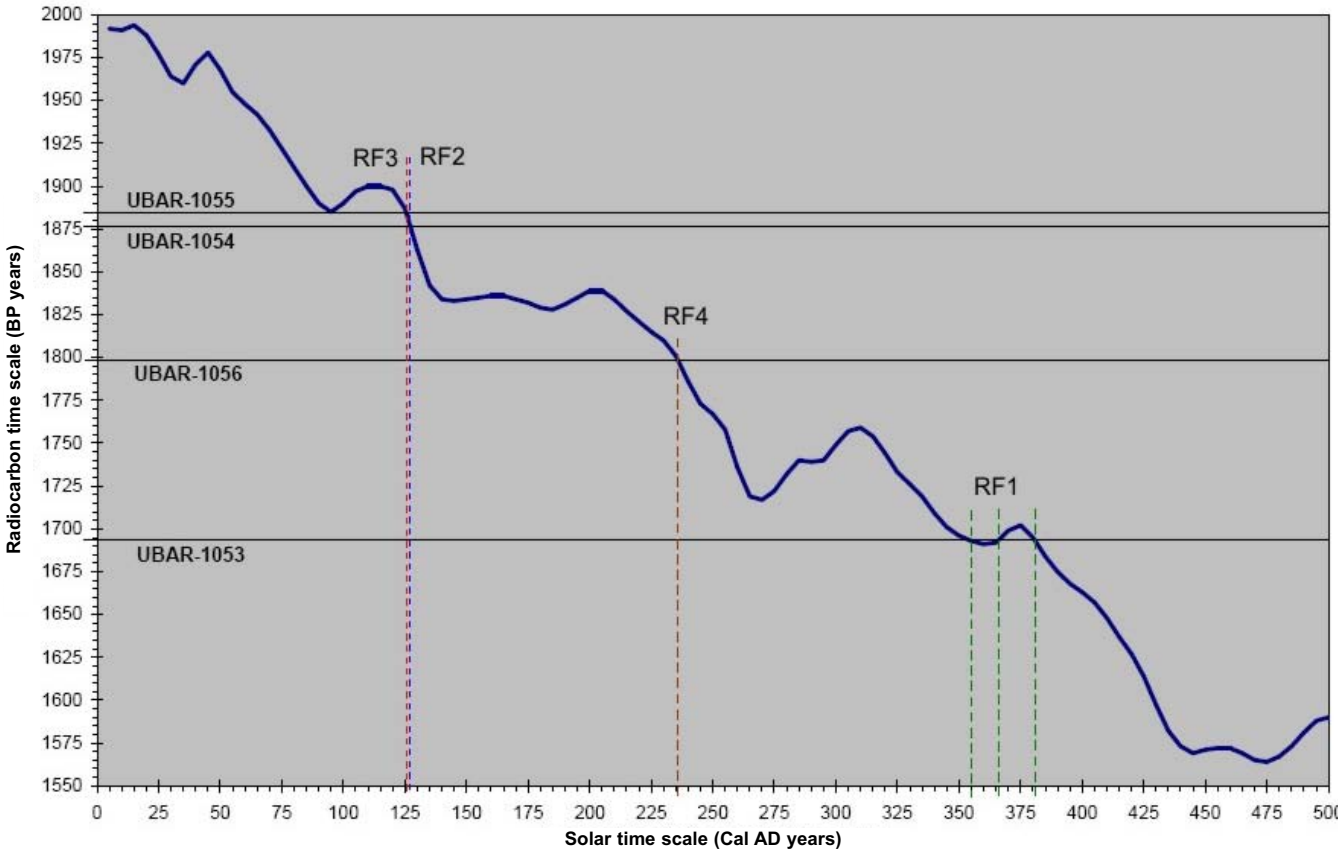


*Figura 1 A-B-C-D*

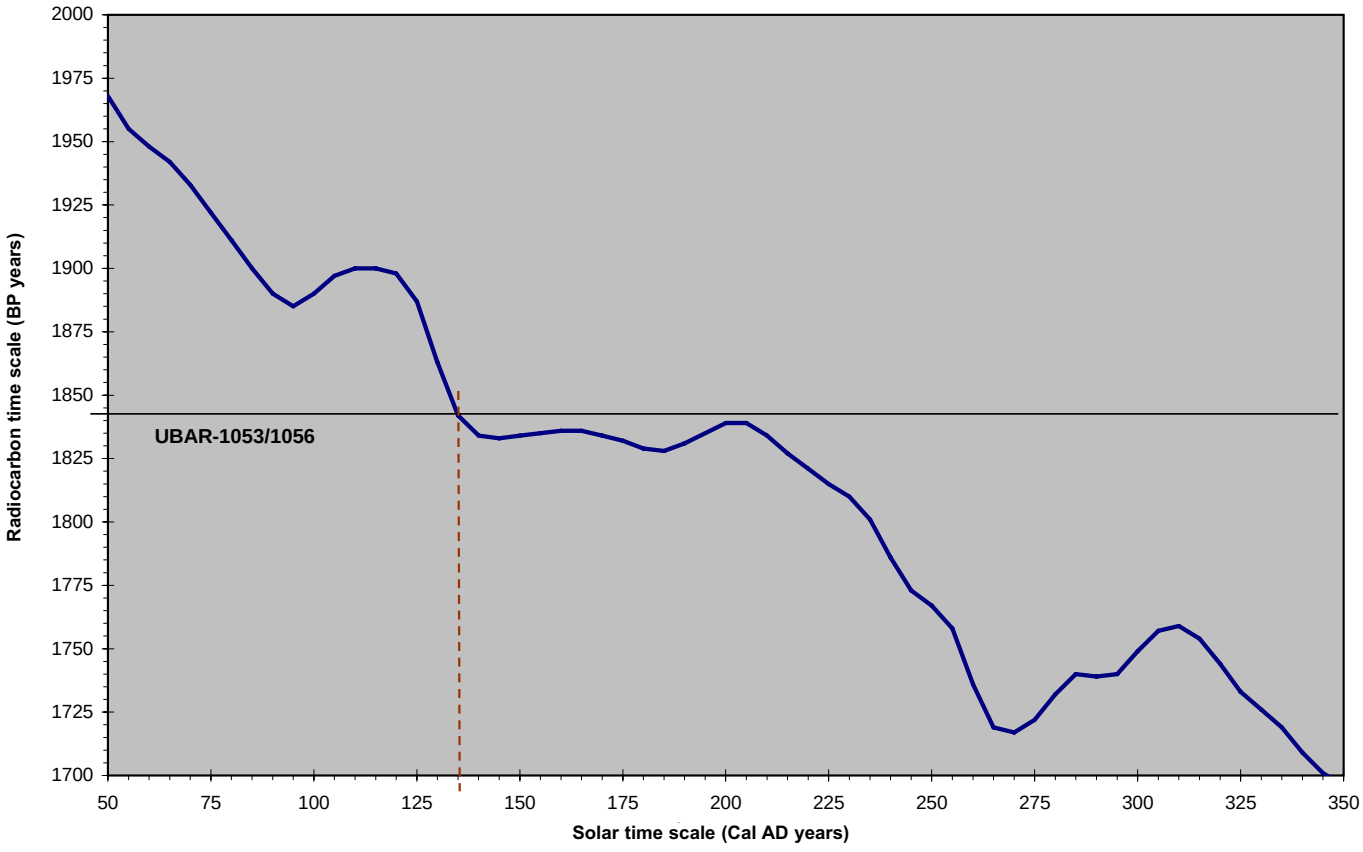


*Figura 1 E*

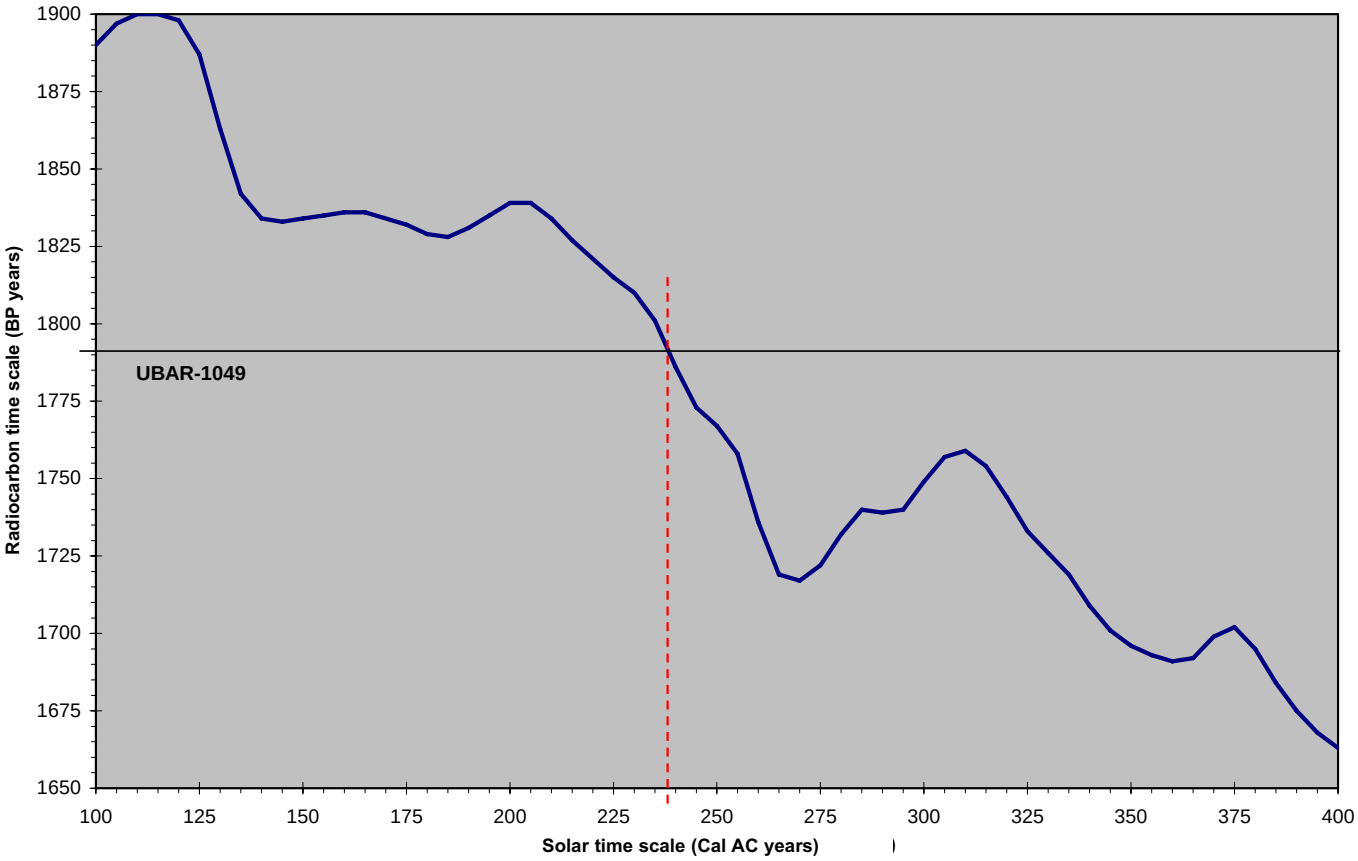


*Figure 1F*

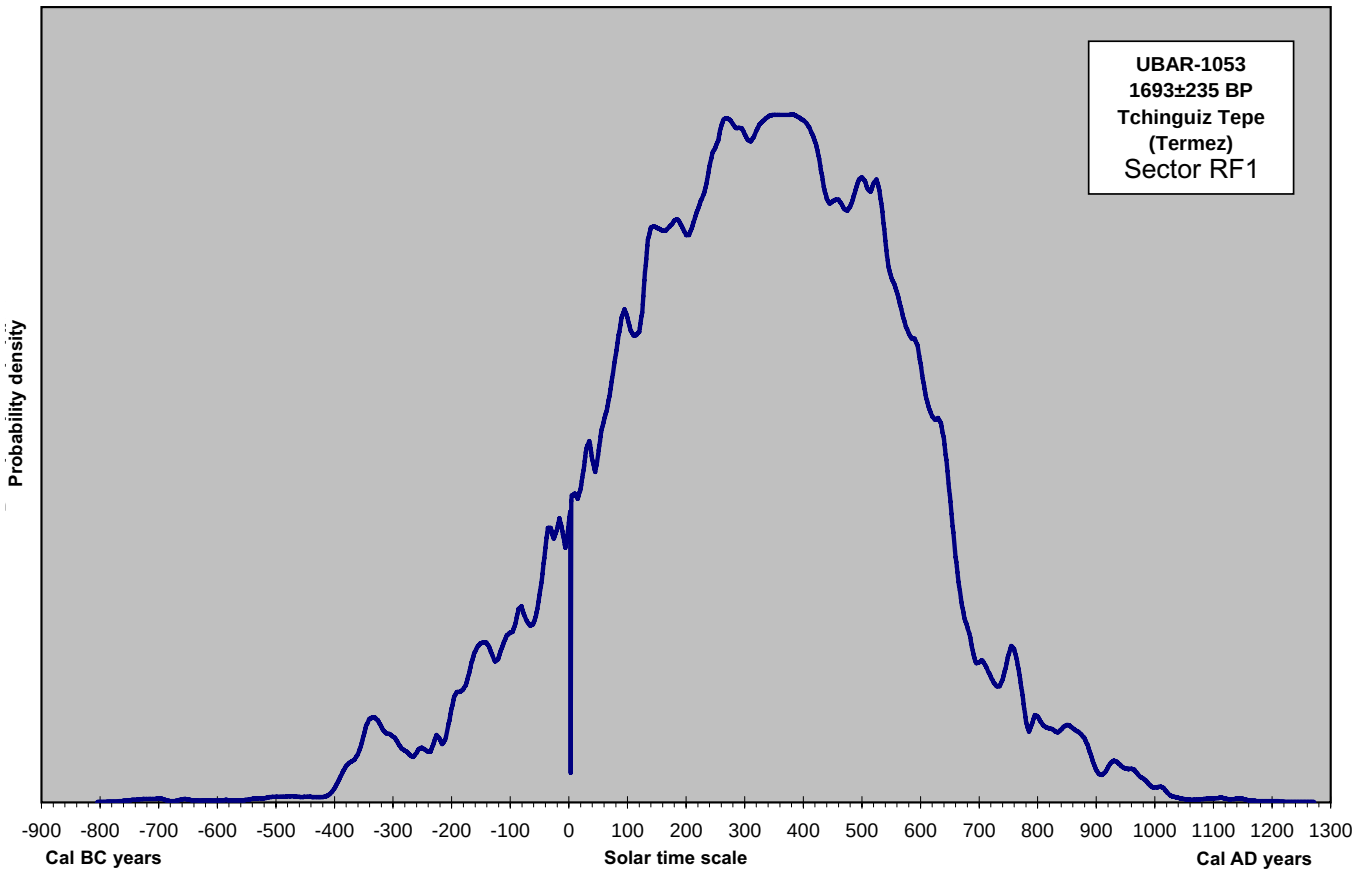


*Figure 2 A*

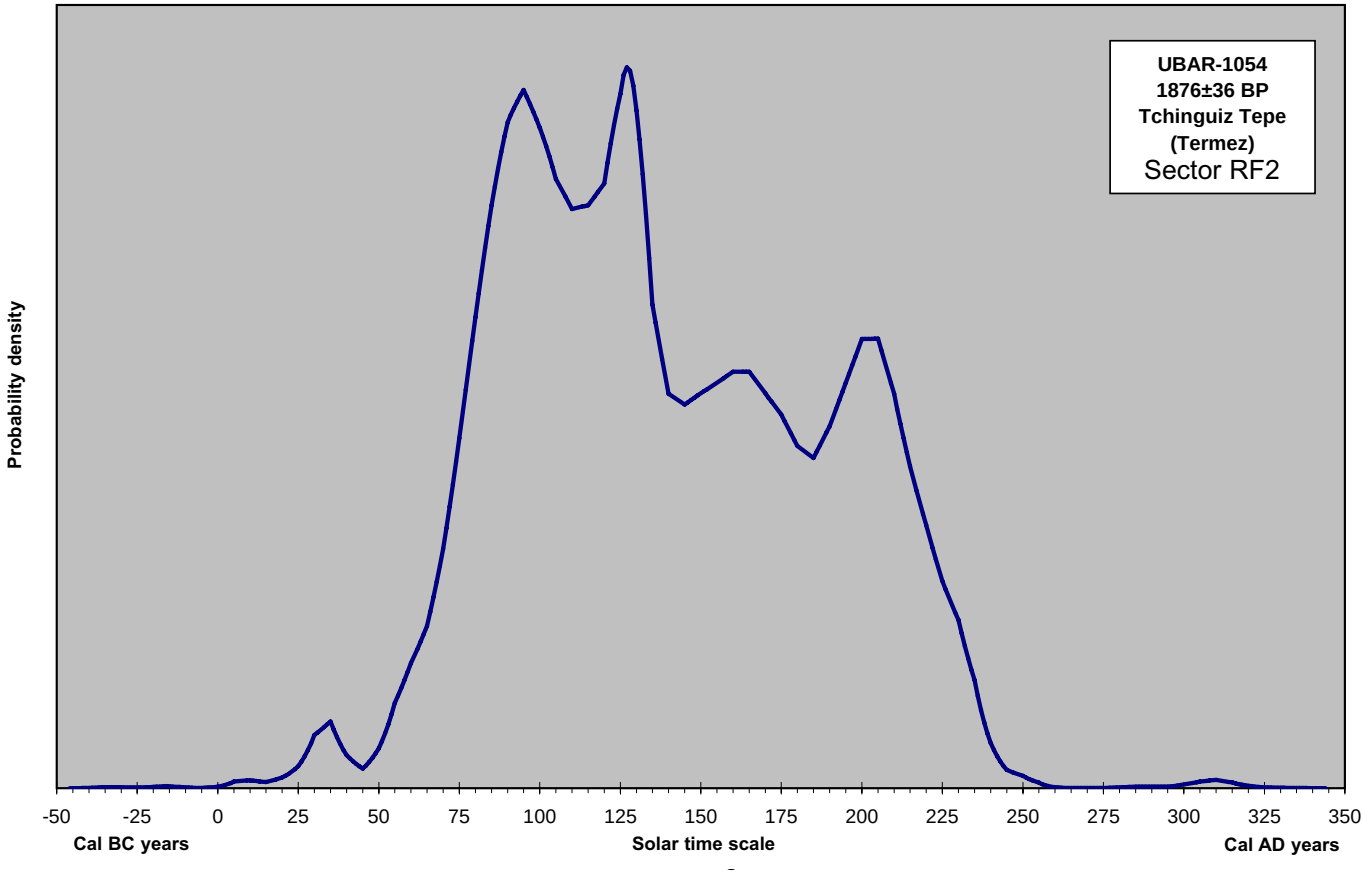


*Figure 2 B*

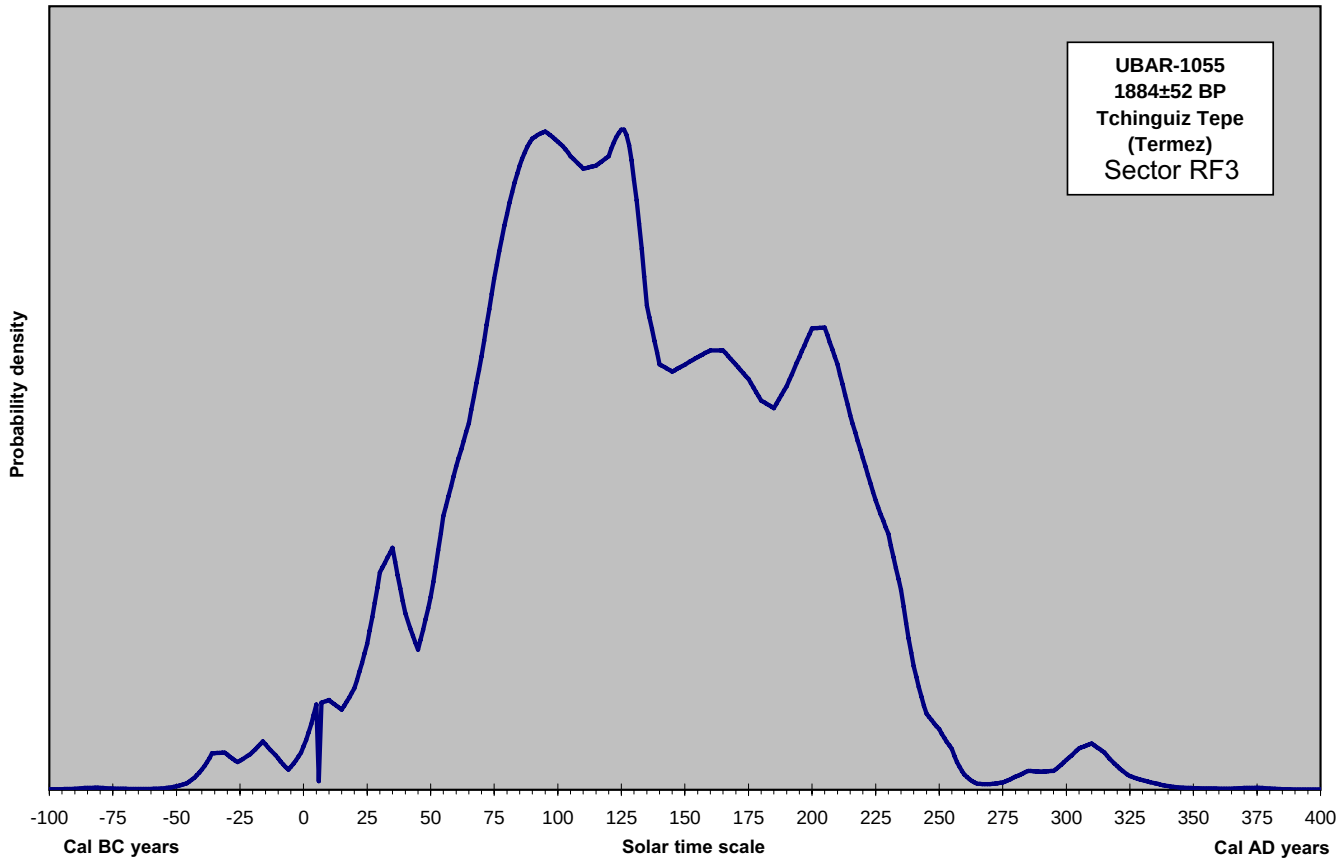


*Figure 2 C*

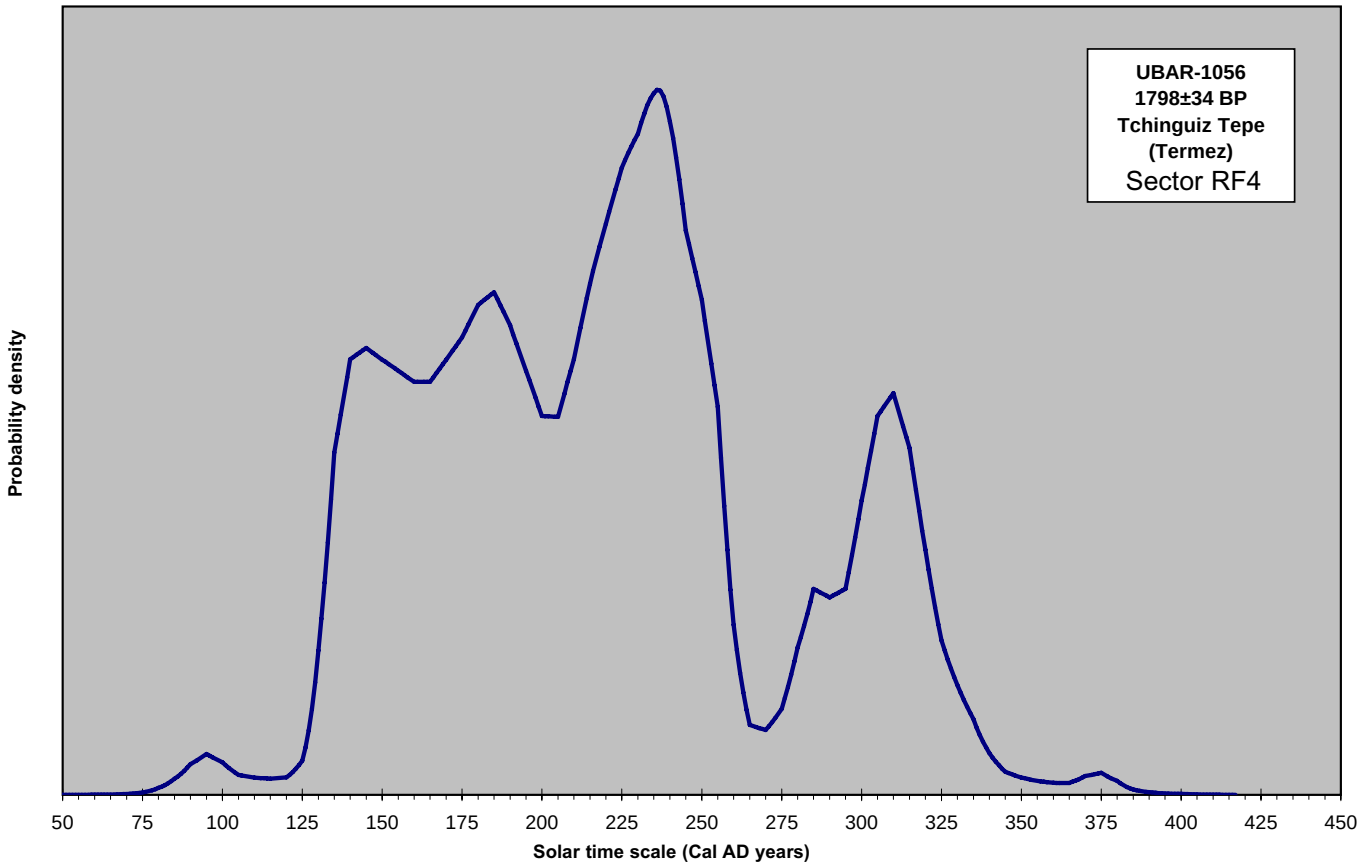


*Figure 2 D*

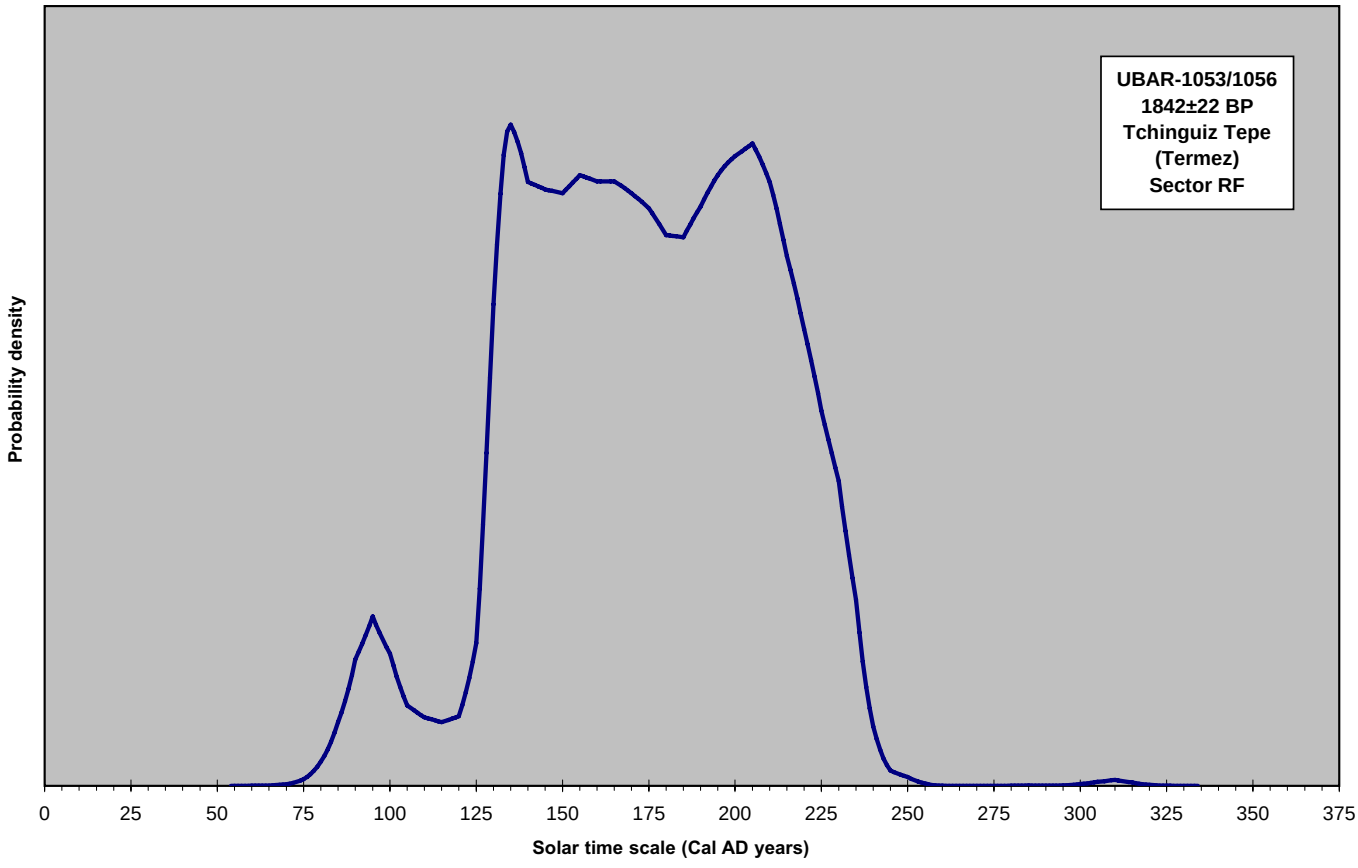


*Figure 2 E*

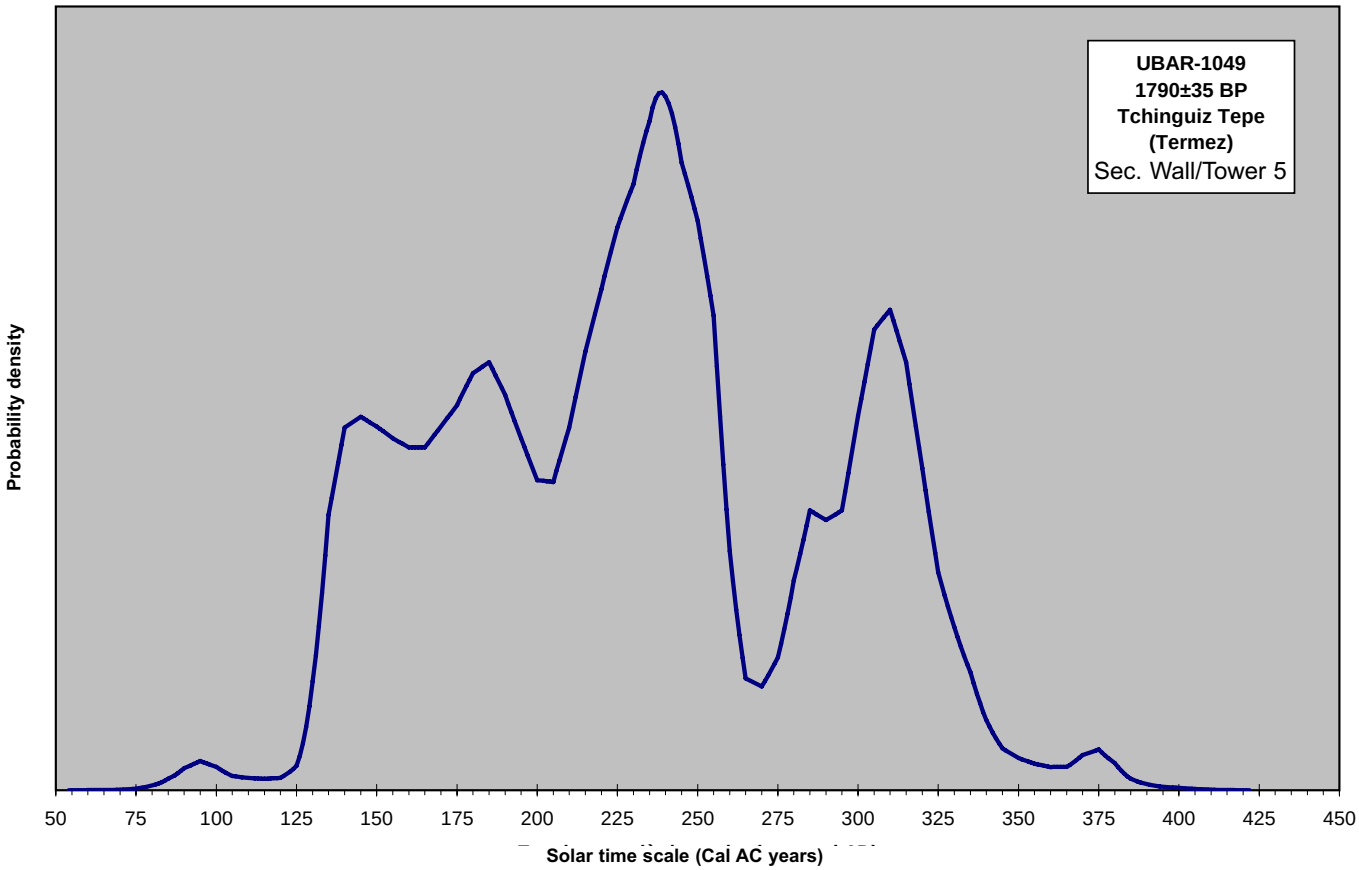


*Figure 2 F*

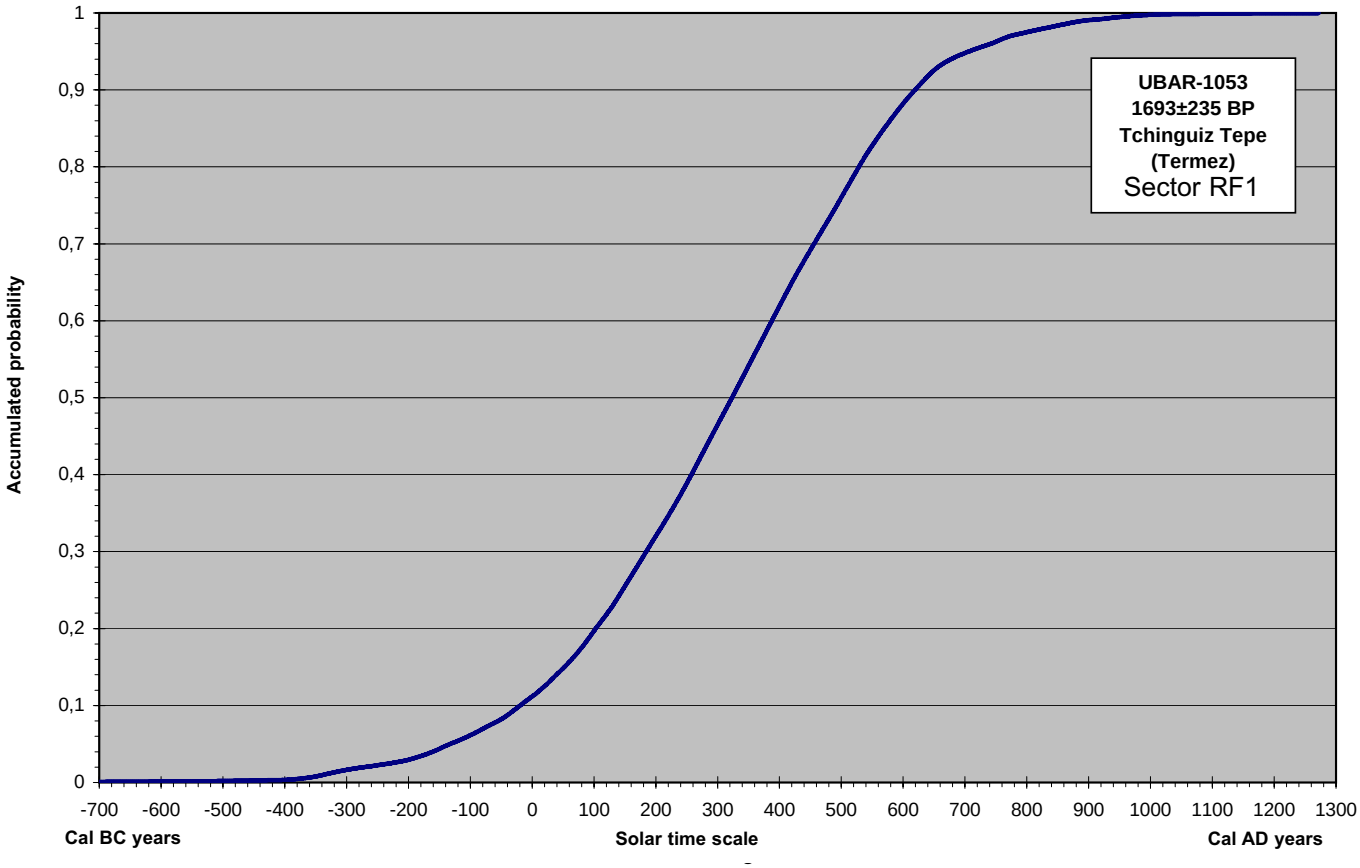


*Figure 3 A*

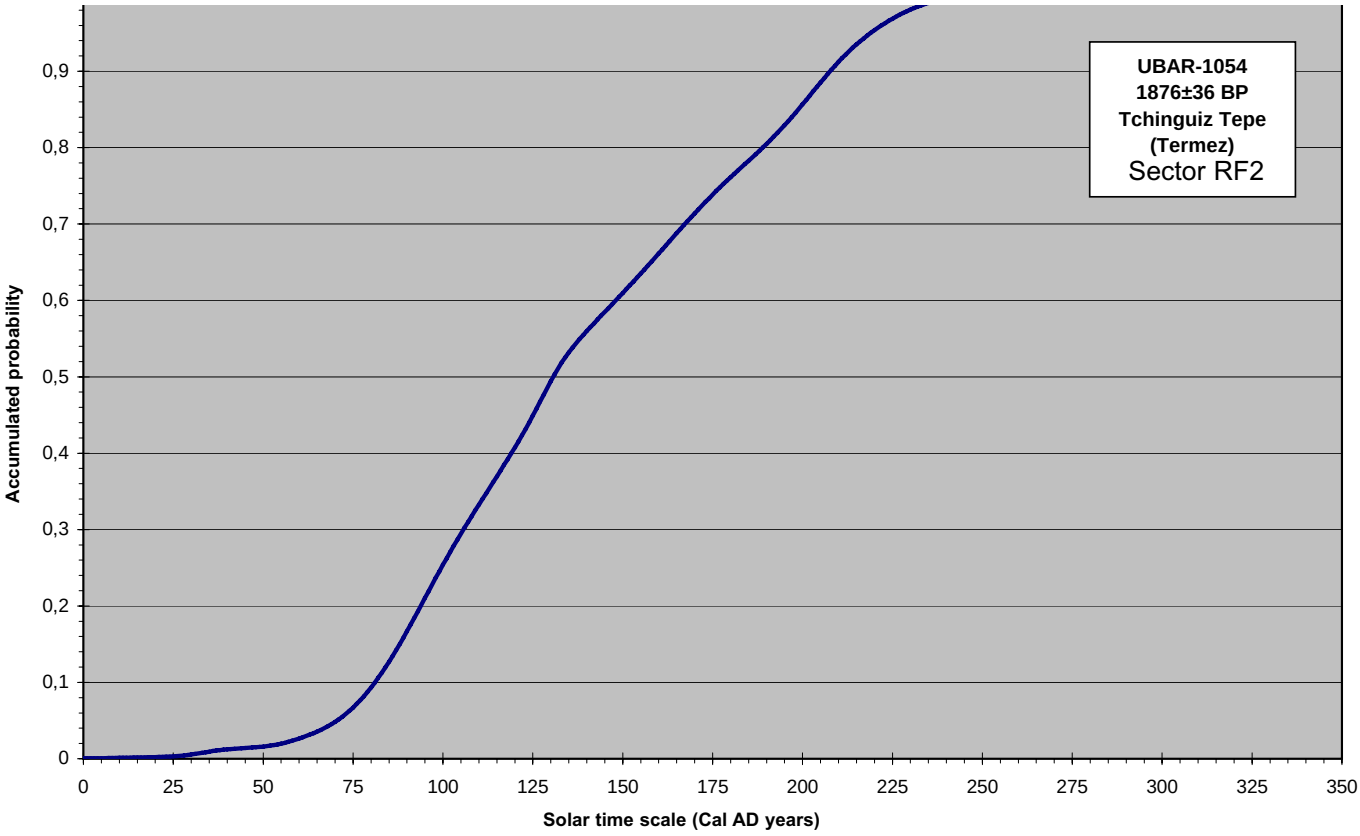


***Figure 3 B***

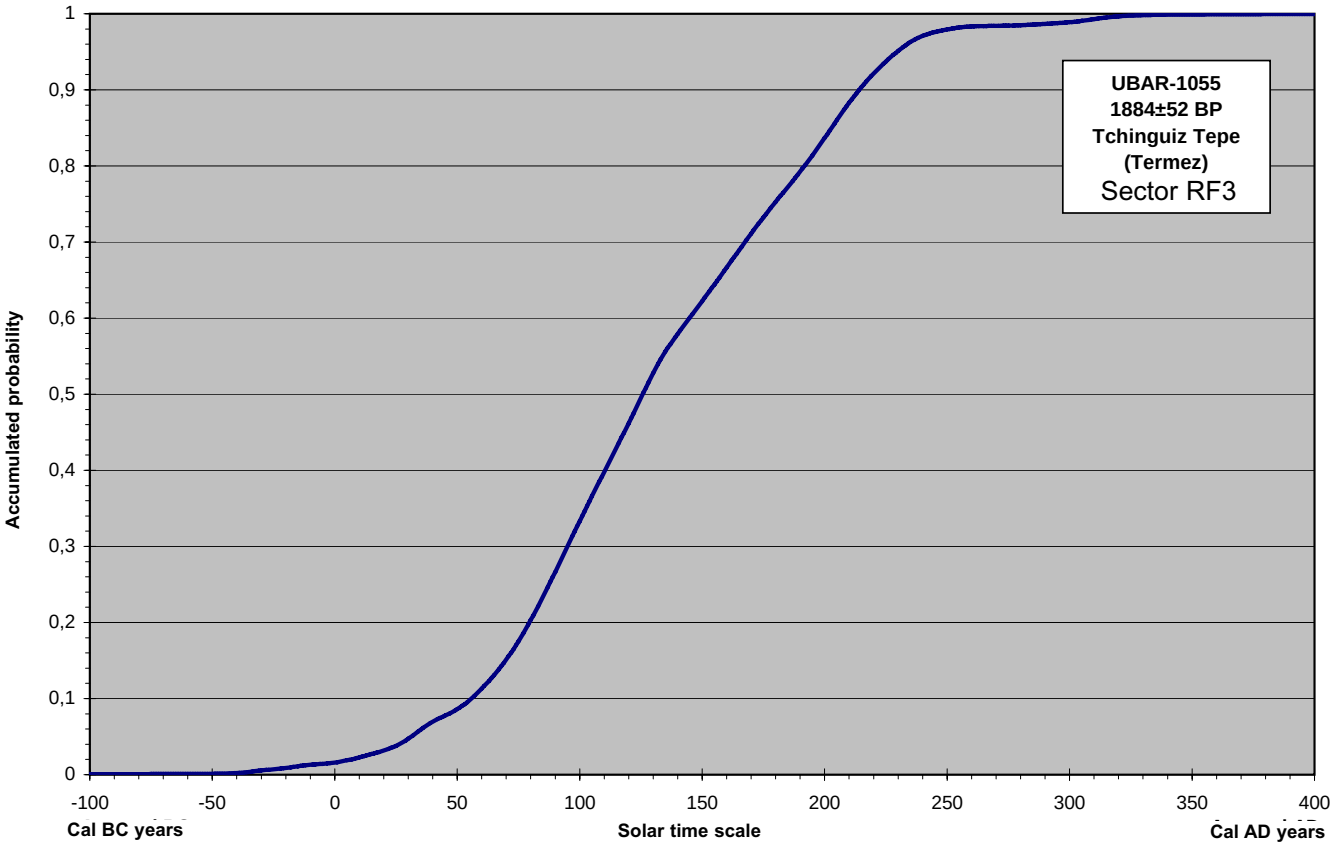


***Figure 3 C***

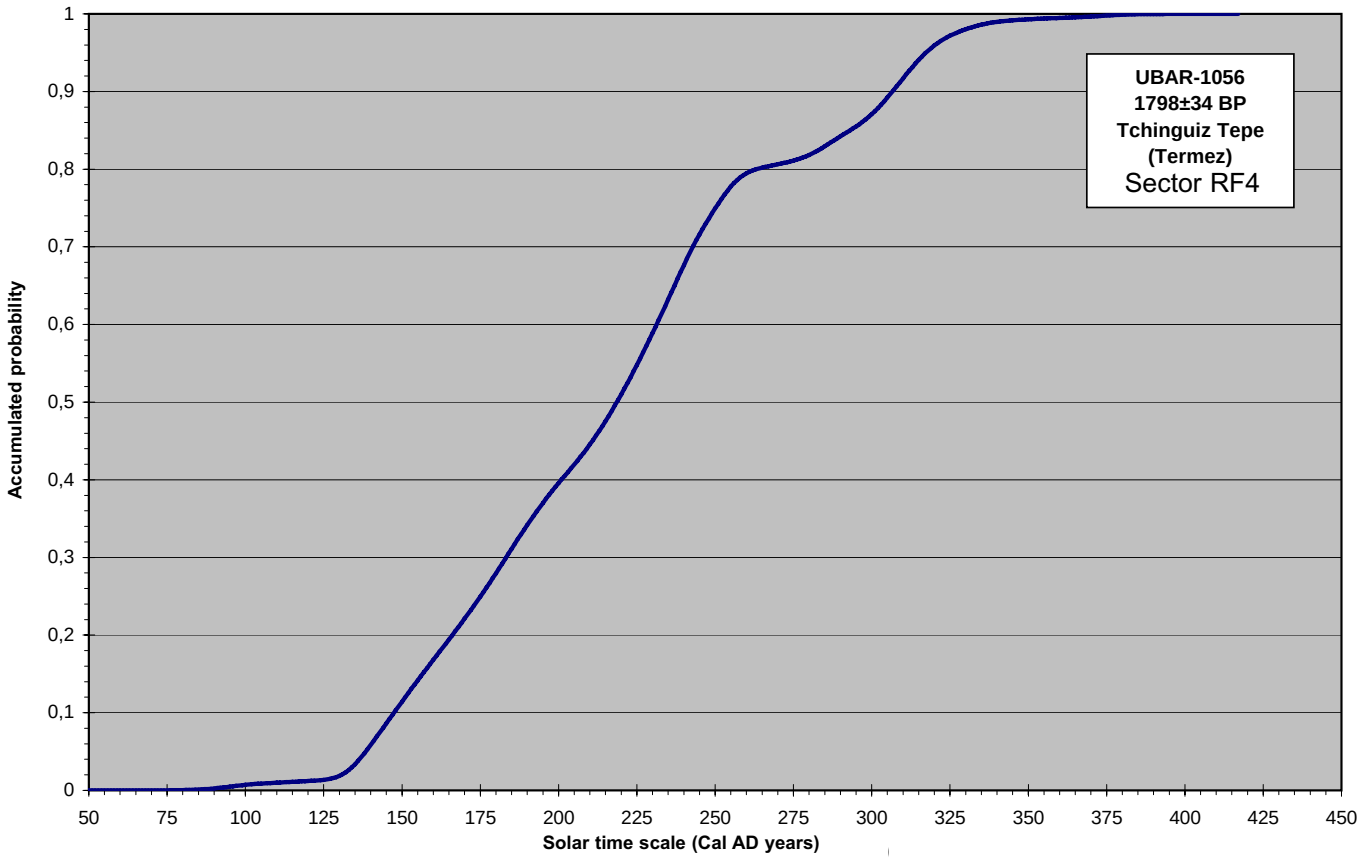


*Figure 3 D*

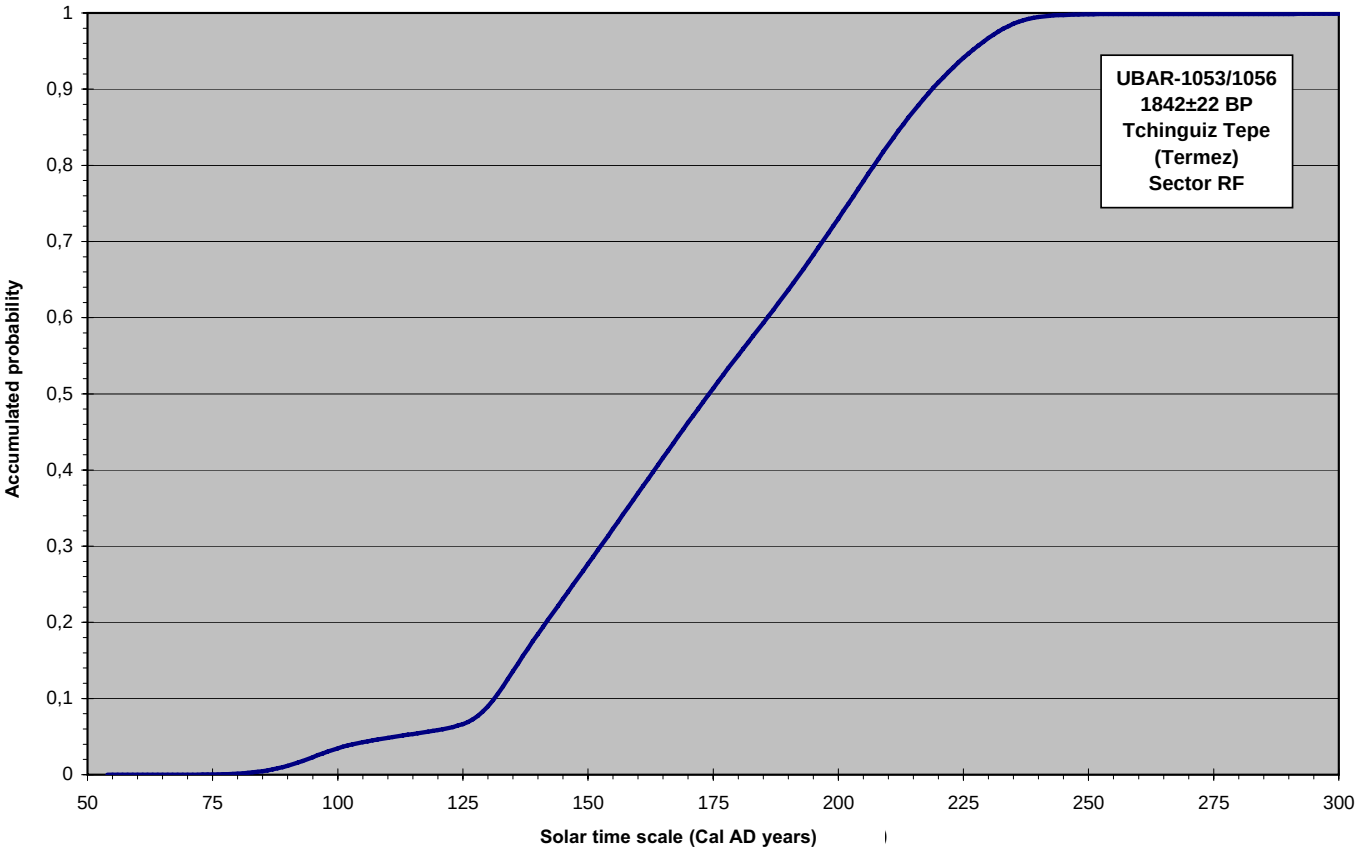


*Figure 3 E*

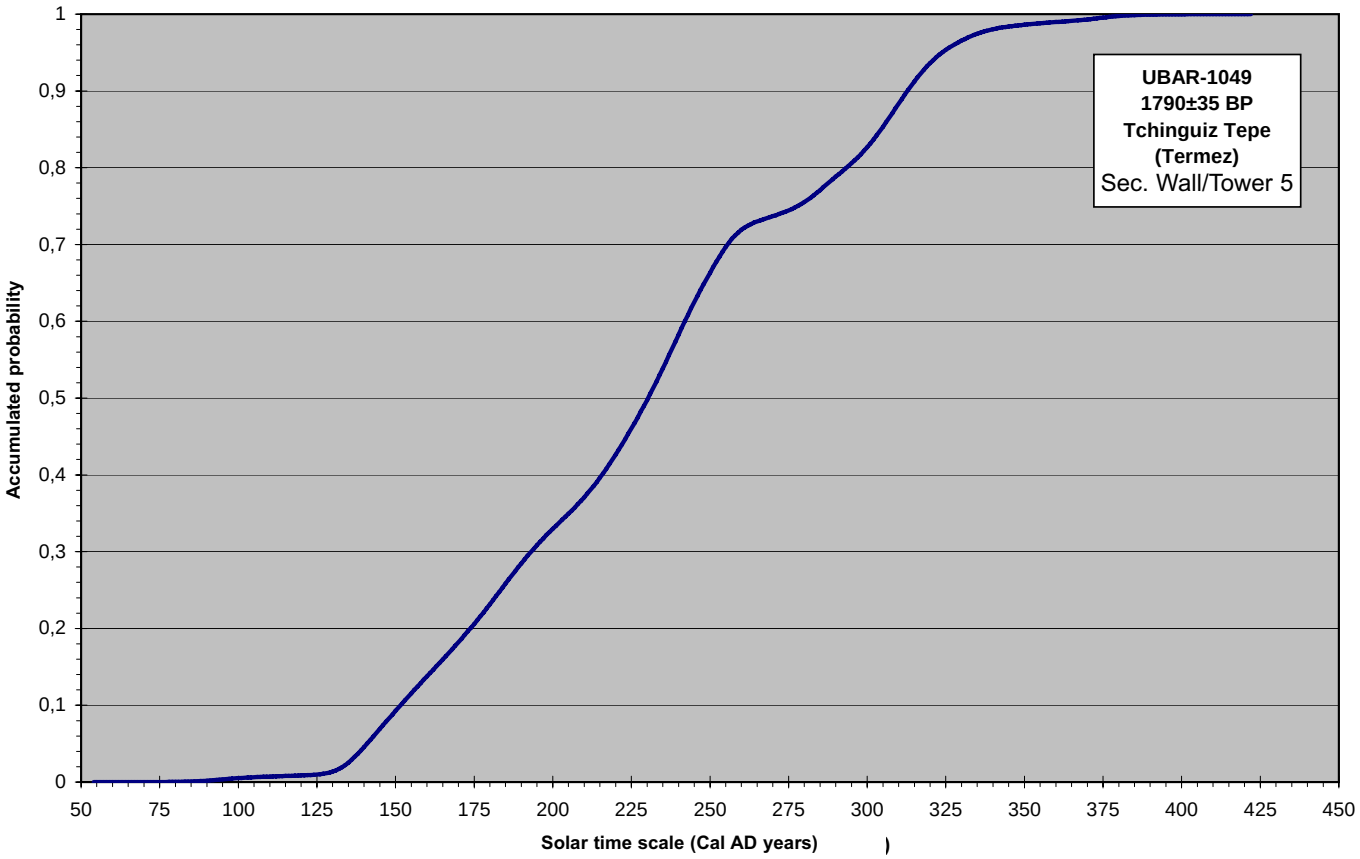
UBAR-1049
1790±35 BP
Tchinguiz Tepe
(Termez)
Sec. Wall/Tower 5
Accumulated probability
Solar time scale (Cal AD years)
1
0,9
0,8
0,7
0,6
0,5
0,4
0,3
0,2
0,1
0
50
75
100
125
150
175
200
225
250
275
300
325
350
375
400
425
450

***Figure 3 F***

# Archaeometrical study of archaeological ceramics. Extension of provenance and technological analysis with new materials from ancient Termez, Kampyr Tepe and Tchurobkurgan sites

**Verònica Martínez, Evanthia Tsantini, Josep M. Gurt and Shakir Pidaev**

## 1. Introduction

The archaeological contexts excavated during the archaeological fieldwork of 2009 at **Termez** proportioned us with important, new pottery contexts dated in a wide chronological range ranging between the Hellenistic and Islamic period. These last artefacts can be added to the high number of ceramic

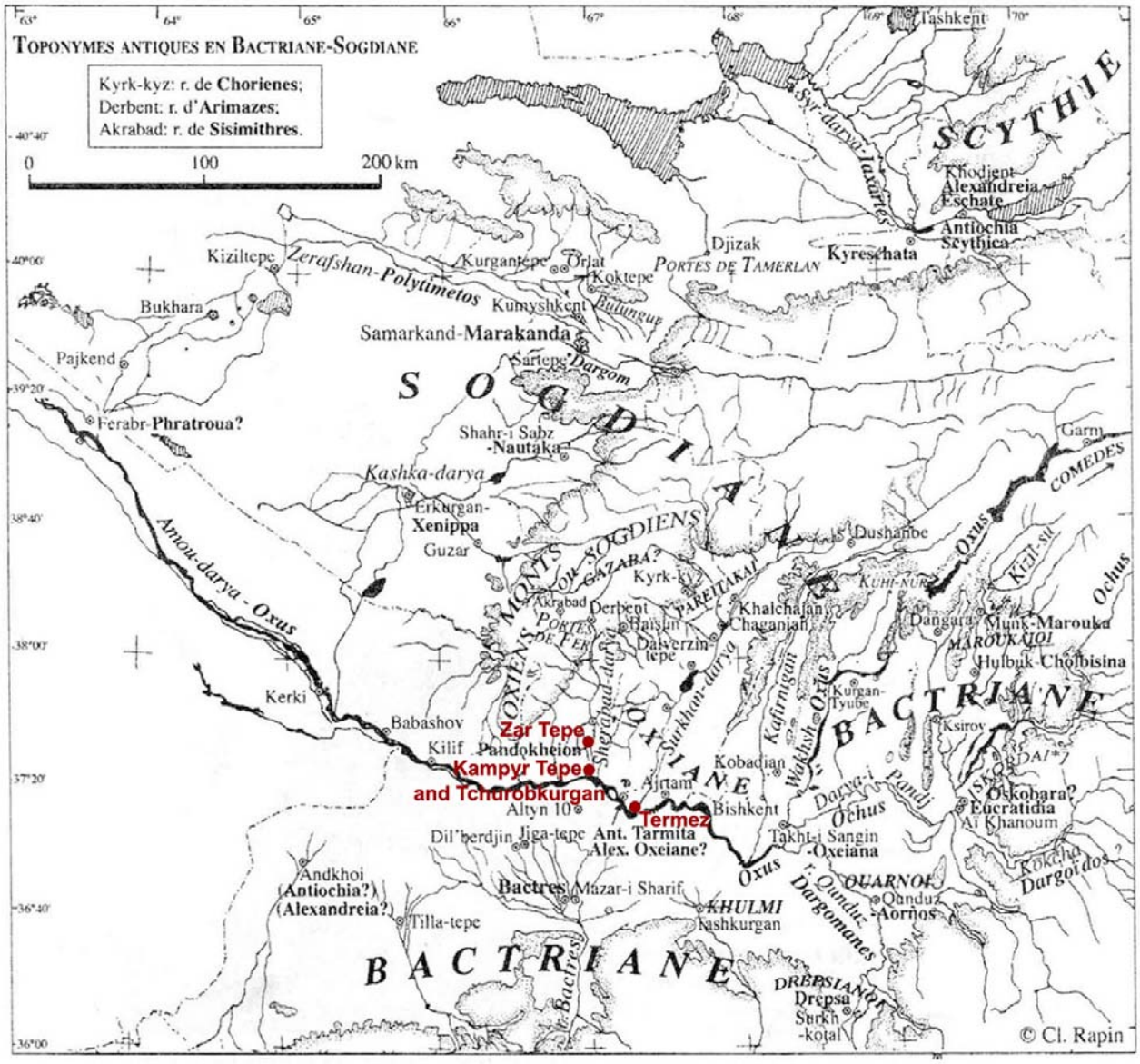


***Figure 1:*** Localization of the studied archaeological sites
The cartographic base used corresponds to the figure number 1 (p. 30) published by:
**Rapin, C.** 2007, Nomads and the Shaping of Central Asia: from the Early Iron Age to the Kushan period. After Alexander. Central Asia before Islam (Joe Cribb and Georgina Herrmann edits.) in *Proceedings of the British Academy* 133, pp. 29-72.

material statigraphically well identified recovered during the yearly excavations carried out between 2006 and 2008 at Termez (Gurt *et al.*, 2007, 2008, 2009). The pottery, from the beginning, has been studied following a double archaeological methodological frame, that, on one hand, involved the expansion of the ceramic finds from the antique **Termez** and, on the other, integrating other numerous pottery from other archaeological sites of the area, such us the Hellenistic-Kushan **Kampyr Tepe**, the Kushan-Sassanian **Zar Tepe** and the Medieval site of **Tchurobkurgan** (Figure 1).

The research carried out, these last years, on clear archaeological contexts and associated pottery has leaded to the construction of a large data base that can be considered as the first archaeological and archaeometrical reference on the production, distribution and composition of archaeological cera-mics at Central Asia. The obtained information not only includes their typological characteristics and decorations but also their chemical, mineralogical and petrographical composition. This, in fact, facilitates their global study starting from their provenance study and the evaluation of the technological aspect involved in their manufacture.

Provenance studies can be done in two different levels one has its aim in identifying the origin or the raw materials applied for the pottery production and the other aims to identify their production centre. In the latest interdisciplinary studies these two levels are combined. Only by knowing the pottery provenance, can one make inferences on the production, distribution and consumption practices followed in Antiquity. The full archaeometric characterization of the pottery also can lead to knowledge on the technological processes involved in their manufacture, such us clay processing, type of modelling, firing temperature and atmosphere. At the same time is the only way to be able to identify possible postdepositional alteration and/or contamination processes.

Obtaining all the above data is the only way to reconstruct the life-cycle of pottery starting from manufacture, moving to use, then to their discard and finally to their deposition in the archaeological layer. Combining and contrasting all this information with the archaeological data, such as chronology, typology and context, is the right way to respond to fundamental question related to the knowledge of the ancient societies that manufactured, used and discarded them latter. For instance: Where they have been produced? Where they have been used and how? Why they have been discarded at some point? Where they have been diffused? How many and which one of them are local? How many and which one of them are imported? The answer to all these questions can not be simply given only by archaeology or only by archaeometry, but by both of them at the same time, as every one of these disciplines could be respond only to one part of the answer. Only an interdisciplinary comparative study between different ceramic productions can make possible the definition of the grade that they were commercialized according the type, the fabric and chronology.

## 2. Study cases and sampling

So far 399 ceramics have been characterized from an archaeological and archaeometrical point of view between 2006 and 2010. These ceramics come from different sites and can be associated to different chronological periods. The analysed material includes jars, plates, bowls of non painted common wares and painted wares covered with a red, brown, grey and black slip and some cooking wares. At Table 1 we listed the location origin and the typology of the ceramics analysed for this work (108 individuals).

The present work is centred on the archaeometrical study of 108 new ceramic samples which correspond only a part of the archaeological finds of 2009. They come mainly from the new sector RC of **Tchinguiz Tepe** (TRZ293 to TRZ312) and the sector **AC2** (Antique Quarters) (TRZ313 to TRZ364) at **Termez**. However, the analytical program includes also new samples from sectors RF (TRZ291 and TRZ292) and RC that was not included in the archaeometrical study of 2008 and some shards from new excavation sites at the Hellenistic settlement of **Kampyr Tepe** (TRZ365 to TRZ389) as well (Martínez *et al.*, 2009: 233). Moreover, ten ceramics from the site **Tchurobkurgan** (TRZ391 to TRZ399) have been also analyzed to expand the archaeometrical study to medieval ceramics produced and diffused in the Surkhan Darya valley (Table 1).

| MATERIAL FROM TERMEZ | | | |
|---|---|---|---|
| **Analytical code** | **Number of inventory** | **Site** | **Type of ceramic** |
| TRZ291 | TZ08-RF-22-4 | TCHINGUIZ TEPE - RF | Common ware, relief dec., reddish slip on inner&outer surfaces |
| TRZ292 | TZ08-RF-26-1 | TCHINGUIZ TEPE - RF | Tap of cooking ware, clear brown paste |
| TRZ293 | TZ08-RC-5-10 | TCHINGUIZ TEPE - RC | Cooking ware, open rim, grey paste and reddish surfaces |
| TRZ294 | TZ08-RC-18-5 | TCHINGUIZ TEPE – RC | Cooking ware, open rim, reddish paste |
| TRZ295 | TZ08-RC-18-6 | TCHINGUIZ TEPE – RC | Cooking ware, open rim, reddish paste |
| TRZ296 | TZ09-RC2-18-1 | TCHINGUIZ TEPE - RC | Common ware, open rim, reddish slip on inner&outer surfaces |
| TRZ297 | TZ09-RC2-18-2 | TCHINGUIZ TEPE – RC | Common ware, plate, incised dec., red slip on inner&outer surfaces |
| TRZ298 | TZ09-RC2-18-3 | TCHINGUIZ TEPE – RC | Cooking ware, open rim |
| TRZ299 | TZ09-RC2-18-4 | TCHINGUIZ TEPE – RC | Common ware, open rim, unpainted |
| TRZ300 | TZ09-RC2-21-1 | TCHINGUIZ TEPE – RC | Common ware, plate, unpainted |
| TRZ301 | TZ09-RC2-21-2 | TCHINGUIZ TEPE – RC | Common ware, open rim, jar, unpainted |
| TRZ302 | TZ09-RC2-21-3 | TCHINGUIZ TEPE – RC | Common ware red slip in internal and external surface |
| TRZ303 | TZ09-RC2-21-4 | TCHINGUIZ TEPE – RC | Common ware, plate, orange slip |
| TRZ304 | TZ09-RC2-21-5 | TCHINGUIZ TEPE – RC | Common ware, incised dec., reddish slip on inner&outer surfaces |
| TRZ305 | TZ09-RC2-25-1 | TCHINGUIZ TEPE – RC | Cooking ware, open rim |
| TRZ306 | TZ09-RC2-25-2 | TCHINGUIZ TEPE – RC | Common ware, open rim, incised dec., red slip on inner&outer s. |
| TRZ307 | TZ09-RC2-25-3 | TCHINGUIZ TEPE – RC | Common ware, base of jar, reddish painted on the outer surface |
| TRZ308 | TZ09-RC2-25-4 | TCHINGUIZ TEPE – RC | Fragment of terracotta, brownish-red paste |
| TRZ309 | TZ09-RC2-28-1 | TCHINGUIZ TEPE – RC | Cooking ware |
| TRZ310 | TZ09-RC2-28-2 | TCHINGUIZ TEPE – RC | Common ware, jar, orange-brown slip on inner-outer surfaces |
| TRZ311 | TZ09-RC2-28-3 | TCHINGUIZ TEPE – RC | Common ware, jar, dark brownish slip on the inner surface |
| TRZ312 | TZ09-RC2-28-4 | TCHINGUIZ TEPE - RC | Common ware, jar, orange-reddish slip on rim and outer surface |
| TRZ313 | TZ09-AC2-11-1 | Ancient Military Quarters 2 | Glazed common ware (white, brown and black), open rim |
| TRZ314 | TZ09-AC2-11-2 | Ancient Military Quarters 2 | Glazed common ware (white, green, yellow, black), open rim |
| TRZ315 | TZ09-AC2-11-3 | Ancient Military Quarters 2 | Glazed common ware (white, brown, black), open rim |
| TRZ316 | TZ09-AC2-11-4 | Ancient Military Quarters 2 | Glazed common ware (white, black, blue, red, yellow), open rim |
| TRZ317 | TZ09-AC2-11-5 | Ancient Military Quarters 2 | Tap of coarse ware of clear paste |
| TRZ318 | TZ09-AC2-11-6 | Ancient Military Quarters 2 | Fragment of jar, common ware, and yellowish paste |
| TRZ319 | TZ09-AC2-11-7 | Ancient Military Quarters 2 | Tap and hang of cooking ware, dark paste |
| TRZ320 | TZ09-AC2-11-8 | Ancient Military Quarters 2 | Cooking ware, open rim |
| TRZ321 | TZ09-AC2-12-1 | Ancient Military Quarters 2 | Common ware, jar, yellowish paste |
| TRZ322 | TZ09-AC2-12-2 | Ancient Military Quarters 2 | Glazed common ware (white, green, yellow, brown), open rim |
| TRZ323 | TZ09-AC2-14-1 | Ancient Military Quarters 2 | Cooking ware, open rim and hang, rose paste |
| TRZ324 | TZ09-AC2-14-2 | Ancient Military Quarters 2 | Glazed common ware (yellow and black), open rim |
| TRZ325 | TZ09-AC2-14-3 | Ancient Military Quarters 2 | Glazed common ware (green), open rim |
| TRZ326 | TZ09-AC2-14-4 | Ancient Military Quarters 2 | Glazed common ware (white), open |
| TRZ327 | TZ09-AC2-15-1 | Ancient Military Quarters 2 | Glazed common ware (white, red, black), open rim |
| TRZ328 | TZ09-AC2-15-2 | Ancient Military Quarters 2 | Glazed common ware (black inscriptions), open rim, |
| TRZ329 | TZ09-AC2-16-1 | Ancient Military Quarters 2 | Glazed common ware (white, black, blue), open rim |
| TRZ330 | TZ09-AC2-16-2 | Ancient Military Quarters 2 | Common ware, decorated with incised motifs |
| TRZ331 | TZ09-AC2-16-3 | Ancient Military Quarters 2 | Glazed common ware (white, black), open rim |
| TRZ332 | TZ09-AC2-17-1 | Ancient Military Quarters 2 | Common ware, open rim, grey paste, unpainted |
| TRZ333 | TZ09-AC2-17-2 | Ancient Military Quarters 2 | Common ware, open rim, reddish slip inner&outer surfaces |
| TRZ334 | TZ09-AC2-17-3 | Ancient Military Quarters 2 | Common ware, open rim, orange-red slip on inner&outer surfaces |
| TRZ335 | TZ09-AC2-17-4 | Ancient Military Quarters 2 | Common ware, open rim, red-brown slip on inner&outer surfaces |
| TRZ336 | TZ09-AC2-17-5 | Ancient Military Quarters 2 | Common ware, open rim, dark brownish slip on the inner surfaces |
| TRZ337 | TZ09-AC2-17-6 | Ancient Military Quarters 2 | Common ware, open rim, red-brown slip on inner&outer surfaces |
| TRZ338 | TZ09-AC2-17-7 | Ancient Military Quarters 2 | Common ware, open rim, dark brown slip on inner&outer surfaces |
| TRZ339 | TZ09-AC2-17-8 | Ancient Military Quarters 2 | Common ware, open rim, orange-brown on inner&outer surfaces |
| TRZ340 | TZ09-AC2-17-9 | Ancient Military Quarters 2 | Common ware, open rim, dark brown painted on inner&outer surfaces |
| TRZ341 | TZ09-AC2-17-10 | Ancient Military Quarters 2 | Common ware, open rim, red-brown painted on inner&outer surfaces |
| TRZ342 | TZ09-AC2-17-11 | Ancient Military Quarters 2 | Common ware, open rim, brown clear paste, unpainted |
| TRZ343 | TZ09-AC2-17-12 | Ancient Military Quarters 2 | Common ware, open rim, dark brown slip on the outer surface |

***Table 1:*** The analysed individuals

| MATERIAL FROM TERMEZ | | | |
|---|---|---|---|
| **Analytical code** | **Number of inventory** | **Site** | **Type of ceramic** |
| TRZ344 | TZ09-AC2-17-13 | Ancient Military Quarters 2 | Big container, open rim and hang, yellowish paste, unpainted |
| TRZ345 | TZ09-AC2-18-1 | Ancient Military Quarters 2 | Glazed common ware (yellow, black, red, green, white), open rim |
| TRZ346 | TZ09-AC2-18-2 | Ancient Military Quarters 2 | Glazed common ware (black, white), open rim |
| TRZ347 | TZ09-AC2-18-3 | Ancient Military Quarters 2 | Big container, open rim with impressive motifs oin the rim, unpainted |
| TRZ348 | TZ09-AC2-20-1 | Ancient Military Quarters 2 | Common ware, open rim, grey slip on inner&outer surfaces |
| TRZ349 | TZ09-AC2-20-2 | Ancient Military Quarters 2 | Common ware, rounded base, grey paste |
| TRZ350 | TZ09-AC2-20-3 | Ancient Military Quarters 2 | Common ware, base, brown slip on inner&outer surfaces |
| TRZ351 | TZ09-AC2-20-4 | Ancient Military Quarters 2 | Common ware, open rim, brown clear paste, unpainted |
| TRZ352 | TZ09-AC2-20-5 | Ancient Military Quarters 2 | Common ware, open rim, orange painted on the inner surface |
| TRZ353 | TZ09-AC2-20-6 | Ancient Military Quarters 2 | Common ware, open rim, red-brown painted on inner&outer surfaces |
| TRZ354 | TZ09-AC2-20-7 | Ancient Military Quarters 2 | Common ware, open rim, orange slip on the outer surface |
| TRZ355 | TZ09-AC2-20-8 | Ancient Military Quarters 2 | Common ware, closed rim, incised motifs, orange slip on inner s. |
| TRZ356 | TZ09-AC2-20-9 | Ancient Military Quarters 2 | Common ware, open rim, orange slip on the inner surface |
| TRZ357 | TZ09-AC2-20-10 | Ancient Military Quarters 2 | Common ware, open rim, reddish slip on inner&outer surfaces |
| TRZ358 | TZ09-AC2-20-11 | Ancient Military Quarters 2 | Common ware, open rim, grey slip on inner&outer surfaces |
| TRZ359 | TZ09-AC2-22-1 | Ancient Military Quarters 2 | Fragment of big jar or container, plane base, unpainted |
| TRZ360 | TZ09-AC2-28-1 | Ancient Military Quarters 2 | Common ware, jar, closed rim, red slip on inner&outer surfaces |
| TRZ361 | TZ09-AC2-28-2 | Ancient Military Quarters 2 | Common ware, open rim, red-brown slip on inner&outer surfaces |
| TRZ362 | TZ09-AC2-28-3 | Ancient Military Quarters 2 | Common ware, closed rim, incised dec., red slip on the outer s. |
| TRZ363 | TZ09-AC2-33-1 | Ancient Military Quarters 2 | Common ware, open rim, rose-brown paste, unpainted |
| TRZ364 | TZ09-AC2-33-2 | Ancient Military Quarters 2 | Common ware, closed rim, jar, brown clear paste, unpainted |

| MATERIAL FROM KAMPYR TEPE | | | |
|---|---|---|---|
| **Analytical code** | **Number of inventory** | **Site** | **Type of ceramic** |
| TRZ365 | KPT-09-V36-1 | Low city, Bloc-V, Area-36a | Common ware, open rim, red slip on inner&outer surfaces |
| TRZ366 | KPT-09-V36-2 | Low city, Bloc-V, Area -36a | Common ware, open rim, brown slip on inner&outer surf. |
| TRZ367 | KPT-09-V36-3 | Low city, Bloc-V, Area -36a | Common ware, open rim, grey slip on inner&outer surfaces |
| TRZ368 | KPT-09-V36-4 | Low city, Bloc-V, Area -36a | Common ware, base, red-brown slip on inner&outer surf. |
| TRZ369 | KPT-09-V36-5 | Low city, Bloc-V, Area -36a | Common ware, base, brown-grey slip in outer surface |
| TRZ370 | KPT-09-V36-6 | Low city, Bloc-V, Area -36a | Common ware, base, brown-grey slip on inner&outer surf. |
| TRZ371 | KPT-09-V36-7 | Low city, Bloc-V, Area -36a | Common ware, open rim, unpainted |
| TRZ372 | KPT-09-V36-8 | Low city, Bloc-V, Area -36a | Common ware, open rim and base, yellowish paste, unpainted |
| TRZ373 | KPT-09-V36-9 | Low city, Bloc-V, Area -36a | Cooking ware, grey black paste |
| TRZ374 | KPT-09-V36-10a | Low city, Bloc-V, Area -36a | Common ware, open rim, black slip on inner&outer surf. |
| TRZ375 | KPT-09-V-34-1 | Low city, Bloc-V, Area -34a, b | Common ware, open rim, red slip on inner&outer surfaces |
| TRZ376 | KPT-09-V-34-2 | Low city, Bloc -V, Area -34a, b | Common ware, jar, orange slip on inner&outer surfaces |
| TRZ377 | KPT-09-V-34-3 | Low city, Bloc -V, Area -34a, b | Common ware, open rim, brown-grey slip on inner&outer s. |
| TRZ378 | KPT-09-V-34-4 | Low city, Bloc -V, Area -34a, b | Common ware, open rim, brown-grey slip on inner&outer s. |
| TRZ379 | KPT-09-V-34-5 | Low city, Bloc -V, Area -34a, b | Common ware, open rim, red slip on the rim |
| TRZ380 | KPT-09-V-34-6 | Low city, Bloc -V, Area -34a, b | Common ware, open rim, black slip on inner&outer surf. |
| TRZ381 | KPT-08-IV H-1 | Citadel S-E, IV H, upper level | Common ware, open rim, red slip on inner&outer surfaces |
| TRZ382 | KPT-08-IV H-2 | Citadel S-E, IV H, upper level | Common ware, open rim, yellowish paste, unpainted |
| TRZ383 | KPT-08-IV H-3 | Citadel S-E, IV H, upper level | Common ware, open rim, red slip on inner&outer surfaces |
| TRZ384 | KPT-08-IV H-4 | Citadel S-E, IV H, upper level | Common ware, open rim, yellow slip on inner&outer surf. |
| TRZ385 | KPT-08-IV H-5 | Citadel S-E, IV H, upper level | Common ware, open rim, yellow slip on inner&outer surf. |
| TRZ386 | KPT-08-IV H-6 | Citadel S-E, IV H, upper level | Common ware, open rim, red slip on inner&outer surfaces |
| TRZ387 | KPT-08-IV H-7 | Citadel S-E, IV H, upper level | Storage jar, open rim, brown clear paste, unpainted |
| TRZ388 | KPT-08-IV H-8 | Citadel S-E, IV H, upper level | Storage jar, open rim, brownish-rose paste |
| TRZ389 | KPT-08-IV H-9 | Citadel S-E, IV H, upper level | Cooking ware, open rim, brownish-black paste |

***Table 1:*** The analysed individuals

| MATERIAL FROM TCHUROBKURGAN | | | |
|---|---|---|---|
| **Analytical code** | **Number of inventory** | **Site** | **Type of ceramic** |
| TRZ390 | Tchurobk-09-1 | TCHUROBKURGAN | Common ware, open rim, reddish slip on inner&outer surfaces |
| TRZ391 | Tchurobk-09-2 | TCHUROBKURGAN | Common ware, open rim, reddish slip on inner&outer surfaces |
| TRZ392 | Tchurobk-09-3 | TCHUROBKURGAN | Common ware, open rim, dark brown slip on inner&outer surfaces |
| TRZ393 | Tchurobk-09-4 | TCHUROBKURGAN | Common ware, open rim, dark brown slip on inner&outer surfaces |
| TRZ394 | Tchurobk-09-5 | TCHUROBKURGAN | Common ware, open rim, reddish slip on inner&outer surfaces |
| TRZ395 | Tchurobk-09-6 | TCHUROBKURGAN | Common ware, open rim, reddish slip on inner surface |
| TRZ396 | Tchurobk-09-7 | TCHUROBKURGAN | Common ware, base, unpainted |
| TRZ397 | Tchurobk-09-8 | TCHUROBKURGAN | Cooking ware, brownish paste |
| TRZ398 | Tchurobk-09-9 | TCHUROBKURGAN | Cooking ware, dark paste |
| TRZ399 | Tchurobk-09-10 | TCHUROBKURGAN | Coarse common ware, open rim, yellowish paste |

***Table 1:*** The analysed individuals

The new results obtained will be presented together with previous analytical results obtained on pottery coming from the same archaeological contexts (Tsantini *et al*., 2007; Martínez *et al*., 2008, 2009). The data is going to be presented following a chronological order.

The following study begins by outlining the archaeometric results of the eldest ceramics dated to the Hellenistic and First Kushan periods from **Termez** and **Kampyr Tepe**. It continues with the ceramics of Kushan-Sassanian period from **Termez** and **Zar Tepe** and ends with the study of medieval and Islamic pottery from **Tchurobkurgan** and **Termez** respectively. Finally, an integrated comparison between contemporary ceramics coming from different sites will follow, to be able to make some inferences upon pottery production and distribution in the broader territory.

**Termez** is located in Surkhan Darya valley, close to the confluence between Amu Darya and Surkhan Darya Rivers. In the past, **Termez** was one of the great centres of Ancient Bactria (Leriche, 2007; Leriche and Pidaev, 2007, 2008). After the conquest of Alexander of Macedonia it was acknowledged as the *Alexandria Oxeiana*, cited by Ptolemaius. It was a major urban site occupied during the Hellenistic, the Kushan and Kushan-Sassanian periods due to its exceptionally important location as a crossroad of many intercontinental routes derived of the Silk Road.

In the ancient city of **Termez**, the oldest pottery has been recovered at the Citadel, a building dated to the Hellenistic period located on the banks of the Amu Darya. The analysed ceramics coming from the Citadel (TRZ093 to TRZ122) were recovered in old archaeological excavations carried out by the Institute of Archaeology of Uzbekistan and they can be dated to the Graeco-Bactrian and Kushan periods (Martínez *et al*., 2008, 2009).

Several structures of the *Kushan* period are located upon **Tchinguiz Tepe's** hill, placed at the northeast of the Citadel, at the right side of the river. At this site a pottery production centre has been located (sector RF). The preserved structure of the kiln is rectangular and measures 6.60 m in length and 2.10 m in width (Martínez, 2009). The archaeological remains are dated from the I$^{st}$ to the 4$^{th}$ c. AD by Radiocarbon Dating. Some of the analysed ceramics from **Tchinguiz Tepe** were recovered inside the kiln structure, at the accumulation layer formed by household trash (TRZ184 to TRZ200, TRZ202, TRZ291 and TRZ292 that correspond to the destruction level of the kiln structures (Martínez *et al*., 2009). Other ceramics come from the surface of the kiln area, recovered by a superficial prospecting (TRZ067 to TRZ072). The rest of the ceramics from **Tchinguiz Tepe** comes from two domestic buildings, that were originally attached to the adobe mentioned brick fortifying wall, delimited as sector RC (TRZ051 to TRZ066, TRZ073 to TRZ087, TRZ157 to TRZ183, TRZ201 and TRZ293 to TRZ312).

Recent excavations carried out by the ERAUB of the Universitat de Barcelona and the Institute of Archaeology of Uzbekistan have revealed a new settlement (sectors **AC1** and **AC2**) over a wide terrace located to the East of **Tchinguiz Tepe**, near to the ancient military quarters. The oldest archaeological

levels define a material horizon that should be —according to traditional terminology—defined as early Kushan, even Hellenistic. Upon this stratigraphy, uninterrupted remains of the settlement when the city was expanded during the Islamic period appear. The analysed samples can be dated to the Hellenistic period (TRZ145 to TRZ156, TRZ360 to TRZ364), the First Kushan period (TRZ332 to TRZ344, TRZ348 to TRZ359) and the Islamic period (TRZ313 to TRZ331 and TRZ345 to TRZ347).

Pottery dated to the Sassanian period appears mostly at **Kara Tepe** hill. There, a ceramic workshop has been excavated, located 1 km northeast from **Tchinguiz Tepe**. The kiln's structure is 3.50 m long and 0.50 to 0.60 m wide and the firing chamber is about 1 m wide. The abandonment layers are dated to the beginning of the 5th c. AD by $C^{14}$ (Ariño *et al*., 2007). The analysed Sassanian ceramics from **Kara Tepe** (Tsantini *et al*., 2007) come from several layers of the preserved space inside the kiln. Some of these layers formed immediately after the abandonment of the kiln by the collapsing of a part of the structure and others deposited once the kiln was used as a dump. Few samples were recovered during ancient excavations from another kiln structure, situated very close to the above mentioned kiln.

Hindu Eastern influences at ancient **Termez** are evidenced by the structures of Buddhist monasteries of **Kara Tepe** and **Tchinguiz Tepe**. This is a general stratigraphic sequence at the site, except in the area of the ancient military quarters where, over the levels of the Kushan period, remains of the Islamic occupation, around X-XII c. AD, have been archaeologically documented (Martínez, in this volume).

**Kampyr Tepe** is located upon the border of the river Amu Darya, 30 kms to the West from **Termez** (Figure 1). This city of 15 hectares of extension was occupied during the Hellenistic period and throughout the first phase of the Kushan period. It is surrounded by a wall with defence towers which is similar to **Tchinguiz Tepe's** fortification. Inside the city there was a citadel protected by a wall that has 4 hectares of extension. The analysed ceramic samples from **Kampyr Tepe** have been provided by the archaeologists of the Oriental Museum of Moscow. All of them (TRZ203 to TRZ242, TRZ365 to TRZ389) can be assigned to the Hellenistic and Early Kushan periods.

**Zar Tepe** is located within the delta of Sherobood, on the North-East of **Kampyr Tepe** (Figure 1). This urban site contains two possible citadels dated on the Kushan or Kushan-Sassanian periods. It is surrounded by a defence wall supported by towers and a moat of 17 hectares of extension. Pottery shards were found on surface after a superficial prospecting carried out by some of the members of our archaeological mission. The individuals TRZ243 to TRZ246 can be dated on the 1st century AD whereas TRZ247 to TRZ249 can be dated on the 2nd century AD. The rest of the samples (TRZ250 to TRZ290) are dated to the Kushan-Sassanian period.

**Tchurobkurgan** is located near of **Kampyr Tepe**, over the first terrace of the Amu Darya River (Figure 1), which is surrounded by numerous streams. In this site a Citadel has been recovered (170x175 m), built on a natural elevation over the floodplain, which was occupied from the Kushan period to the post-Mongol period. On the West of the Citadel lies the city (20 ha) which is divided into three sectors by the passage of the streams. Only some stratigraphic levels, at the northern sector, have been dated to the Kushan period, but the site was mainly occupied during the Early Middle Ages. All analysed ceramics (TRZ290 to TRZ399) are dated to the first half of the VIII c. AD.

## 3. The analytical programme and methodology

The archaeometrical study upon the total of new 109 ceramic individuals has been carried out applying chemical and mineralogical techniques. The chemical composition has been determined by X-Ray Fluorescence (XRF), and the mineralogy has been studied using X-Ray Diffraction (XRD). We still need to complete these results with SEM and OM study.

XRF was performed using a Phillips PW 2400 spectrometer with a Rh excitation source. A portion of specimens were dried at 100°C for 24 h. Major and minor elements were determined by preparing duplicate of glassy pills using 0.3 g of powdered specimen in an alkaline fusion with lithium tetraborate at 1/20 dilution. Trace elements and $Na_2O$ were determined by powdered pills made from 5 g of specimen

mixed with Elvacite agglutinating agent placed over boric acid in an aluminiumm capsule and pressed for 60 s at 200 kN. The quantification of the concentrations was obtained by using a calibration line performed with 60 International Geological Standards (Hein *et al.,* 2002). The identified elements are: identified comprised $Fe_2O_3$ (as total Fe), $Al_2O_3$, MnO, $P_2O_5$, $TiO_2$, MgO, CaO, $Na_2O$, $K_2O$, $SiO_2$, Ba, Rb, Mo, Th, Nb, Pb, Zr, Y, Sr, Sn, Ce, Co, Ga, V, Zn, W, Cu, Ni and Cr. The loss on ignition (LOI) was determined by firing 0.3 g of dried specimen at 950°C for 3 h.

XRD analyses were carried out by using the same specimens prepared for XRF. The measurements were performed using a Siemens D-500 diffractometer working with the Cu Kα radiation (λ=1.5406 Å), and graphite monochromator in the diffracted beam, at 1.2 kW (40 kV, 30 mA). Spectra were taken from 4 to 70°2Θ, at 1°2Θ/min (step size=0.05°2Θ; time=3 s). The evaluation of crystalline phases was carried out using the X'Pert program of Panalytical.

Petrographic analysis was carried out upon selected individuals by thin-sections using an Olympus BX-41 polarising microscope working under magnification between 40X and 400X. Each ceramic specimen was impregnated with epoxy resin and mounted using Loctite UV glue and sectioned using a Struers Discoplan TS. The thin sections were finished by hand using a powder abrasive until reaching a thickness of 30 micrometers in which quartz presents a grey-white first order interference colour. The observations were carried out with Olympus BX41 microscope equipped with objectives of x4, x10, x20, x40 working between 40 and 400 magnifications. Photographs were taken using a digital camera Olympus DP-70 attached to the microscope controlled by specific computer software.

JEOL JSM-840study Scanning Electron Microscope (SEM) equipped with Secondary Electron (SE) detector and Energy Dispersive X-ray Micro Analyser (EDXA) was used for the quantitative micro-chemical analysis of the paste and surface slip of several samples. The observations were performed under vacuum at the external surface of the polished sections and the secondary electron image was taken at several magnifications. The acceleration voltage was equal to 20kV and the intensity to 3x10-9 A. The preparation of the samples has been done by fixing the fresh fractures upon a standard metallic base of 1cm diameter with silicon and in order to insure the continuous conductivity between the sample and its base and to avoid the overloading of the surface, the polished sections were covered with silver and then the whole sample was covered with carbon.

## 4. General Geological description of the studied area

In the marc of provenance analyses, is very important to know the geological composition of the studied areas. According to the postulate of provenance, the intra-source variability must be smaller than the inter-source variability, which means that the pottery produced with the same or common raw materials must be much more similar chemically than the pottery produced with raw materials originated at different geological areas.

**Termez** is located in Surkhan Darya valley, which is integrated in the Afghano-Tadjic depression, limited in the east by Pamir Mountains and in the south by Hindukush mountains. Amu Darya and Surkhan Darya rivers are the main collector of Afghano-Tadjic depression and the major Aral Sea tributaries.

The basement is hercinic, formed by metamorphic and crystallitic rocks. The Mesozoic and Cenozoic sediments filling this basement are constituted by sandstones, claystones and limonite with salt levels and anhydrites. The Cretaceous is formed basically by red and grey sandstone alternating with green-grey claystone and limestone with shells. The Upper Cretaceous contains claystone, sandstone, marlstone, siltstone, limestone and gypsum. The main constituents of the Paleogene are sediments of marine phases. The lowest levels contain limestone, dolomite and gypsum, while the highest levels contain claystone, siltstone, sandstone, limestone and marlstone. The Oligocene and Neogene sediments are mainly represented by deltaic and alluvial phases composed by greyish-blue and red sandstone, siltstone and claystone; red and ochre sandstone, reddish-brown siltstone and claystone. In the Pliocene, siltstone, claystone and sandstone forms a unique sequence of considerable potential. Quaternary sediment is formed by Upper Oligocene, Miocene and Pliocene materials (Sánchez del Corral, 2009).

**Tchinguiz Tepe** is geologically formed by detritic rocks (sandstone, siltstone and claystone) from the Miocene that are very similar to the rocks grouped regionally. The lowest formation, corresponding to the Oligocene-Miocene, made up of reddish brown sandstone, siltstone and claystone (440 m of potential). The Upper Miocene: red and reddish grey sandstone, siltstone and claystone with a variable potential of between 500 m and 1300 m (Sánchez del Corral, 2009).

To improve the archeometrical study apart of the geological study using geological maps, some geological samples have been added to the work. From sector **AC2** at **Termez**, two clay sediments **G-TRZ27** and **G-TRZ28** were sampled for chemical (XRF) (Table 2) and mineralogical (XRD) analysis (Figure 2a). The clay **G-TRZ27** presents quartz, calcite, plagioclase illite-muscovite, kaolinite and chloride as predominant mineralogical phases together with few k-feldspar. The clay **G-TRZ28** contains quartz, calcite, and plagioclase as main phases together with k-feldspar, illite-muscovite, kaolinite and few hematite.

Three other specimens were selected from the wall of two different small domestic kilns at **Kampyr Tepe** to prove if raw materials used for the brick production are similar to those of the pottery from **Kampyr Tepe**. G-TRZ29 and G-TRZ30 comes from the kiln num. 5 and they correspond to an over fired brick and to the sediment covering the external surface of the kiln structure respectively. XRD analysis of **G-TRZ29** and **G-TRZ30** shows some differences in their diffractograms related to two different firing temperatures (Figure 2b). The effect of the heat due to the use as domestic kiln is obvious by the XRD spectrum of G-TRZ29, which corresponds to a brick sampled from the interior of this kiln, that is characterized by the simultaneous presence of primary phases (quartz, calcite, muscovite, plagioclase, k-feldspar) and firing phases (hematite, pyroxene and gehlenite) in its diffractogram, compared to G-TRZ30, that have been sampled from the outside of the same kiln, and characterised only by primary mineralogical phases such as quartz, calcite, chloride illite-muscovite, plagioclase and k-feldspar. Therefore the estimated temperature for G-TRZ29 is around 950-1000ºC. Finally, the XRD analysis ofthe sample **G-TRZ31** that corresponds to sediment from the surface of the domestic kiln num. 6, dated to the Seleucid period, indicates that this part of the oven was exposed to a low firing temperature because only primary mineralogical phases (quartz, calcite, plagioclase, muscovite, k-feldspar and few hematite) have been identified (Figure 2b).

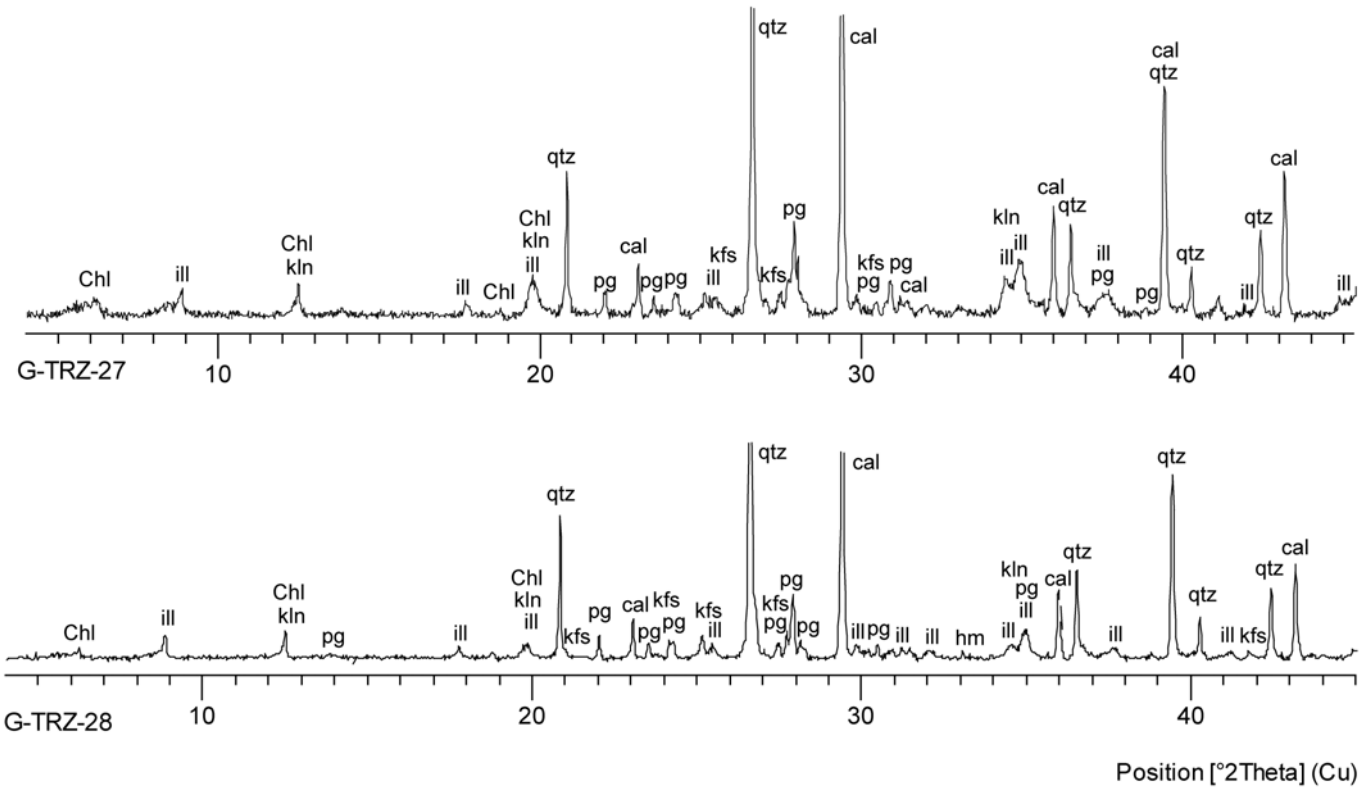


***Figure 2a:*** Diffractograms of the clay samples G-TRZ-27 and G-TRZ-28 from sector Ancient Military Quarters (Termez)

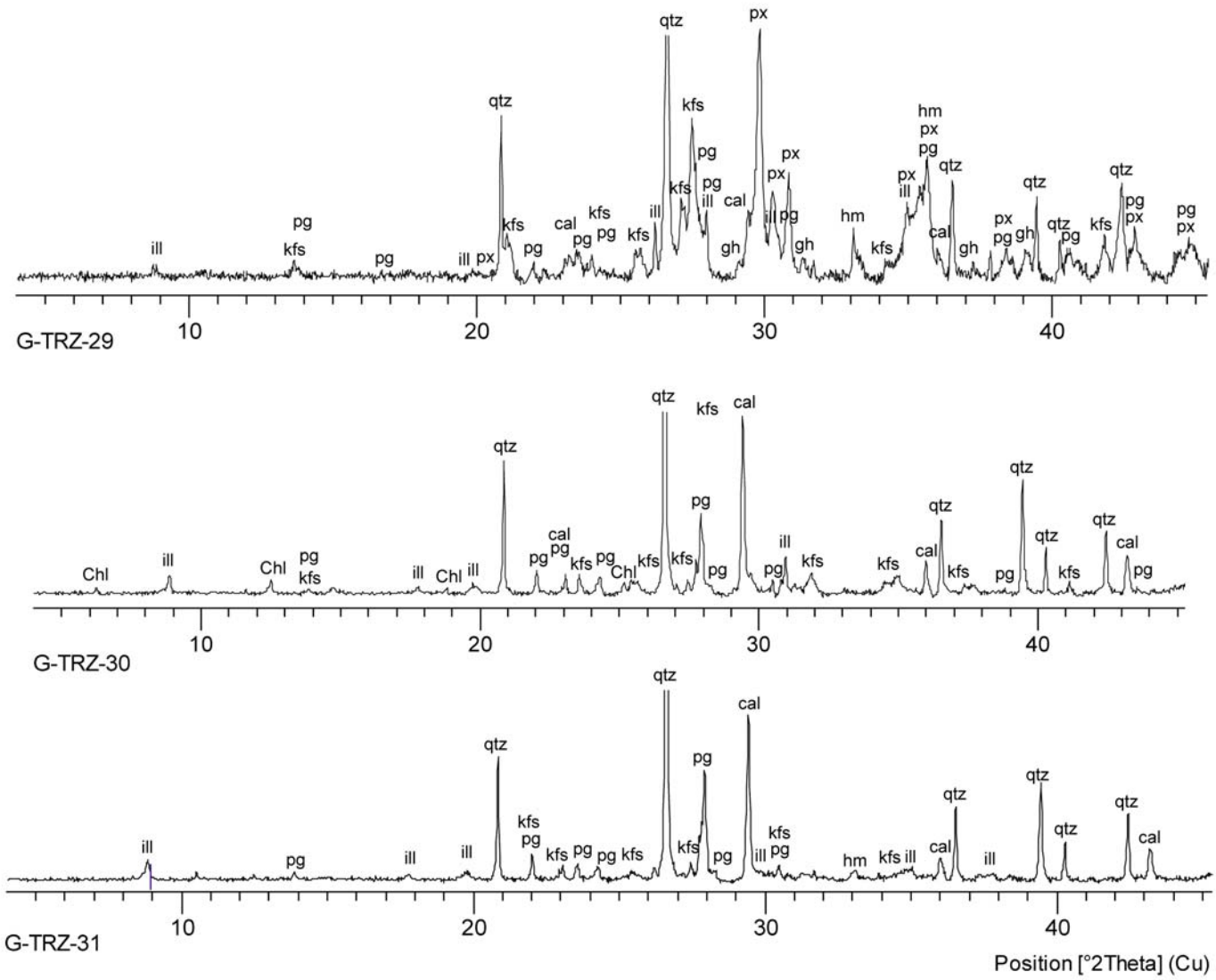


***Figure 2b:*** Diffractograms of the bricks of two domestic kilns, num. 5 (G-TRZ-29 and G-TRZ-30) amd num. 6 (G-TRZ-31) from Kampir Tepe

In order to provide data for the definition of petrographical composition of the geological substrate of the **Tchinguiz Tepe** hill, a sandstone rock fragment from the sector **AC2** was analysed by thin section analysis (Figure 3). Sandstone has been classified as litharenite with carbonate cement (sparite), although some of the sandstone types show more traces of clay than others, containing plagioclase, microcline, quartz, polycrystalline quartz and muscovite, together with some clay. There are also grains of slate which, together with muscovite, is an indicator of highly varied source areas.

A limestone fragment found at the superficial level of **Tchinguiz Tepe**, in a secondary deposition layer, was also analysed using the petrography (Figure 3). Thin section analysis shows that it is a sedimentary carbonate rock formed by calcareous foraminiferous microfossils (gastropods, miliolids, nummulites and so on).

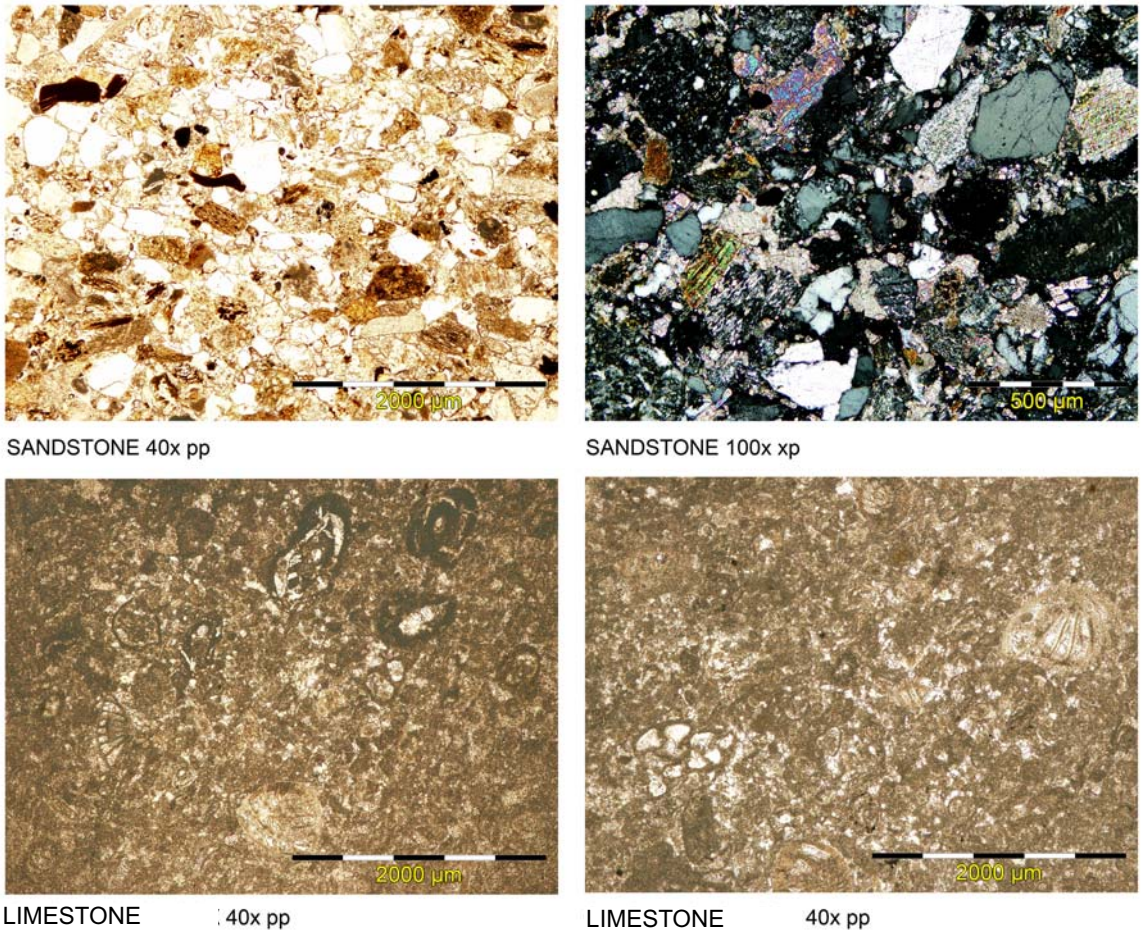


***Figure 3:*** Microphotographs by plane polars (pp) and crossed polars (xp) of the sandstone sampled at sector 2 of Ancient Military Quarters and the limestone sampled at Tchinguiz Tepe (Termez)

## 5. Ceramics from the Hellenistic-First Kushan period. Integrated results of the archaeometrical analysis

### *5.1. Termez: Sector of Ancient Military Quarter*

From the 41 samples analysed, 12 come from Ancient Military Quarter sector 1 (**AC1**: TRZ145 to TRZ156) (Gurt, 2009) and 29 from Ancient Military Quarter sector 2 (**AC2**: TRZ332 to TRZ344 and TRZ349 to TRZ364) (Martínez, in this volume).

All the analysed shards from **AC1**, except TRZ152 and TRZ156, are common wares (Table 1). Unfortunately, at present we have no absolute chronology for the two archaeological stratigraphical units (s.u. 11 and s.u. 12) from which the ceramics were sampled. Although the two stratigraphical units have a secondary character, the presence of some fragments of pottery Yuezhi, even if possibly waste materials, constitutes a reference of a relatively old material. It is important to take into account that the pottery forms of **AC1** are clear parallels appeared at the site of **Kampyr Tepe**. This fact leads to draw a chronological frame for these vessels between the Hellenistic and the First Kushan periods.

TRZ156 is a cooking ware, whereas the function of TRZ152 is still unknown. Nevertheless, it must have cooking or storage functions (Table 1). Within the variety of common wares, some rims and bases belong to cups (TRZ145, TRZ147, TRZ148, TRZ153 and TRZ154). Some cups are straight and present high vertical wall and others are wide with short walls, very similar to those found at **Kampyr Tepe**. The rest are rims and bases of plates or bowls (TRZ146, TRZ149, TRZ150 and TRZ151). Typologically, the group is formed by plates of Hellenistic tradition but attributed to productions of the tribes Yuezhi. Finally, TRZ155 could be considered a big plate (Martínez *et al*., 2009: 261). The surface of all these common wares seems to be recovered with a slip, more evident in some cases that in others. The slip is predominantly reddish (TRZ145, TRZ146, TRZ147, TRZ148, TRZ153 and TRZ153) but also greyish in three samples (TRZ149, TRZ150 and TRZ151).

Ceramics from sector 2 of Ancient Military Quarters (**AC2**) correspond to a wide range of common ceramic types (Table 1). Most of the vessels are plates, bowls, cups and jars. Most of these ceramics are totally or partially covered with a slip. Slips are mostly reddish (TRZ333, TRZ334, TRZ335, TRZ336, TRZ343, TRZ352, TRZ353, TRZ357 and TRZ360), but in some ceramics orange (TRZ339, TRZ356 and TRZ362) or brown (TRZ337, TRZ338, TRZ340, TRZ341, TRZ350 and TRZ361). In a few cases, the ceramics have been fired under reducing atmosphere and their pastes have a greyish colour (TRZ332, TRZ348, TRZ349 and TRZ358). Although so far we do not have absolute chronologies for archaeological contexts of origin of these ceramics, all of them can be attributed to the Hellenistic and First Kushan periods by their typological characteristics.

#### *5.1.1. Chemical composition (XRF analysis)*

The normalised chemical composition of 41 analysed ceramics is given in Table 2. One of the most important steps for the statistical evaluation of the chemical data is to calculate somehow the variability in the data set. One of the common ways is to calculate the Compositional Variation Matrix (CVM) (Buxeda, 1999; Buxeda and Kilikoglou, 2003), which includes the total variation and the variability that each element is introducing in the data set.

The CVM has been calculated over the 41 ceramic individuals using the subcomposition: $Fe_2O_3$ (as total Fe), $Al_2O_3$, $TiO_2$, MgO, CaO, $Na_2O$, $K_2O$, $SiO_2$, Ba, Rb, Th, Nb, Zr, Y, Sr, Ce, Ga, V, Zn, Cu, Ni and Cr. Some elements have not been considered: Mo and Sn because can introduce a false high variability in the data set due to analytical imprecision; Co and W because their values might have been altered during sample preparation process and $P_2O_5$, Pb and MnO because they are very susceptible to suffer postdepositional contaminations.

| Ic | Fe2O3 | Al2O3 | MnO | P2O5 | TiO2 | MgO | CaO | Na2O | K2O | SiO2 | Ba | Rb | Th | Nb | Pb | Zr | Y | Sr | Ce | Ga | V | Zn | Cu | Ni | Cr |
|---|---|---|---|---|---|---|---|---|---|---|---|---|---|---|---|---|---|---|---|---|---|---|---|---|---|
| **TRZ292** | 6.31 | 15.73 | 0.09 | 0.21 | 0.69 | 3.42 | 7.71 | 1.52 | 3.44 | 60.70 | 0.0597 | 0.0142 | 0.0018 | 0.0018 | 0.0024 | 0.0170 | 0.0030 | 0.0353 | 0.0063 | 0.0020 | 0.0105 | 0.0100 | 0.0038 | 0.0053 | 0.0084 |
| **TRZ293** | 6.03 | 16.81 | 0.06 | 0.16 | 0.73 | 3.73 | 1.13 | 1.59 | 4.26 | 65.33 | 0.0437 | 0.0142 | 0.0014 | 0.0018 | 0.0029 | 0.0188 | 0.0032 | 0.0152 | 0.0082 | 0.0019 | 0.0117 | 0.0118 | 0.0034 | 0.0045 | 0.0083 |
| **TRZ294** | 5.81 | 17.09 | 0.06 | 0.16 | 0.74 | 3.68 | 0.96 | 1.57 | 4.20 | 65.58 | 0.0431 | 0.0143 | 0.0014 | 0.0018 | 0.0028 | 0.0188 | 0.0032 | 0.0154 | 0.0076 | 0.0019 | 0.0121 | 0.0118 | 0.0034 | 0.0045 | 0.0087 |
| **TRZ295** | 5.77 | 17.05 | 0.06 | 0.16 | 0.75 | 3.71 | 1.00 | 1.57 | 4.21 | 65.57 | 0.0426 | 0.0144 | 0.0015 | 0.0019 | 0.0029 | 0.0187 | 0.0031 | 0.0156 | 0.0071 | 0.0020 | 0.0121 | 0.0118 | 0.0033 | 0.0046 | 0.0086 |
| **TRZ296** | 6.15 | 15.60 | 0.10 | 0.24 | 0.67 | 4.44 | 9.76 | 1.38 | 3.37 | 58.13 | 0.0446 | 0.0121 | 0.0011 | 0.0017 | 0.0025 | 0.0146 | 0.0026 | 0.0388 | 0.0046 | 0.0018 | 0.0106 | 0.0107 | 0.0030 | 0.0046 | 0.0079 |
| **TRZ097** | 6.43 | 16.01 | 0.10 | 0.21 | 0.69 | 3.57 | 10.57 | 1.44 | 3.56 | 57.24 | 0.0593 | 0.0134 | 0.0013 | 0.0016 | 0.0028 | 0.0150 | 0.0027 | 0.0364 | 0.0057 | 0.0018 | 0.0097 | 0.0093 | 0.0035 | 0.0050 | 0.0080 |
| **TRZ298** | 6.20 | 15.67 | 0.09 | 0.19 | 0.67 | 3.36 | 9.92 | 1.38 | 3.29 | 59.07 | 0.0511 | 0.0123 | 0.0013 | 0.0016 | 0.0025 | 0.0146 | 0.0024 | 0.0369 | 0.0049 | 0.0018 | 0.0103 | 0.0091 | 0.0031 | 0.0045 | 0.0075 |
| **TRZ299** | 5.81 | 14.65 | 0.10 | 0.20 | 0.64 | 3.19 | 11.84 | 1.45 | 3.10 | 58.85 | 0.0534 | 0.0121 | 0.0011 | 0.0016 | 0.0022 | 0.0153 | 0.0025 | 0.0372 | 0.0059 | 0.0017 | 0.0091 | 0.0088 | 0.0030 | 0.0046 | 0.0069 |
| **TRZ300** | 6.24 | 15.55 | 0.10 | 0.40 | 0.66 | 3.90 | 11.83 | 1.49 | 3.20 | 56.46 | 0.0475 | 0.0123 | 0.0014 | 0.0016 | 0.0018 | 0.0148 | 0.0027 | 0.0383 | 0.0060 | 0.0019 | 0.0098 | 0.0111 | 0.0036 | 0.0050 | 0.0076 |
| **TRZ301** | 6.29 | 15.83 | 0.11 | 0.26 | 0.68 | 3.73 | 9.16 | 1.67 | 3.36 | 58.73 | 0.0563 | 0.0125 | 0.0014 | 0.0016 | 0.0025 | 0.0150 | 0.0025 | 0.0376 | 0.0048 | 0.0018 | 0.0090 | 0.0103 | 0.0035 | 0.0048 | 0.0078 |
| **TRZ302** | 6.22 | 15.66 | 0.10 | 0.25 | 0.67 | 3.95 | 11.00 | 1.30 | 3.38 | 57.30 | 0.0467 | 0.0128 | 0.0012 | 0.0017 | 0.0026 | 0.0153 | 0.0026 | 0.0400 | 0.0062 | 0.0018 | 0.0094 | 0.0104 | 0.0031 | 0.0048 | 0.0076 |
| **TRZ303** | 6.53 | 16.18 | 0.11 | 0.25 | 0.68 | 3.96 | 11.06 | 1.36 | 3.36 | 56.35 | 0.0485 | 0.0129 | 0.0012 | 0.0016 | 0.0026 | 0.0147 | 0.0025 | 0.0406 | 0.0044 | 0.0018 | 0.0103 | 0.0105 | 0.0036 | 0.0048 | 0.0077 |
| **TRZ304** | 6.06 | 15.50 | 0.10 | 0.24 | 0.67 | 3.82 | 11.21 | 1.25 | 3.54 | 57.42 | 0.0500 | 0.0131 | 0.0012 | 0.0017 | 0.0025 | 0.0152 | 0.0027 | 0.0439 | 0.0050 | 0.0018 | 0.0102 | 0.0108 | 0.0033 | 0.0049 | 0.0074 |
| **TRZ305** | 5.89 | 15.73 | 0.08 | 0.30 | 0.73 | 3.04 | 5.84 | 1.72 | 3.86 | 62.64 | 0.0506 | 0.0120 | 0.0013 | 0.0017 | 0.0029 | 0.0166 | 0.0025 | 0.0307 | 0.0055 | 0.0017 | 0.0099 | 0.0065 | 0.0025 | 0.0045 | 0.0076 |
| **TRZ306** | 6.15 | 15.26 | 0.11 | 0.19 | 0.69 | 3.88 | 10.35 | 1.50 | 3.16 | 58.55 | 0.0585 | 0.0130 | 0.0014 | 0.0018 | 0.0028 | 0.0167 | 0.0027 | 0.0344 | 0.0078 | 0.0019 | 0.0084 | 0.0100 | 0.0038 | 0.0050 | 0.0083 |
| **TRZ307** | 6.32 | 15.96 | 0.10 | 0.21 | 0.67 | 3.97 | 10.92 | 1.41 | 3.29 | 56.97 | 0.0502 | 0.0131 | 0.0012 | 0.0016 | 0.0023 | 0.0149 | 0.0025 | 0.0378 | 0.0061 | 0.0018 | 0.0101 | 0.0099 | 0.0031 | 0.0049 | 0.0077 |
| **TRZ309** | 6.46 | 17.39 | 0.07 | 0.17 | 0.79 | 3.73 | 2.28 | 1.51 | 4.29 | 63.13 | 0.0534 | 0.0150 | 0.0015 | 0.0019 | 0.0035 | 0.0188 | 0.0034 | 0.0198 | 0.0069 | 0.0020 | 0.0133 | 0.0139 | 0.0039 | 0.0058 | 0.0100 |
| **TRZ310** | 6.38 | 16.56 | 0.08 | 0.21 | 0.70 | 3.32 | 10.86 | 1.16 | 3.50 | 57.04 | 0.0401 | 0.0141 | 0.0013 | 0.0015 | 0.0024 | 0.0160 | 0.0026 | 0.0622 | 0.0059 | 0.0020 | 0.0108 | 0.0098 | 0.0031 | 0.0045 | 0.0075 |
| **TRZ311** | 5.99 | 15.36 | 0.12 | 0.24 | 0.67 | 4.38 | 6.41 | 1.50 | 3.64 | 61.53 | 0.0491 | 0.0101 | 0.0013 | 0.0016 | 0.0026 | 0.0152 | 0.0026 | 0.0538 | 0.0048 | 0.0016 | 0.0092 | 0.0106 | 0.0031 | 0.0046 | 0.0080 |
| **TRZ312** | 6.00 | 15.18 | 0.09 | 0.22 | 0.66 | 3.83 | 11.58 | 1.35 | 3.34 | 57.59 | 0.0459 | 0.0127 | 0.0012 | 0.0016 | 0.0025 | 0.0149 | 0.0025 | 0.0427 | 0.0062 | 0.0018 | 0.0099 | 0.0105 | 0.0033 | 0.0047 | 0.0076 |
| **TRZ313** | 6.20 | 15.66 | 0.10 | 0.27 | 0.69 | 3.46 | 9.84 | 1.46 | 3.20 | 58.82 | 0.0525 | 0.0134 | 0.0017 | 0.0018 | 0.1341 | 0.0165 | 0.0032 | 0.0366 | 0.0061 | 0.0028 | 0.0096 | 0.0109 | 0.0062 | 0.0048 | 0.0078 |
| **TRZ314** | 5.98 | 15.49 | 0.10 | 0.20 | 0.70 | 3.48 | 10.08 | 1.39 | 3.08 | 58.64 | 0.0466 | 0.0099 | 0.0016 | 0.0017 | 0.6667 | 0.0176 | 0.0042 | 0.0339 | 0.0044 | 0.0065 | 0.0099 | 0.0103 | 0.0353 | 0.0053 | 0.0077 |
| **TRZ315** | 7.44 | 12.97 | 0.13 | 0.18 | 0.70 | 7.66 | 20.34 | 1.76 | 0.75 | 47.86 | 0.0214 | 0.0063 | 0.0012 | 0.0018 | 0.0426 | 0.0130 | 0.0022 | 0.0391 | 0.0035 | 0.0021 | 0.0100 | 0.0100 | 0.0099 | 0.0278 | 0.0165 |
| **TRZ316** | 6.18 | 15.57 | 0.10 | 0.28 | 0.71 | 3.23 | 9.93 | 1.40 | 3.14 | 58.95 | 0.0472 | 0.0108 | 0.0017 | 0.0018 | 0.3370 | 0.0175 | 0.0036 | 0.0381 | 0.0049 | 0.0043 | 0.0093 | 0.0109 | 0.0074 | 0.0047 | 0.0077 |
| **TRZ317** | 5.26 | 14.38 | 0.09 | 0.17 | 0.60 | 3.10 | 12.17 | 1.66 | 2.82 | 59.56 | 0.0562 | 0.0125 | 0.0018 | 0.0017 | 0.0017 | 0.0157 | 0.0026 | 0.0385 | 0.0063 | 0.0019 | 0.0089 | 0.0089 | 0.0037 | 0.0045 | 0.0075 |
| **TRZ318** | 6.48 | 15.59 | 0.12 | 0.17 | 0.67 | 3.55 | 13.60 | 1.92 | 2.45 | 55.27 | 0.0594 | 0.0096 | 0.0019 | 0.0018 | 0.0013 | 0.0152 | 0.0028 | 0.0321 | 0.0048 | 0.0021 | 0.0099 | 0.0104 | 0.0032 | 0.0056 | 0.0080 |
| **TRZ319** | 6.74 | 18.12 | 0.06 | 0.17 | 0.84 | 2.20 | 1.68 | 1.89 | 3.34 | 64.80 | 0.0374 | 0.0154 | 0.0018 | 0.0017 | 0.0023 | 0.0192 | 0.0032 | 0.0185 | 0.0068 | 0.0022 | 0.0150 | 0.0105 | 0.0035 | 0.0039 | 0.0098 |
| **TRZ320** | 4.42 | 18.66 | 0.06 | 0.09 | 0.66 | 1.38 | 3.51 | 1.09 | 3.66 | 66.29 | 0.0608 | 0.0184 | 0.0021 | 0.0020 | 0.0020 | 0.0207 | 0.0034 | 0.0227 | 0.0075 | 0.0023 | 0.0107 | 0.0050 | 0.0026 | 0.0035 | 0.0082 |
| **TRZ321** | 6.15 | 15.17 | 0.10 | 0.17 | 0.66 | 3.35 | 13.22 | 1.62 | 2.90 | 56.46 | 0.0569 | 0.0126 | 0.0016 | 0.0018 | 0.0033 | 0.0167 | 0.0028 | 0.0353 | 0.0056 | 0.0020 | 0.0093 | 0.0085 | 0.0033 | 0.0053 | 0.0077 |
| **TRZ322** | 5.95 | 15.36 | 0.09 | 0.24 | 0.67 | 3.34 | 11.48 | 1.37 | 3.12 | 58.04 | 0.0520 | 0.0132 | 0.0015 | 0.0018 | 0.1401 | 0.0172 | 0.0033 | 0.0433 | 0.0062 | 0.0028 | 0.0091 | 0.0106 | 0.0086 | 0.0047 | 0.0105 |
| **TRZ323** | 3.38 | 20.77 | 0.03 | 0.10 | 0.90 | 0.76 | 2.72 | 0.74 | 3.71 | 66.76 | 0.0299 | 0.0175 | 0.0020 | 0.0021 | 0.0013 | 0.0227 | 0.0034 | 0.0211 | 0.0086 | 0.0023 | 0.0110 | 0.0023 | 0.0033 | 0.0033 | 0.0082 |
| **TRZ324** | 6.38 | 16.06 | 0.10 | 0.26 | 0.70 | 3.59 | 9.97 | 1.46 | 3.24 | 57.90 | 0.0544 | 0.0138 | 0.0016 | 0.0019 | 0.1484 | 0.0165 | 0.0032 | 0.0377 | 0.0062 | 0.0031 | 0.0092 | 0.0110 | 0.0091 | 0.0052 | 0.0080 |
| **TRZ325** | 6.08 | 15.46 | 0.10 | 0.33 | 0.66 | 3.67 | 10.28 | 1.39 | 3.18 | 54.89 | 0.0382 | 0.0002 | 0.0011 | 0.0017 | 3.5528 | 0.0194 | 0.0099 | 0.0352 | 0.0035 | 0.0278 | 0.0101 | 0.0142 | 0.2173 | 0.0088 | 0.0072 |
| **TRZ326** | 4.93 | 12.69 | 0.09 | 0.20 | 0.59 | 2.95 | 19.75 | 1.61 | 1.45 | 54.92 | 0.0376 | 0.0036 | 0.0013 | 0.0017 | 0.6615 | 0.0191 | 0.0038 | 0.0462 | 0.0028 | 0.0062 | 0.0083 | 0.0092 | 0.0093 | 0.0056 | 0.0068 |
| **TRZ327** | 5.97 | 15.07 | 0.11 | 0.26 | 0.67 | 3.50 | 12.92 | 1.32 | 3.08 | 56.89 | 0.0515 | 0.0136 | 0.0018 | 0.0018 | 0.0307 | 0.0166 | 0.0029 | 0.0554 | 0.0049 | 0.0022 | 0.0090 | 0.0106 | 0.0045 | 0.0047 | 0.0070 |
| **TRZ328** | 6.52 | 16.26 | 0.11 | 0.27 | 0.71 | 3.66 | 9.98 | 1.31 | 3.39 | 57.08 | 0.0498 | 0.0114 | 0.0020 | 0.0019 | 0.5346 | 0.0169 | 0.0041 | 0.0420 | 0.0058 | 0.0058 | 0.0103 | 0.0116 | 0.0050 | 0.0059 | 0.0078 |
| **TRZ329** | 6.05 | 15.13 | 0.11 | 0.23 | 0.70 | 3.33 | 11.39 | 1.38 | 3.10 | 58.24 | 0.0496 | 0.0130 | 0.0018 | 0.0018 | 0.1593 | 0.0170 | 0.0033 | 0.0486 | 0.0053 | 0.0030 | 0.0090 | 0.0105 | 0.0069 | 0.0046 | 0.0072 |
| **TRZ330** | 6.05 | 15.15 | 0.10 | 0.17 | 0.67 | 3.51 | 12.06 | 1.98 | 2.78 | 57.36 | 0.0519 | 0.0114 | 0.0019 | 0.0018 | 0.0013 | 0.0165 | 0.0028 | 0.0326 | 0.0064 | 0.0020 | 0.0091 | 0.0090 | 0.0026 | 0.0052 | 0.0072 |
| **TRZ331** | 7.05 | 17.64 | 0.12 | 0.20 | 0.76 | 3.60 | 7.94 | 1.42 | 3.67 | 57.27 | 0.0547 | 0.0158 | 0.0020 | 0.0019 | 0.1434 | 0.0169 | 0.0038 | 0.0300 | 0.0072 | 0.0033 | 0.0113 | 0.0120 | 0.0054 | 0.0057 | 0.0085 |

***Table 2:*** The normalised chemical composition of the analysed ceramic material from Termez, Kampyr Tepe and Tchurobkurgan

| Ic | Fe2O3 | Al2O3 | MnO | P2O5 | TiO2 | MgO | CaO | Na2O | K2O | SiO2 | Ba | Rb | Th | Nb | Pb | Zr | Y | Sr | Ce | Ga | V | Zn | Cu | Ni | Cr |
|---|---|---|---|---|---|---|---|---|---|---|---|---|---|---|---|---|---|---|---|---|---|---|---|---|---|
| **TRZ332** | 6.36 | 16.07 | 0.09 | 0.21 | 0.69 | 3.42 | 10.54 | 1.34 | 3.25 | 57.85 | 0.0573 | 0.0148 | 0.0018 | 0.0017 | 0.0025 | 0.0159 | 0.0029 | 0.0385 | 0.0066 | 0.0021 | 0.0110 | 0.0105 | 0.0036 | 0.0057 | 0.0083 |
| **TRZ333** | 6.71 | 16.63 | 0.10 | 0.19 | 0.69 | 3.33 | 8.57 | 1.19 | 3.45 | 58.95 | 0.0541 | 0.0154 | 0.0017 | 0.0018 | 0.0028 | 0.0159 | 0.0029 | 0.0375 | 0.0056 | 0.0021 | 0.0114 | 0.0102 | 0.0044 | 0.0053 | 0.0082 |
| **TRZ334** | 6.68 | 16.43 | 0.11 | 0.19 | 0.70 | 3.82 | 9.27 | 1.29 | 3.23 | 58.08 | 0.0552 | 0.0142 | 0.0016 | 0.0018 | 0.0023 | 0.0163 | 0.0029 | 0.0389 | 0.0066 | 0.0022 | 0.0108 | 0.0107 | 0.0044 | 0.0056 | 0.0082 |
| **TRZ335** | 6.04 | 15.31 | 0.11 | 0.26 | 0.69 | 3.98 | 11.00 | 1.32 | 3.08 | 58.03 | 0.0553 | 0.0133 | 0.0017 | 0.0018 | 0.0016 | 0.0166 | 0.0030 | 0.0447 | 0.0063 | 0.0019 | 0.0097 | 0.0102 | 0.0042 | 0.0052 | 0.0076 |
| **TRZ336** | 6.22 | 16.11 | 0.09 | 0.21 | 0.68 | 3.87 | 9.97 | 1.40 | 3.12 | 58.17 | 0.0490 | 0.0141 | 0.0018 | 0.0018 | 0.0008 | 0.0156 | 0.0027 | 0.0346 | 0.0067 | 0.0021 | 0.0108 | 0.0102 | 0.0034 | 0.0055 | 0.0085 |
| **TRZ337** | 5.92 | 15.65 | 0.09 | 0.21 | 0.63 | 3.91 | 10.33 | 1.55 | 2.91 | 58.63 | 0.0511 | 0.0131 | 0.0017 | 0.0017 | 0.0025 | 0.0151 | 0.0028 | 0.0395 | 0.0049 | 0.0020 | 0.0104 | 0.0097 | 0.0034 | 0.0050 | 0.0083 |
| **TRZ338** | 6.14 | 15.95 | 0.10 | 0.21 | 0.67 | 3.76 | 9.73 | 1.61 | 2.89 | 58.77 | 0.0510 | 0.0131 | 0.0018 | 0.0018 | 0.0011 | 0.0153 | 0.0027 | 0.0354 | 0.0059 | 0.0020 | 0.0109 | 0.0099 | 0.0034 | 0.0052 | 0.0080 |
| **TRZ339** | 6.35 | 15.98 | 0.10 | 0.22 | 0.71 | 4.03 | 10.54 | 1.81 | 2.45 | 57.65 | 0.0476 | 0.0102 | 0.0018 | 0.0018 | 0.0028 | 0.0168 | 0.0028 | 0.0325 | 0.0053 | 0.0021 | 0.0098 | 0.0105 | 0.0037 | 0.0054 | 0.0079 |
| **TRZ340** | 5.74 | 15.06 | 0.10 | 0.58 | 0.63 | 3.60 | 10.69 | 1.44 | 3.00 | 58.97 | 0.0554 | 0.0136 | 0.0018 | 0.0018 | 0.0019 | 0.0154 | 0.0027 | 0.0460 | 0.0043 | 0.0020 | 0.0102 | 0.0110 | 0.0040 | 0.0049 | 0.0078 |
| **TRZ341** | 6.42 | 16.45 | 0.11 | 0.20 | 0.69 | 3.71 | 8.88 | 1.46 | 3.12 | 58.77 | 0.0584 | 0.0137 | 0.0017 | 0.0018 | 0.0021 | 0.0160 | 0.0029 | 0.0349 | 0.0063 | 0.0021 | 0.0108 | 0.0106 | 0.0040 | 0.0053 | 0.0083 |
| **TRZ342** | 7.00 | 16.75 | 0.12 | 0.22 | 0.72 | 3.63 | 9.74 | 1.12 | 3.48 | 57.03 | 0.0567 | 0.0146 | 0.0017 | 0.0018 | 0.0032 | 0.0155 | 0.0030 | 0.0436 | 0.0065 | 0.0021 | 0.0117 | 0.0117 | 0.0049 | 0.0054 | 0.0084 |
| **TRZ343** | 5.90 | 15.30 | 0.10 | 0.22 | 0.65 | 3.78 | 10.62 | 1.48 | 2.90 | 58.87 | 0.0537 | 0.0129 | 0.0016 | 0.0017 | 0.0007 | 0.0164 | 0.0028 | 0.0393 | 0.0066 | 0.0019 | 0.0104 | 0.0088 | 0.0037 | 0.0051 | 0.0080 |
| **TRZ344** | 6.42 | 16.09 | 0.11 | 0.19 | 0.71 | 3.37 | 9.65 | 1.27 | 3.31 | 58.68 | 0.0570 | 0.0143 | 0.0017 | 0.0018 | 0.0027 | 0.0163 | 0.0029 | 0.0408 | 0.0055 | 0.0021 | 0.0104 | 0.0103 | 0.0041 | 0.0051 | 0.0078 |
| **TRZ345** | 6.19 | 15.67 | 0.10 | 0.25 | 0.68 | 3.82 | 11.99 | 1.63 | 2.68 | 56.26 | 0.0500 | 0.0082 | 0.0018 | 0.0019 | 0.5621 | 0.0166 | 0.0043 | 0.0407 | 0.0061 | 0.0059 | 0.0101 | 0.0119 | 0.0065 | 0.0057 | 0.0074 |
| **TRZ346** | 5.86 | 15.21 | 0.10 | 0.22 | 0.68 | 3.49 | 10.41 | 1.54 | 2.81 | 58.78 | 0.0470 | 0.0086 | 0.0017 | 0.0018 | 0.7239 | 0.0180 | 0.0043 | 0.0340 | 0.0066 | 0.0070 | 0.0099 | 0.0107 | 0.0057 | 0.0055 | 0.0076 |
| **TRZ347** | 6.45 | 16.44 | 0.09 | 0.24 | 0.70 | 3.31 | 8.28 | 1.35 | 3.39 | 59.58 | 0.0635 | 0.0151 | 0.0017 | 0.0018 | 0.0032 | 0.0158 | 0.0029 | 0.0387 | 0.0069 | 0.0022 | 0.0108 | 0.0119 | 0.0045 | 0.0053 | 0.0080 |
| **TRZ349** | 6.11 | 15.84 | 0.10 | 0.25 | 0.68 | 3.34 | 9.06 | 1.72 | 2.96 | 59.75 | 0.0633 | 0.0120 | 0.0016 | 0.0017 | 0.0024 | 0.0161 | 0.0029 | 0.0479 | 0.0057 | 0.0021 | 0.0110 | 0.0098 | 0.0038 | 0.0050 | 0.0085 |
| **TRZ350** | 6.23 | 15.91 | 0.11 | 0.21 | 0.66 | 3.66 | 10.61 | 1.29 | 3.22 | 57.93 | 0.0540 | 0.0145 | 0.0016 | 0.0017 | 0.0028 | 0.0161 | 0.0028 | 0.0382 | 0.0052 | 0.0020 | 0.0096 | 0.0100 | 0.0035 | 0.0054 | 0.0082 |
| **TRZ351** | 5.80 | 15.00 | 0.10 | 0.25 | 0.67 | 3.08 | 10.71 | 1.36 | 3.21 | 59.63 | 0.0682 | 0.0140 | 0.0016 | 0.0018 | 0.0017 | 0.0165 | 0.0028 | 0.0430 | 0.0053 | 0.0019 | 0.0099 | 0.0085 | 0.0036 | 0.0052 | 0.0078 |
| **TRZ352** | 5.87 | 15.01 | 0.12 | 0.26 | 0.68 | 3.20 | 7.49 | 1.28 | 3.15 | 62.74 | 0.0577 | 0.0132 | 0.0017 | 0.0018 | 0.0033 | 0.0165 | 0.0027 | 0.0443 | 0.0061 | 0.0019 | 0.0103 | 0.0095 | 0.0053 | 0.0043 | 0.0074 |
| **TRZ353** | 6.02 | 15.93 | 0.13 | 0.20 | 0.70 | 3.48 | 7.86 | 1.39 | 3.24 | 60.87 | 0.0571 | 0.0139 | 0.0018 | 0.0018 | 0.0027 | 0.0163 | 0.0029 | 0.0424 | 0.0069 | 0.0020 | 0.0111 | 0.0114 | 0.0046 | 0.0049 | 0.0083 |
| **TRZ354** | 6.35 | 15.72 | 0.12 | 0.21 | 0.68 | 3.74 | 11.86 | 1.21 | 3.06 | 56.87 | 0.0561 | 0.0133 | 0.0017 | 0.0018 | 0.0024 | 0.0157 | 0.0031 | 0.0317 | 0.0065 | 0.0020 | 0.0096 | 0.0107 | 0.0042 | 0.0053 | 0.0075 |
| **TRZ355** | 5.98 | 15.29 | 0.11 | 0.20 | 0.68 | 3.11 | 8.47 | 1.18 | 3.15 | 61.66 | 0.0531 | 0.0140 | 0.0018 | 0.0019 | 0.0029 | 0.0178 | 0.0028 | 0.0380 | 0.0054 | 0.0020 | 0.0104 | 0.0100 | 0.0040 | 0.0053 | 0.0080 |
| **TRZ356** | 6.44 | 16.06 | 0.11 | 0.22 | 0.71 | 3.34 | 9.72 | 1.23 | 3.33 | 58.64 | 0.0595 | 0.0146 | 0.0019 | 0.0019 | 0.0019 | 0.0164 | 0.0027 | 0.0386 | 0.0057 | 0.0020 | 0.0106 | 0.0101 | 0.0036 | 0.0056 | 0.0083 |
| **TRZ357** | 6.90 | 16.02 | 0.08 | 0.22 | 0.74 | 3.11 | 6.64 | 1.17 | 3.34 | 61.59 | 0.0508 | 0.0133 | 0.0017 | 0.0019 | 0.0027 | 0.0167 | 0.0028 | 0.0439 | 0.0058 | 0.0019 | 0.0117 | 0.0114 | 0.0048 | 0.0045 | 0.0085 |
| **TRZ358** | 5.93 | 15.12 | 0.11 | 0.25 | 0.67 | 3.13 | 9.85 | 1.19 | 3.18 | 60.39 | 0.0519 | 0.0138 | 0.0016 | 0.0018 | 0.0026 | 0.0157 | 0.0026 | 0.0502 | 0.0058 | 0.0019 | 0.0106 | 0.0104 | 0.0039 | 0.0047 | 0.0084 |
| **TRZ359** | 6.10 | 15.41 | 0.11 | 0.21 | 0.68 | 3.09 | 10.57 | 1.24 | 3.13 | 59.28 | 0.0535 | 0.0134 | 0.0015 | 0.0018 | 0.0025 | 0.0164 | 0.0028 | 0.0401 | 0.0052 | 0.0019 | 0.0101 | 0.0097 | 0.0038 | 0.0046 | 0.0078 |
| **TRZ360** | 6.07 | 15.14 | 0.11 | 0.18 | 0.66 | 3.32 | 10.82 | 1.39 | 2.94 | 59.21 | 0.0554 | 0.0126 | 0.0018 | 0.0018 | 0.0021 | 0.0165 | 0.0027 | 0.0327 | 0.0054 | 0.0019 | 0.0091 | 0.0092 | 0.0038 | 0.0053 | 0.0078 |
| **TRZ361** | 6.51 | 16.70 | 0.11 | 0.19 | 0.68 | 3.49 | 8.30 | 1.21 | 3.35 | 59.28 | 0.0540 | 0.0150 | 0.0019 | 0.0018 | 0.0029 | 0.0154 | 0.0029 | 0.0352 | 0.0059 | 0.0020 | 0.0107 | 0.0108 | 0.0038 | 0.0052 | 0.0087 |
| **TRZ362** | 6.53 | 16.15 | 0.11 | 0.20 | 0.72 | 3.31 | 9.46 | 1.10 | 3.34 | 58.91 | 0.0498 | 0.0142 | 0.0017 | 0.0018 | 0.0030 | 0.0162 | 0.0028 | 0.0419 | 0.0046 | 0.0020 | 0.0107 | 0.0106 | 0.0041 | 0.0051 | 0.0078 |
| **TRZ363** | 6.37 | 15.29 | 0.15 | 0.22 | 0.67 | 3.31 | 12.16 | 1.26 | 3.14 | 57.25 | 0.0579 | 0.0136 | 0.0016 | 0.0018 | 0.0024 | 0.0162 | 0.0027 | 0.0519 | 0.0065 | 0.0020 | 0.0093 | 0.0086 | 0.0039 | 0.0052 | 0.0078 |
| **TRZ364** | 6.49 | 16.13 | 0.12 | 0.19 | 0.67 | 3.61 | 8.98 | 1.43 | 3.26 | 58.94 | 0.0560 | 0.0146 | 0.0017 | 0.0017 | 0.0026 | 0.0160 | 0.0027 | 0.0393 | 0.0060 | 0.0020 | 0.0098 | 0.0106 | 0.0041 | 0.0053 | 0.0081 |
| **TRZ365** | 5.94 | 15.55 | 0.09 | 0.25 | 0.69 | 3.18 | 9.65 | 1.66 | 3.36 | 59.48 | 0.0476 | 0.0131 | 0.0011 | 0.0016 | 0.0021 | 0.0182 | 0.0026 | 0.0305 | 0.0055 | 0.0019 | 0.0098 | 0.0092 | 0.0024 | 0.0039 | 0.0069 |
| **TRZ366** | 6.22 | 15.96 | 0.09 | 0.26 | 0.71 | 3.27 | 10.06 | 1.52 | 3.57 | 58.20 | 0.0408 | 0.0133 | 0.0011 | 0.0016 | 0.0024 | 0.0160 | 0.0027 | 0.0339 | 0.0052 | 0.0018 | 0.0097 | 0.0087 | 0.0029 | 0.0041 | 0.0068 |
| **TRZ367** | 6.38 | 16.32 | 0.10 | 0.19 | 0.70 | 3.30 | 7.44 | 1.62 | 3.51 | 60.30 | 0.0484 | 0.0135 | 0.0013 | 0.0017 | 0.0024 | 0.0151 | 0.0026 | 0.0262 | 0.0051 | 0.0019 | 0.0102 | 0.0100 | 0.0024 | 0.0047 | 0.0081 |
| **TRZ368** | 5.79 | 15.62 | 0.08 | 0.34 | 0.69 | 3.09 | 7.56 | 1.94 | 3.50 | 61.20 | 0.0453 | 0.0141 | 0.0015 | 0.0018 | 0.0024 | 0.0171 | 0.0029 | 0.0502 | 0.0074 | 0.0020 | 0.0098 | 0.0089 | 0.0024 | 0.0047 | 0.0085 |
| **TRZ369** | 5.70 | 14.88 | 0.08 | 0.34 | 0.68 | 3.24 | 9.00 | 1.64 | 3.37 | 60.91 | 0.0452 | 0.0121 | 0.0011 | 0.0016 | 0.0023 | 0.0188 | 0.0026 | 0.0334 | 0.0053 | 0.0017 | 0.0100 | 0.0100 | 0.0026 | 0.0038 | 0.0069 |
| **TRZ370** | 6.44 | 16.26 | 0.10 | 0.24 | 0.70 | 3.86 | 11.86 | 2.02 | 2.39 | 55.97 | 0.0451 | 0.0104 | 0.0014 | 0.0017 | 0.0018 | 0.0163 | 0.0027 | 0.0392 | 0.0063 | 0.0019 | 0.0104 | 0.0096 | 0.0031 | 0.0049 | 0.0071 |
| **TRZ371** | 6.38 | 16.52 | 0.09 | 0.33 | 0.71 | 3.49 | 9.46 | 1.31 | 3.47 | 58.07 | 0.0484 | 0.0142 | 0.0011 | 0.0016 | 0.0024 | 0.0166 | 0.0028 | 0.0316 | 0.0060 | 0.0019 | 0.0088 | 0.0107 | 0.0033 | 0.0047 | 0.0068 |
| **TRZ372** | 5.81 | 15.12 | 0.09 | 0.22 | 0.67 | 3.40 | 11.46 | 1.55 | 2.98 | 58.53 | 0.0472 | 0.0121 | 0.0012 | 0.0016 | 0.0019 | 0.0161 | 0.0025 | 0.0355 | 0.0065 | 0.0017 | 0.0086 | 0.0096 | 0.0028 | 0.0041 | 0.0064 |
| **TRZ373** | 3.65 | 10.05 | 0.06 | 0.27 | 0.46 | 1.90 | 34.39 | 1.15 | 2.60 | 45.31 | 0.0184 | 0.0093 | 0.0010 | 0.0013 | 0.0013 | 0.0143 | 0.0016 | 0.0801 | 0.0033 | 0.0013 | 0.0077 | 0.0080 | 0.0016 | 0.0018 | 0.0048 |
| **TRZ374** | 6.12 | 16.08 | 0.09 | 0.34 | 0.71 | 2.81 | 8.57 | 1.86 | 3.99 | 59.27 | 0.0398 | 0.0122 | 0.0013 | 0.0016 | 0.0022 | 0.0163 | 0.0025 | 0.0355 | 0.0053 | 0.0017 | 0.0110 | 0.0096 | 0.0030 | 0.0032 | 0.0070 |

***Table 2:*** The normalised chemical composition of the analysed ceramic material from Termez, Kampyr Tepe and Tchurobkurgan

| Ic | Fe2O3 | Al2O3 | MnO | P2O5 | TiO2 | MgO | CaO | Na2O | K2O | SiO2 | Ba | Rb | Th | Nb | Pb | Zr | Y | Sr | Ce | Ga | V | Zn | Cu | Ni | Cr |
|---|---|---|---|---|---|---|---|---|---|---|---|---|---|---|---|---|---|---|---|---|---|---|---|---|---|
| **TRZ375** | 6.29 | 15.82 | 0.10 | 0.25 | 0.70 | 3.66 | 10.22 | 1.95 | 3.82 | 57.03 | 0.0418 | 0.0125 | 0.0012 | 0.0016 | 0.0024 | 0.0161 | 0.0025 | 0.0401 | 0.0056 | 0.0017 | 0.0103 | 0.0102 | 0.0026 | 0.0045 | 0.0072 |
| **TRZ376** | 5.86 | 15.01 | 0.10 | 0.47 | 0.69 | 3.23 | 8.88 | 2.50 | 3.52 | 59.58 | 0.0452 | 0.0114 | 0.0013 | 0.0016 | 0.0023 | 0.0166 | 0.0027 | 0.0359 | 0.0074 | 0.0016 | 0.0103 | 0.0086 | 0.0020 | 0.0040 | 0.0075 |
| **TRZ377** | 5.40 | 14.10 | 0.08 | 0.26 | 0.64 | 4.94 | 9.63 | 3.54 | 3.77 | 57.47 | 0.0426 | 0.0119 | 0.0014 | 0.0017 | 0.0026 | 0.0170 | 0.0025 | 0.0561 | 0.0060 | 0.0017 | 0.0090 | 0.0123 | 0.0025 | 0.0046 | 0.0073 |
| **TRZ378** | 5.87 | 15.10 | 0.09 | 0.27 | 0.68 | 3.45 | 9.05 | 2.19 | 3.49 | 59.63 | 0.0455 | 0.0140 | 0.0016 | 0.0018 | 0.0098 | 0.0194 | 0.0030 | 0.0364 | 0.0057 | 0.0020 | 0.0102 | 0.0089 | 0.0030 | 0.0043 | 0.0071 |
| **TRZ379** | 5.74 | 14.90 | 0.09 | 0.20 | 0.66 | 3.51 | 12.26 | 2.23 | 2.86 | 57.38 | 0.0423 | 0.0110 | 0.0017 | 0.0018 | 0.0013 | 0.0190 | 0.0029 | 0.0424 | 0.0070 | 0.0019 | 0.0092 | 0.0089 | 0.0028 | 0.0046 | 0.0065 |
| **TRZ380** | 6.58 | 15.48 | 0.11 | 0.39 | 0.66 | 4.42 | 10.68 | 2.40 | 3.67 | 55.41 | 0.0506 | 0.0140 | 0.0014 | 0.0018 | 0.0024 | 0.0165 | 0.0029 | 0.0770 | 0.0056 | 0.0020 | 0.0113 | 0.0116 | 0.0025 | 0.0047 | 0.0075 |
| **TRZ381** | 5.16 | 14.15 | 0.07 | 0.48 | 0.66 | 5.97 | 9.89 | 1.72 | 3.70 | 58.05 | 0.0361 | 0.0116 | 0.0016 | 0.0017 | 0.0014 | 0.0188 | 0.0025 | 0.0374 | 0.0058 | 0.0017 | 0.0107 | 0.0106 | 0.0023 | 0.0038 | 0.0071 |
| **TRZ382** | 5.31 | 13.91 | 0.08 | 0.63 | 0.65 | 2.88 | 11.02 | 1.66 | 3.05 | 60.65 | 0.0435 | 0.0118 | 0.0017 | 0.0017 | 0.0014 | 0.0199 | 0.0028 | 0.0428 | 0.0069 | 0.0017 | 0.0085 | 0.0090 | 0.0024 | 0.0041 | 0.0064 |
| **TRZ383** | 6.30 | 16.01 | 0.09 | 0.30 | 0.66 | 4.05 | 10.84 | 1.70 | 3.66 | 56.20 | 0.0493 | 0.0144 | 0.0016 | 0.0018 | 0.0026 | 0.0162 | 0.0027 | 0.0601 | 0.0044 | 0.0021 | 0.0089 | 0.0115 | 0.0040 | 0.0052 | 0.0073 |
| **TRZ384** | 6.31 | 16.03 | 0.09 | 0.27 | 0.67 | 3.74 | 9.45 | 1.72 | 3.54 | 58.01 | 0.0515 | 0.0144 | 0.0019 | 0.0017 | 0.0020 | 0.0158 | 0.0028 | 0.0323 | 0.0067 | 0.0020 | 0.0108 | 0.0106 | 0.0032 | 0.0050 | 0.0075 |
| **TRZ385** | 5.94 | 14.98 | 0.09 | 0.22 | 0.67 | 3.54 | 12.67 | 2.15 | 2.00 | 57.59 | 0.0420 | 0.0075 | 0.0017 | 0.0017 | 0.0010 | 0.0178 | 0.0027 | 0.0344 | 0.0054 | 0.0019 | 0.0097 | 0.0094 | 0.0028 | 0.0050 | 0.0070 |
| **TRZ386** | 4.87 | 14.46 | 0.08 | 0.64 | 0.67 | 2.74 | 9.53 | 1.61 | 3.66 | 61.54 | 0.0499 | 0.0132 | 0.0013 | 0.0018 | 0.0020 | 0.0196 | 0.0029 | 0.0481 | 0.0071 | 0.0018 | 0.0096 | 0.0105 | 0.0023 | 0.0032 | 0.0068 |
| **TRZ387** | 5.67 | 14.76 | 0.09 | 0.53 | 0.68 | 3.28 | 8.24 | 1.99 | 4.10 | 60.49 | 0.0452 | 0.0129 | 0.0014 | 0.0017 | 0.0023 | 0.0183 | 0.0028 | 0.0413 | 0.0063 | 0.0018 | 0.0102 | 0.0127 | 0.0022 | 0.0042 | 0.0074 |
| **TRZ388** | 6.45 | 15.84 | 0.11 | 0.40 | 0.72 | 3.17 | 10.11 | 2.07 | 4.56 | 56.40 | 0.0454 | 0.0138 | 0.0018 | 0.0018 | 0.0024 | 0.0168 | 0.0029 | 0.0355 | 0.0067 | 0.0020 | 0.0113 | 0.0142 | 0.0034 | 0.0052 | 0.0075 |
| **TRZ389** | 6.04 | 14.89 | 0.08 | 0.98 | 0.64 | 3.47 | 10.06 | 1.98 | 4.29 | 57.38 | 0.0488 | 0.0131 | 0.0016 | 0.0017 | 0.0027 | 0.0151 | 0.0026 | 0.0547 | 0.0061 | 0.0020 | 0.0108 | 0.0125 | 0.0033 | 0.0047 | 0.0074 |
| **TRZ391** | 6.52 | 16.36 | 0.09 | 0.43 | 0.67 | 4.14 | 9.48 | 0.99 | 4.02 | 57.10 | 0.0553 | 0.0149 | 0.0018 | 0.0019 | 0.0025 | 0.0155 | 0.0030 | 0.0491 | 0.0061 | 0.0022 | 0.0114 | 0.0103 | 0.0032 | 0.0058 | 0.0086 |
| **TRZ392** | 6.09 | 15.85 | 0.09 | 0.22 | 0.68 | 3.21 | 9.65 | 1.39 | 3.40 | 59.25 | 0.0471 | 0.0145 | 0.0015 | 0.0017 | 0.0012 | 0.0180 | 0.0028 | 0.0291 | 0.0052 | 0.0020 | 0.0093 | 0.0094 | 0.0030 | 0.0045 | 0.0071 |
| **TRZ393** | 6.35 | 16.08 | 0.09 | 0.30 | 0.68 | 3.74 | 8.49 | 1.42 | 3.57 | 59.11 | 0.0413 | 0.0142 | 0.0014 | 0.0016 | 0.0017 | 0.0175 | 0.0028 | 0.0394 | 0.0059 | 0.0020 | 0.0103 | 0.0096 | 0.0032 | 0.0052 | 0.0078 |
| **TRZ394** | 5.77 | 15.34 | 0.08 | 0.33 | 0.66 | 4.13 | 7.97 | 2.81 | 3.75 | 58.96 | 0.0580 | 0.0140 | 0.0016 | 0.0017 | 0.0025 | 0.0162 | 0.0027 | 0.0479 | 0.0065 | 0.0020 | 0.0105 | 0.0097 | 0.0031 | 0.0044 | 0.0075 |
| **TRZ395** | 5.95 | 15.77 | 0.09 | 0.29 | 0.63 | 3.55 | 7.96 | 1.40 | 3.65 | 60.54 | 0.0547 | 0.0144 | 0.0018 | 0.0017 | 0.0020 | 0.0155 | 0.0028 | 0.0332 | 0.0067 | 0.0020 | 0.0099 | 0.0097 | 0.0036 | 0.0051 | 0.0082 |
| **TRZ396** | 6.44 | 15.41 | 0.11 | 0.18 | 0.68 | 3.73 | 12.56 | 1.71 | 2.90 | 56.11 | 0.0567 | 0.0123 | 0.0020 | 0.0019 | 0.0020 | 0.0166 | 0.0029 | 0.0276 | 0.0061 | 0.0020 | 0.0093 | 0.0104 | 0.0047 | 0.0060 | 0.0073 |
| **TRZ397** | 7.63 | 19.10 | 0.03 | 0.35 | 0.87 | 2.50 | 1.43 | 1.83 | 3.32 | 62.75 | 0.0443 | 0.0163 | 0.0019 | 0.0019 | 0.0023 | 0.0185 | 0.0034 | 0.0357 | 0.0057 | 0.0023 | 0.0328 | 0.0105 | 0.0025 | 0.0043 | 0.0183 |
| **TRZ398** | 6.98 | 18.36 | 0.04 | 0.26 | 0.84 | 2.31 | 2.33 | 1.50 | 3.53 | 63.65 | 0.0379 | 0.0166 | 0.0017 | 0.0020 | 0.0022 | 0.0191 | 0.0032 | 0.0328 | 0.0072 | 0.0023 | 0.0226 | 0.0114 | 0.0026 | 0.0042 | 0.0244 |
| **TRZ399** | 5.92 | 15.26 | 0.09 | 0.23 | 0.69 | 3.26 | 10.48 | 1.23 | 3.27 | 59.40 | 0.0493 | 0.0140 | 0.0016 | 0.0018 | 0.0024 | 0.0186 | 0.0030 | 0.0401 | 0.0053 | 0.0020 | 0.0099 | 0.0092 | 0.0030 | 0.0045 | 0.0070 |
| **GTRZ27** | 6.15 | 15.27 | 0.10 | 0.22 | 0.66 | 4.19 | 14.27 | 0.82 | 3.11 | 55.03 | 0.0629 | 0.0141 | 0.0018 | 0.0018 | 0.0028 | 0.0150 | 0.0028 | 0.0292 | 0.0059 | 0.0018 | 0.0120 | 0.0107 | 0.0036 | 0.0050 | 0.0081 |
| **GTRZ28** | 5.51 | 13.02 | 0.14 | 0.17 | 0.67 | 2.74 | 15.03 | 0.96 | 2.75 | 58.88 | 0.0454 | 0.0127 | 0.0018 | 0.0020 | 0.0030 | 0.0193 | 0.0025 | 0.0216 | 0.0054 | 0.0016 | 0.0095 | 0.0088 | 0.0035 | 0.0042 | 0.0070 |
| **GTRZ29** | 4.88 | 12.65 | 0.08 | 0.23 | 0.64 | 3.28 | 12.76 | 2.49 | 4.83 | 58.00 | 0.0432 | 0.0104 | 0.0016 | 0.0017 | 0.0007 | 0.0209 | 0.0028 | 0.0314 | 0.0043 | 0.0017 | 0.0080 | 0.0085 | 0.0031 | 0.0037 | 0.0061 |
| **GTRZ30** | 4.39 | 11.84 | 0.10 | 0.43 | 0.61 | 2.85 | 13.33 | 1.77 | 2.87 | 61.63 | 0.0454 | 0.0107 | 0.0013 | 0.0016 | 0.0021 | 0.0214 | 0.0025 | 0.0350 | 0.0071 | 0.0014 | 0.0083 | 0.0082 | 0.0022 | 0.0031 | 0.0073 |
| **GTRZ31** | 4.49 | 11.99 | 0.10 | 0.26 | 0.62 | 2.55 | 12.55 | 2.08 | 3.20 | 62.00 | 0.0464 | 0.0105 | 0.0015 | 0.0017 | 0.0024 | 0.0219 | 0.0026 | 0.0367 | 0.0061 | 0.0015 | 0.0082 | 0.0072 | 0.0017 | 0.0032 | 0.0073 |

***Table 2:*** The normalised chemical composition of the analysed ceramic material from Termez, Kampyr Tepe and Tchurobkurgan

The total variation (vt) in this data set according to the CVM (Table 3a) is very low (0.1855), which generally indicates an homogeneous composition. The variability introduced by all the elements is relatively low, although $Na_2O_3$ ($\tau._{Na2O3}$ = 0.615), CaO ($\tau._{CaO}$ = 0.604), Cu ($\tau._{Cu}$ = 0.574), Ce ($\tau._{Ce}$ = 0.550), Sr ($\tau._{Sr}$ = 0.538) and Ba ($\tau._{Ba}$ = 0.531) have the most variable concentrations.

The variability introduced by CaO is clearly linked to some differences in the calcareous character of the material, although all individuals were produced using calcareous clays. Nonetheless, the variability introduced by CaO, Ba and Sr could be results of the crystallisation of secondary calcite inside the pores of some vessels (Buxeda and Cau, 1995; Cau, Day, Montana, 2002), as it has been observed at TRZ148 by thin section analysis. The variability introduced mathematically by Cu cannot be trusted as it is an element that can easily present postdepositional alterations. Finally, some of the variability introduced by $Na_2O$ can be explained by the existence of a characteristic postdepositional alteration related to the formation of the Na-zeolite analcime ($Na[AlSi_2O_6]\cdot 6H_2O$), as it has been already detected in previous archaeometric works we have carried out on the pottery of **Termez** (Tsantini *et al.*, 2007; Martínez *et al*., 2008, 2009). Furthermore, relevant number of the previously analysed shards by SEM-EDX exhibit NaCl crystals. The crystallization of both minerals must be related to the same alteration and/or contamination process occurred during burial at a dessert environment, rich in salt efflorescences stemming from the emergence of salts originated in Mesozoic salt beds, due to halocinetic processes (Martínez *et al*., 2008; Sánchez del Corral, 2009). For these reasons, $Na_2O$, Ba, Sr and Cu were excluded of the statistical evaluation of the chemical data.

Repeating the same statistical routine without considering these three elements, the vt resulted of the new CVM is more lower (vt = 0.113). A total variation of that range indicates a very homogeneous data set. In geochemical terms, this range of vt points towards the same or very similar geochemical origin of the raw materials used for the production of all the analysed individuals, without this necessa-rily meaning that all of them belong into the same production. Then, the subcomposition $Fe_2O_3$, $Al_2O_3$, $TiO_2$, MgO, CaO, $K_2O$, $SiO_2$, Rb, Th, Nb, Zr, Y, Ce, Ga, V, Zn, Cu, Ni and Cr were transformed into logratios following the considerations of Aitchison (1986) and Buxeda (1999) on compositional data, where $Al_2O_3$ was used as divisor, as according to the CVM it was the element less contributing to the chemical variability (Buxeda and Kilikoglou, 2003).

The dendrogram representing the results of the cluster analysis performed using the Square Euclidean distance and the centroid algorithm with S-plus2000 (MathSoft, 1999) and $Al_2O_3$ as divisor in the logratio transformation, is presented in Figure 4. The analysed individuals are grouped forming five main groups (**AC1-A**, **AC1-B**, **AC2-A**, **AC2-B** and **AC2-C**) whereas the cooking ware TRZ152 and the possible storage jar TRZ156 remain isolated at the right side of the dendrogram. Looking at the raw chemical data, **TRZ152** and **TRZ156** differ of the rest of the vessels because they present the lowest values in MgO and Ni of all the analysed pottery. Nevertheless these two individuals present chemical differences even between them, as TRZ152 have high values in $Al_2O_3$, $Na_2O$, Ba and Sr and also the lowest value in Zn, whereas TRZ156 have high values in Ce and Cu and low values in $Fe_2O_3$, $Na_2O$, Ba, Th, Ga and Ni. On the left side of the dendrogram, the samples **TRZ339** and **TRZ357** are linked to the rest of the ceramics at a major ultra-metrical distance, which indicates some differences in their chemical composition. TRZ339 is characteristic by high $Fe_2O_3$, $TiO_2$, Nb and Zn and TRZ357 presents the highest value in MgO but low concentration in $K_2O$, $SiO_2$, Rb, Sr, Ce and V. The normalised chemical composition of the ceramic outliers **TRZ152**, **TRZ156, TRZ339 and TRZ357** is given at Table 4 and the typology of all these vessels is represented in Figure 5.

The rest of the ceramics are distributed into two main groups, **AC1** and **AC2**, which are divided in several subgroups. **AC1**, formed by samples from Ancient Military Quarter Sector 1 (u.s. 11 and 12), is composed by the subgroups **AC1-A** and **AC-1B**. Pottery belonging to **AC1-A** (TRZ147, 148, 149 and 150) are cups painted with a red slip (TRZ147 and TRZ148), plates and bowls painted with a grey slip (TRZ149 and TRZ150). These individuals are middle-calcareous, with high $Al_2O_3$, Th and Cr values and low Zr relative content. The subgroup **AC1-B** is formed by cups (TRZ145, 153 and 154) and one plate (TRZ146) painted with a red slip, one bowl painted with a grey slip (TRZ151) and one big plate painted

| (AC) | $Fe_2O_3$ | $Al_2O_3$ | $TiO_2$ | MgO | CaO | $Na_2O$ | $K_2O$ | $SiO_2$ | Ba | Rb | Th | Nb | Zr | Y | Sr | Ce | Ga | V | Zn | Cu | Ni | Cr |
|---|---|---|---|---|---|---|---|---|---|---|---|---|---|---|---|---|---|---|---|---|---|---|
| $\tau_{\cdot i}$ | 0.224 | 0.204 | 0.212 | 0.397 | 0.604 | 0.615 | 0.267 | 0.219 | 0.531 | 0.289 | 0.441 | 0.443 | 0.236 | 0.343 | 0.538 | 0.550 | 0.261 | 0.299 | 0.306 | 0.574 | 0.375 | 0.235 |
| $vt/\tau_{\cdot i}$ | 0.830 | 0.907 | 0.875 | 0.467 | 0.307 | 0.302 | 0.695 | 0.847 | 0.350 | 0.641 | 0.421 | 0.418 | 0.787 | 0.540 | 0.345 | 0.337 | 0.711 | 0.621 | 0.607 | 0.323 | 0.495 | 0.788 |
| $r_{v,\tau}$ | 0.973 | 0.983 | 0.966 | 0.686 | 0.673 | 0.677 | 0.862 | 0.939 | 0.631 | 0.952 | 0.776 | 0.685 | 0.947 | 0.681 | 0.732 | 0.878 | 0.816 | 0.884 | 0.940 | 0.779 | 0.765 | 0.924 |
| vt | 0.185 | | | | | | | | | | | | | | | | | | | | | |

***Table 3a:*** Compositional Variation Matrix (CVM) calculated upon the 41 ceramics from the Hellenistic and First Kushan periods sampled at **Ancient Military Quarters** (Termez)

| (KT) | $Fe_2O_3$ | $Al_2O_3$ | $TiO_2$ | MgO | CaO | $Na_2O$ | $K_2O$ | $SiO_2$ | Ba | Rb | Th | Nb | Zr | Y | Sr | Ce | Ga | V | Zn | Cu | Ni | Cr |
|---|---|---|---|---|---|---|---|---|---|---|---|---|---|---|---|---|---|---|---|---|---|---|
| $\tau_{\cdot i}$ | 0.454 | 0.408 | 0.396 | 0.653 | 1.751 | 1.017 | 0.707 | 0.423 | 0.681 | 0.588 | 0.614 | 0.419 | 0.556 | 0.403 | 1.733 | 0.852 | 0.428 | 0.477 | 0.580 | 0.775 | 0.753 | 0.434 |
| $vt/\tau_{\cdot i}$ | 0.756 | 0.841 | 0.868 | 0.526 | 0.196 | 0.337 | 0.485 | 0.812 | 0.504 | 0.584 | 0.559 | 0.818 | 0.617 | 0.851 | 0.198 | 0.403 | 0.802 | 0.720 | 0.592 | 0.443 | 0.456 | 0.791 |
| $r_{v,\tau}$ | 0.973 | 0.988 | 0.994 | 0.970 | 0.004 | 0.876 | 0.949 | 0.980 | 0.964 | 0.962 | 0.981 | 0.985 | 0.911 | 0.994 | -0.164 | 0.969 | 0.986 | 0.994 | 0.979 | 0.941 | 0.946 | 0.987 |
| vt | 0.343 | | | | | | | | | | | | | | | | | | | | | |

***Table 3b:*** Compositional Variation Matrix (CVM) calculated upon the 65 ceramics from the Hellenistic and First Kushan periods sampled at **Kampyr Tepe**

| (AC&KT) | $Fe_2O_3$ | $Al_2O_3$ | $TiO_2$ | MgO | CaO | $Na_2O$ | $K_2O$ | $SiO_2$ | Ba | Rb | Th | Nb | Zr | Y | Sr | Ce | Ga | V | Zn | Cu | Ni | Cr |
|---|---|---|---|---|---|---|---|---|---|---|---|---|---|---|---|---|---|---|---|---|---|---|
| $\tau_{\cdot i}$ | 0.460 | 0.423 | 0.422 | 0.650 | 1.424 | 1.604 | 0.760 | 0.445 | 0.825 | 0.565 | 0.886 | 0.521 | 0.583 | 0.476 | 1.377 | 0.867 | 0.475 | 0.501 | 0.588 | 1.413 | 0.782 | 0.493 |
| $vt/\tau_{\cdot i}$ | 0.817 | 0.888 | 0.892 | 0.578 | 0.264 | 0.234 | 0.495 | 0.845 | 0.456 | 0.665 | 0.424 | 0.721 | 0.645 | 0.789 | 0.273 | 0.433 | 0.792 | 0.750 | 0.639 | 0.266 | 0.481 | 0.763 |
| $r_{v,\tau}$ | 0.960 | 0.988 | 0.991 | 0.957 | 0.572 | 0.681 | 0.871 | 0.970 | 0.842 | 0.975 | 0.783 | 0.970 | 0.826 | 0.974 | 0.541 | 0.929 | 0.956 | 0.989 | 0.951 | 0.818 | 0.831 | 0.928 |
| vt | 0.376 | | | | | | | | | | | | | | | | | | | | | |

***Table 3c:*** Compositional Variation Matrix (CVM) calculated upon the 111 ceramics and sediments from the Hellenistic and First Kushan periods sampled at **Ancient Military Quarters** (Termez) and **Kampyr Tepe**

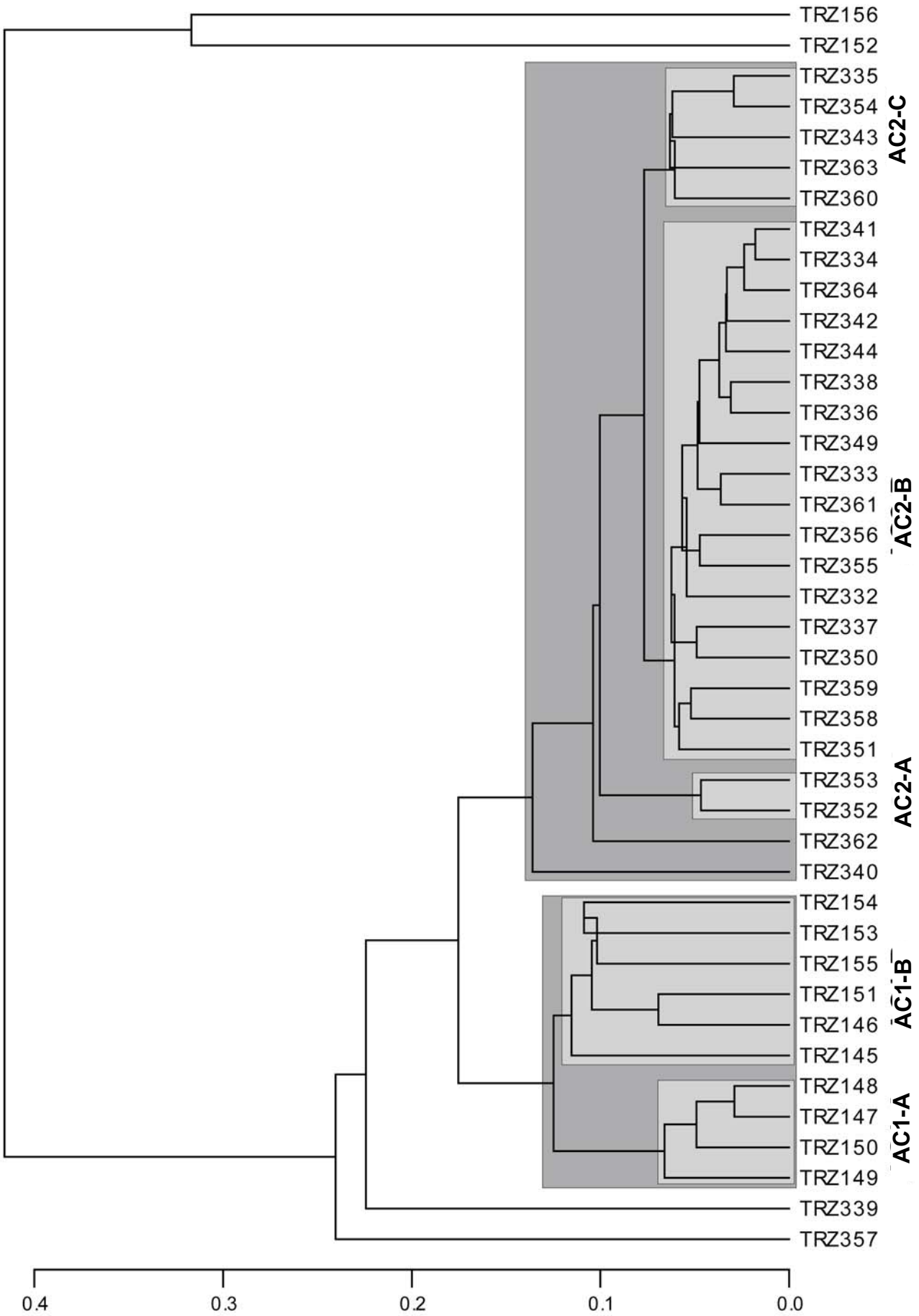


***Figure 4:*** Dendrogram resulted from the cluster analysis performed on the subcomposition $Fe_2O_3$, $TiO_2$, MgO, CaO, $K_2O$, $SiO_2$, Rb, Th, Nb, Zr, Y, Ce, Ga, V, Zn, Cu, Ni, Cr and $Al_2O_3$ used as divisor of 41 individuals sampled at sector Ancient Military Quarters (Termez), using the Square Euclidean distance and the centroid algorithm

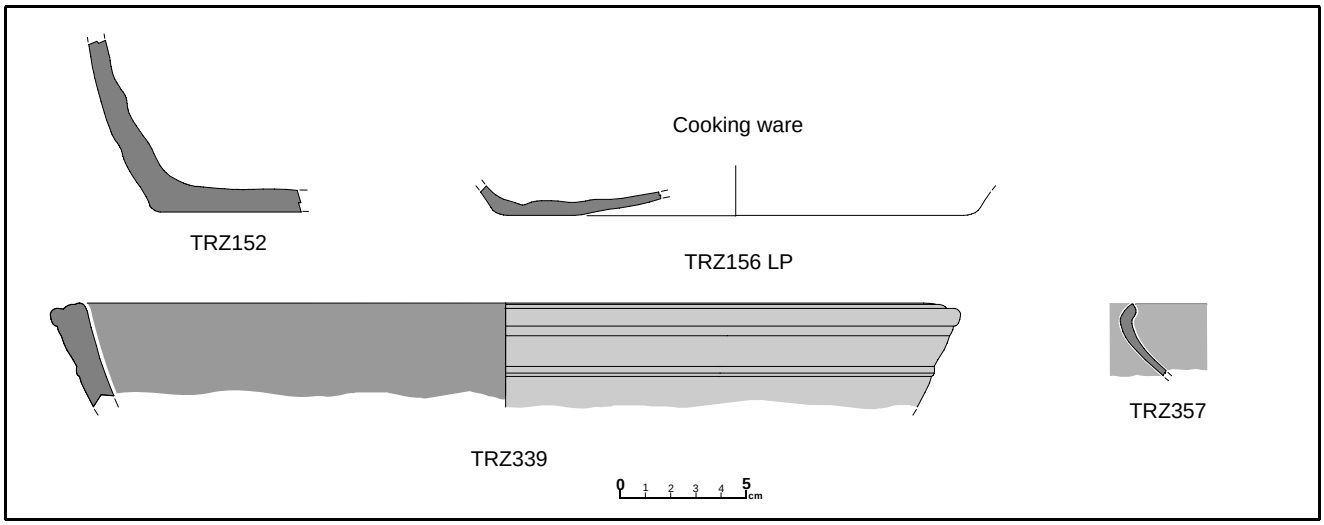


***Figure 5:*** Typology of the ceramic outliers of sectors **AC1** and **AC2** from Ancient Military Quarters (TRZ152, TRZ156, TRZ339 and TRZ357)

with a yellowish slip and incised decoration (TRZ155). All these ceramics are calcareous with low V relative content. The mean chemical composition and the standard deviation of **AC1-A** and **AC1-B** are given in Table 4. The typologies of the vessels belonging to these subgroups are presented in Figure 6. Due to the luck recovered pottery workshops in the area of the Ancient Military Quarters and to the impossibility to archaeologically relate these individuals to any kiln **AC1-A** and **AC1-B** must be considered as PCRU (Paste Compositional Reference Units) of the Hellenistic and First Kushan pottery production of the Antique Military Quarter's sector 1 of **Termez**.

The samples taken from Ancient Military Quarter sector 2 are grouped in **AC2**, except **TRZ339** and **TRZ357. AC2** can be divided into three subgroups (**AC2-A**, **AC2-B** and **AC2-C**) (look at the chemical differences at Table 4). **AC2-A** is formed by two middle-calcareous plates painted with a red slip (TRZ352 and TRZ353) from the u.s. 20. **AC2-B** is the most important subgroup because of the respectively high number and variety of ceramics from u.s. 17, 20, 22 and 28. Contains 10 bowls, plates and jars painted with a reddish or brownish slip (TRZ333, TRZ334, TRZ336, TRZ337, TRZ338, TRZ341, TRZ350, TRZ355, TRZ356 and TRZ361), one painted bowl with a greyish slip (TRZ358) and some unpainted common wares (TRZ332 and TRZ349 with greyish paste, TRZ342, TRZ344, TRZ351, TRZ359 and TRZ364 with clear brown paste). All these ceramics were produced with calcareous clay and their chemical composition reflects relatively higher Rb respect to the rest of the material. Finally, five vessels are grouped in the subgroup **AC2-C** (TRZ335 and TRZ343 from u.s. 17, TRZ354 from u.s. 20, TRZ360 from u.s. 28 and TRZ363 from u.s. 33). Most of them are big plates or big bowls and only TRZ363 is unpainted. All of them are calcareous ceramics with low concentration in $Al_2O_3$ and V. The mean chemical composition and the standard deviation of **AC2-A**, **AC2-B** and **AC2-C** are given in Table 4. The typologies of the vessels belonging to the three subgroups are represented in Figure 7. **AC2-A**, **AC2-B** and **AC2-C** should be as PCRU's, because they can not be attributed to any known production centre dated on the Hellenistic and the first Kushan period at **Termez**. Finally, **TRZ340** from u.s. 17 and **TRZ362** from u.s. 28 are separated from **AC2** due to slight chemical differences. Nevertheless, they have in common a slightly lower Ce relative content.

| Elements | AC1-A (n=4) | | AC1-B (n=6) | | AC2-A (n= 2) | | AC2-B (n= 18) | | AC2-C (n= 5) | | TRZ339 | TRZ357 | TRZ152 | TRZ156 |
|---|---|---|---|---|---|---|---|---|---|---|---|---|---|---|
| | m | sd | m | sd | m | sd | m | sd | m | sd | nc | nc | nc | nc |
| $Fe_2O_3$ (%) | 6.48 | 0.17 | 6.43 | 0.17 | 5.97 | 0.11 | 6.32 | 0.32 | 6.16 | 0.21 | 6.92 | 6.37 | 5.74 | 5.69 |
| $Al_2O_3$ (%) | 16.33 | 0.44 | 16.09 | 0.49 | 15.52 | 0.65 | 16.03 | 0.52 | 15.40 | 0.22 | 16.07 | 16.07 | 16.39 | 15.46 |
| $TiO_2$ (%) | 0.70 | 0.02 | 0.70 | 0.01 | 0.69 | 0.01 | 0.68 | 0.02 | 0.67 | 0.01 | 0.75 | 0.71 | 0.68 | 0.69 |
| MgO (%) | 3.37 | 0.24 | 3.35 | 0.12 | 3.35 | 0.19 | 3.49 | 0.28 | 3.64 | 0.30 | 3.12 | 4.04 | 2.29 | 2.63 |
| CaO (%) | 7.96 | 0.38 | 9.63 | 0.88 | 7.70 | 0.26 | 9.64 | 0.78 | 11.33 | 0.68 | 6. 66 | 10.57 | 8.28 | 8.88 |
| $Na_2O$ (%) | 1.10 | 0.08 | 1.21 | 0.16 | 1.34 | 0.08 | 1.34 | 0.16 | 1.34 | 0.11 | 1. 17 | 1.82 | 1.50 | 0.93 |
| $K_2O$ (%) | 3.26 | 0.06 | 3.25 | 0.07 | 3.21 | 0.06 | 3.21 | 0.17 | 3.04 | 0.10 | 3.35 | 2.46 | 3.35 | 3.35 |
| $SiO_2$ (%) | 60.61 | 0.96 | 59.16 | 0.71 | 62.02 | 1.36 | 59.10 | 1.05 | 58.24 | 1 | 61.78 | 57.84 | 61.56 | 62.20 |
| Ba (ppm) | 667 | 94 | 647 | 24 | 576 | 4 | 559 | 47 | 559 | 15 | 509 | 477 | 791 | 400 |
| Rb (ppm) | 129 | 6 | 127 | 4 | 136 | 5 | 141 | 8 | 132 | 4 | 133 | 103 | 132 | 120 |
| Th (ppm) | 22 | 1 | 20 | 2 | 17 | 1 | 17 | 1 | 17 | 1 | 17 | 18 | 19 | 15 |
| Nb (ppm) | 14 | 1 | 14 | 0 | 18 | 0 | 18 | 1 | 18 | 0 | 19 | 18 | 13 | 13 |
| Zr (ppm) | 155 | 5 | 161 | 7 | 165 | 1 | 161 | 6 | 163 | 4 | 167 | 169 | 163 | 169 |
| Y (ppm) | 23 | 1 | 24 | 1 | 28 | 2 | 28 | 1 | 29 | 2 | 28 | 28 | 23 | 25 |
| Sr (ppm) | 429 | 36 | 395 | 53 | 435 | 14 | 398 | 43 | 402 | 85 | 440 | 326 | 511 | 393 |
| Ce (ppm) | 71 | 6 | 58 | 7 | 65 | 6 | 58 | 5 | 63 | 5 | 59 | 53 | 62 | 76 |
| Ga (ppm) | 19 | 1 | 18 | 1 | 19 | 1 | 21 | 1 | 20 | 0 | 19 | 21 | 19 | 15 |
| V (ppm) | 115 | 2 | 98 | 6 | 108 | 5 | 107 | 5 | 97 | 5 | 117 | 99 | 116 | 115 |
| Zn (ppm) | 102 | 4 | 98 | 9 | 105 | 14 | 102 | 7 | 95 | 9 | 114 | 106 | 89 | 108 |
| Cu (ppm) | 40 | 8 | 45 | 4 | 50 | 5 | 39 | 4 | 39 | 2 | 48 | 38 | 42 | 54 |
| Ni (ppm) | 55 | 2 | 54 | 4 | 46 | 4 | 53 | 3 | 52 | 1 | 45 | 54 | 40 | 33 |
| Cr (ppm) | 89 | 2 | 82 | 4 | 79 | 6 | 82 | 3 | 78 | 2 | 85 | 79 | 87 | 71 |

***Table 4:*** The mean chemical composition (m) and the standard deviation (sd) using normalised data of **AC1-A**, **AC1-B**, **AC2-A**, **AC2-B** and **AC2-C** chemical groups and the raw normalised chemical composition (nc) of the ceramics outliers **TRZ339**, **TRZ357**, **TRZ152**, **TRZ156** from Ancient Military Quarters sector (**Termez**).

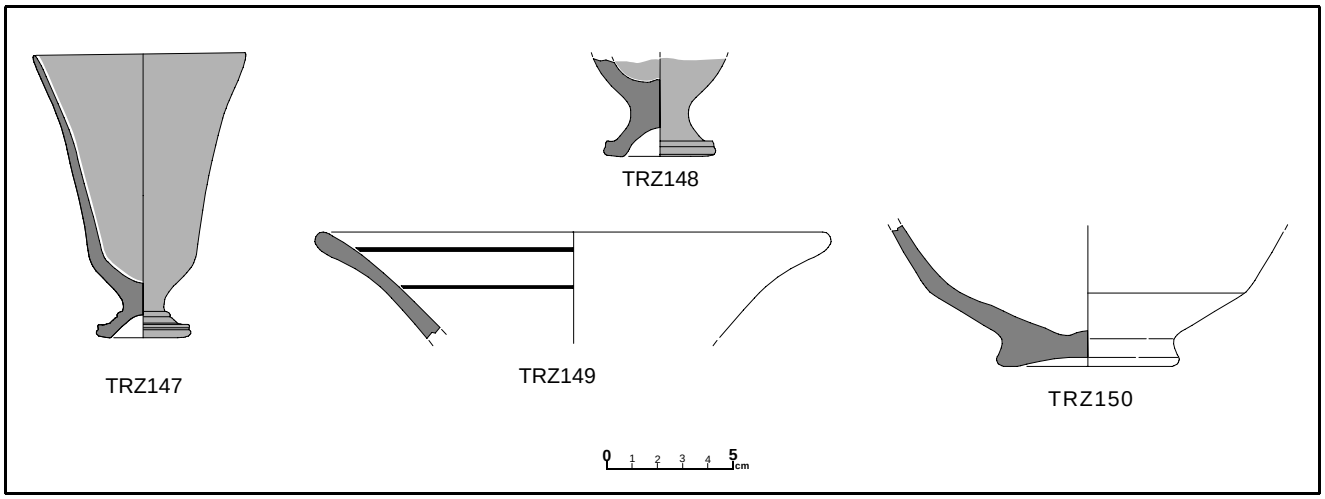


***Figure 6a:*** Typology of the **AC1-A** group (TRZ147, TRZ148, TRZ149 and TRZ150)

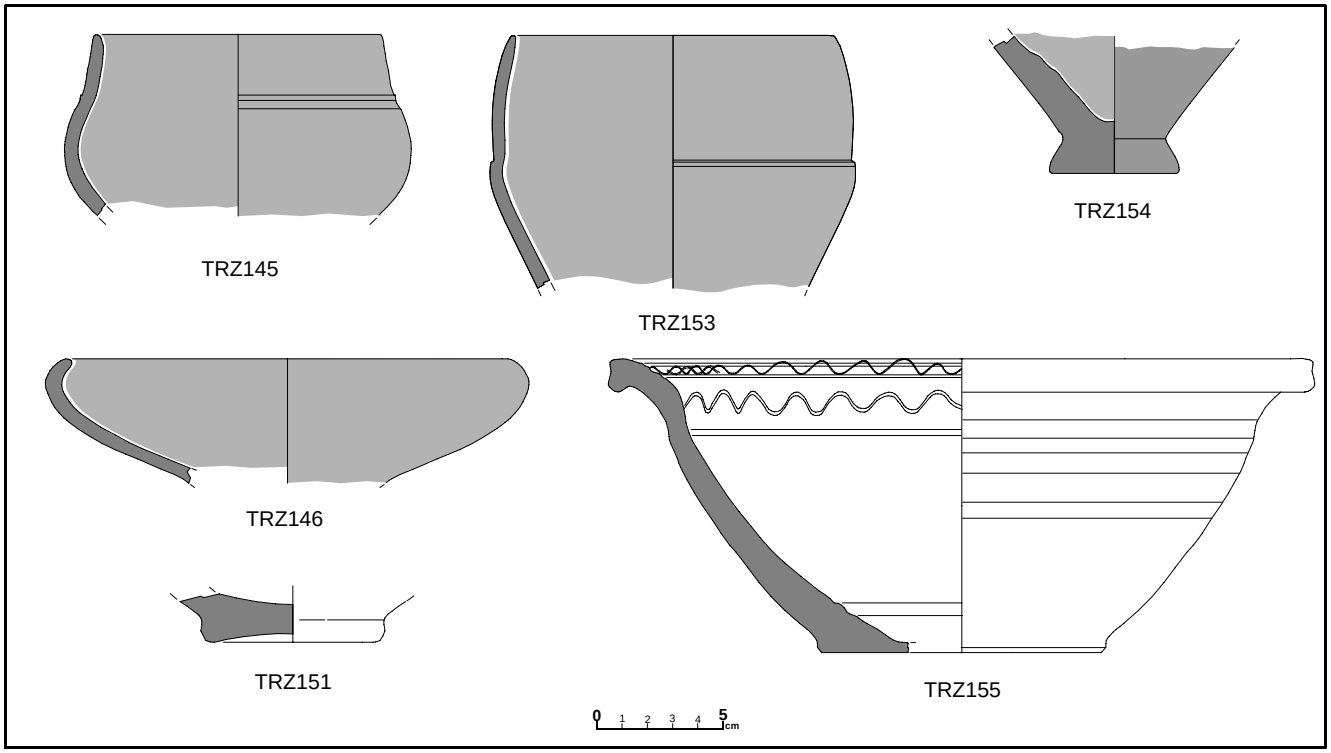


***Figure 6b:*** Typology of the **AC1-B** group (TRZ145, TRZ153, TRZ154, TRZ146, TRZ151 and TRZ155)

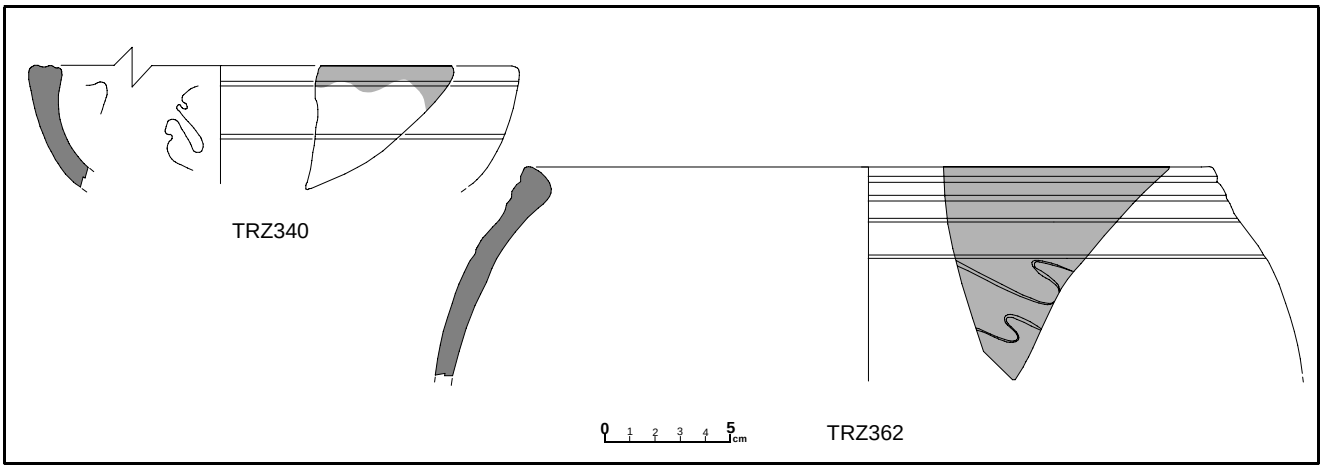


***Figure 7a:*** Typology of the two ceramic outliers similar to **AC2** group (TRZ340 and TRZ362)

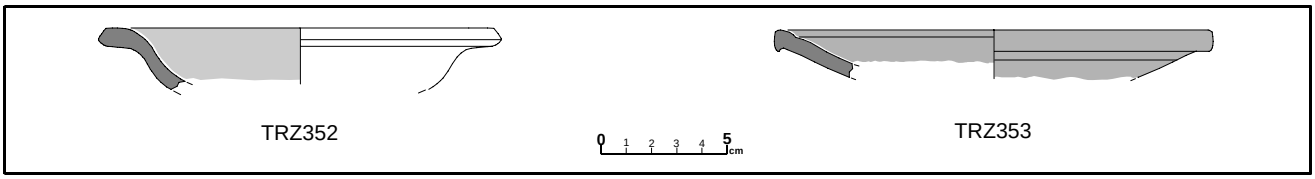


***Figure 7b:*** Typology of the **AC2-A** group (TRZ352 and TRZ353)

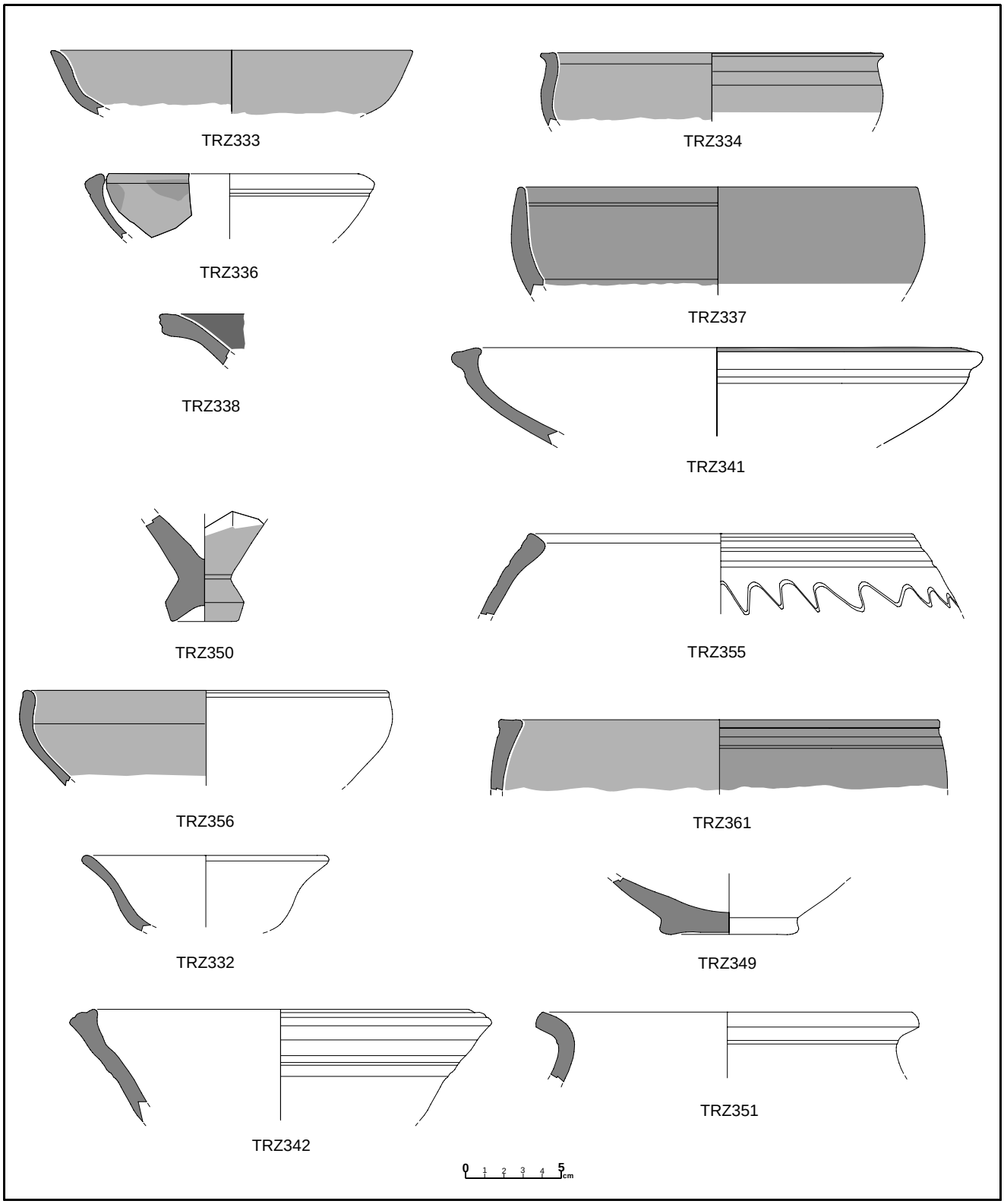


***Figure 7c:*** Typology of the **AC2-B** group (TRZ333, TRZ334, TRZ336, TRZ337, TRZ338, TRZ341, TRZ350, TRZ355, TRZ356, TRZ361, TRZ332, TRZ349, TRZ342, TRZ344, TRZ351, TRZ359 and TRZ364)

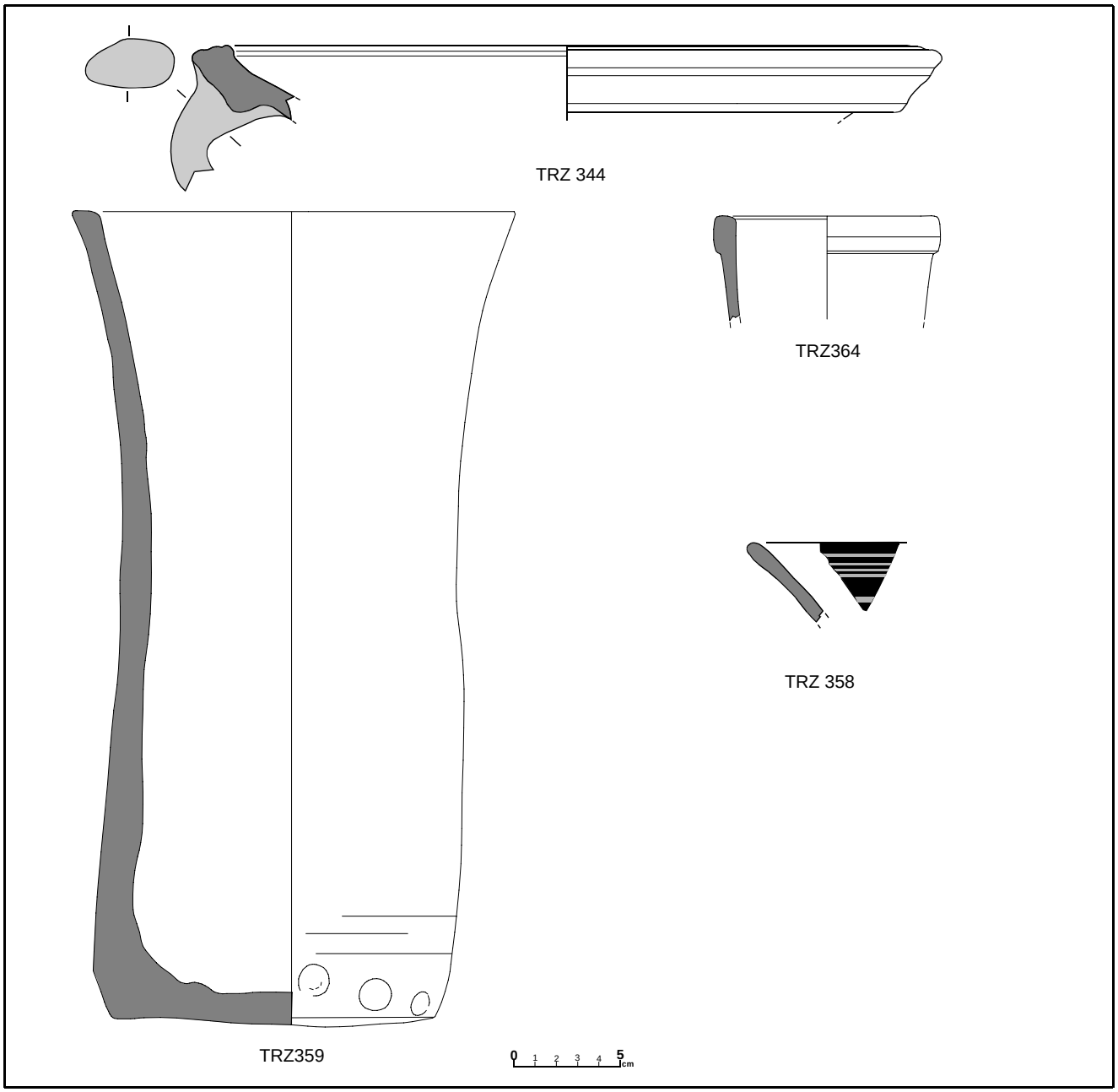


***Figure 7c:*** Typology of the **AC2-B** group (TRZ333, TRZ334, TRZ336, TRZ337, TRZ338, TRZ341, TRZ344, TRZ350, TRZ355, TRZ356, TRZ358, TRZ361, TRZ332, TRZ349, TRZ342, TRZ344, TRZ351, TRZ359 and TRZ364)

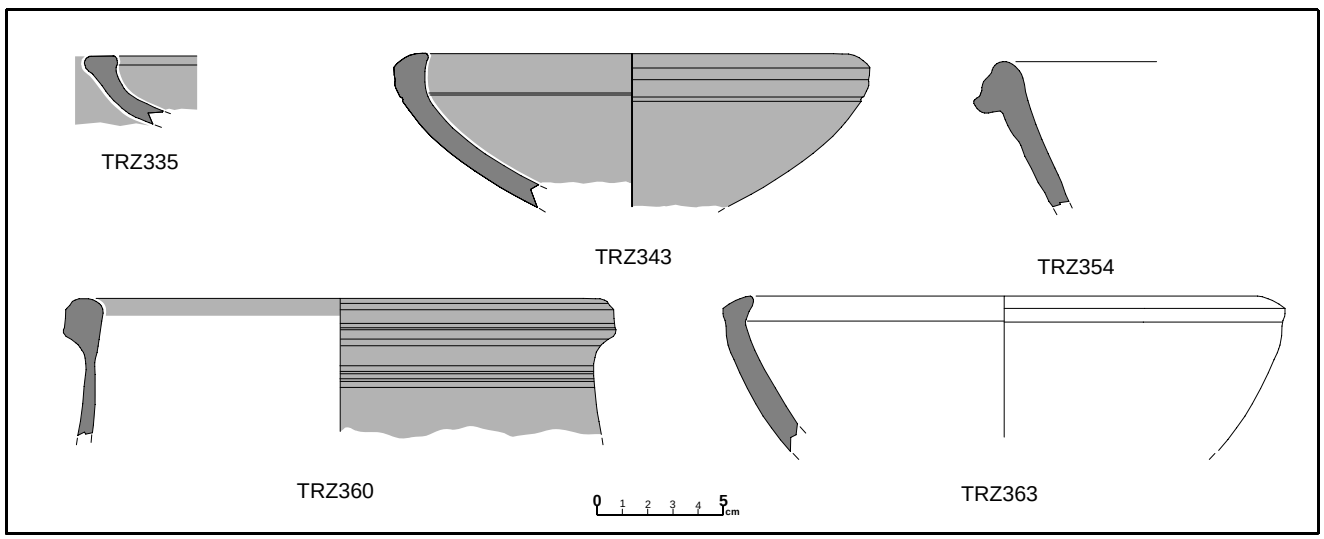


***Figure 7d:*** Typology of the **AC2-C** group (TRZ335, TRZ343, TRZ354, TRZ360 and TRZ363)

### *5.1.2. Petrographical composition (thin section analysis)*

Petrographical analysis has been carried out upon 9 ceramics from Ancient Military Quarter sector 1 (**AC1**). All of them, except the cooking ware TRZ156, had a similar petrographical composition, which is compatible with the range of geological deposits in the broader local area. However, all these ceramics can be grouped in two different petrographic fabrics (***F-AC1A*** and ***F-AC1B***) because of slight differences in frequency and size of non plastic inclusions (Whitbread *et al*., 1997; Whitbread, 2001).

- ***F-AC1-A*: TRZ148, 149, 150**. Thin section analysis points to a similar petrographical composition of these vessels. However, TRZ150 can be attributed to a different petrographic subfabric because of the higher percentage of aplastic inclusions and a higher carbonate component. Clay matrix: Ca-rich (semi-vitrified). Groundmass (very scarce and very fine): quartz, muscovite and micritic calcite (dominant). Coarser inclusions (≤ 0.75 mm): few, sub-angular to sub-rounded, moderately to well sorted, open-spaced, bimodal grain-size distribution. Predominant to dominant: quartz, muscovite and quartz-mica schist; Dominant to frequent: biotite and micritic calcite; Common to few: chert, amphibole; Few to occasional: opaques. Predominant to dominant mesovoids (vughs and vesicles), some of them partially filled by secondary micritic calcite (Figure 8).

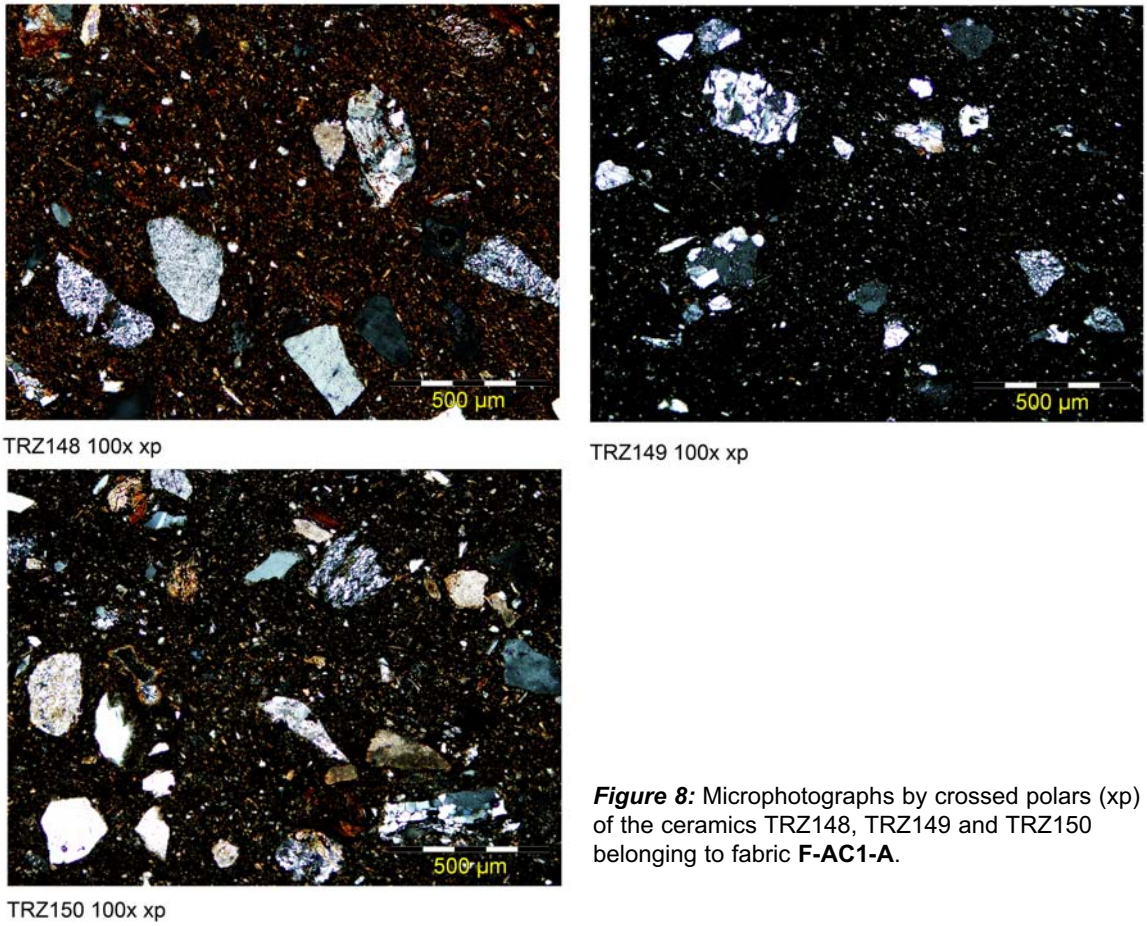


***Figure 8:*** Microphotographs by crossed polars (xp) of the ceramics TRZ148, TRZ149 and TRZ150 belonging to fabric **F-AC1-A**.

***F-AC1-B***: Samples **TRZ145, 146, 153, 155**.

Clay matrix: Ca-rich (poorly vitrified in most cases). Groundmass (scarce and fine): quartz, muscovite, micritic calcite (dominant), plagioclase, amphibole and epidote (accessory). Coarser inclusions (≤ 0.5 mm): moderately abundant, sub-angular to sub-rounded, moderately to poorly sorted, open-spaced (at times single-spaced), unimodal grain-size distribution. Predominant to dominant: quartz, k-feldspar and plagioclase crystals, quartz-mica schist rocks; Dominant to frequent: sandstone grains, biotite and muscovite lames; Common to few: amphibole, volcanic rocks (alterated basalt and traquite), chert and garnet; Few to occasional: epidote crystals and opaques (Figure 9). Predominant to dominant mesovoids (vesicles).

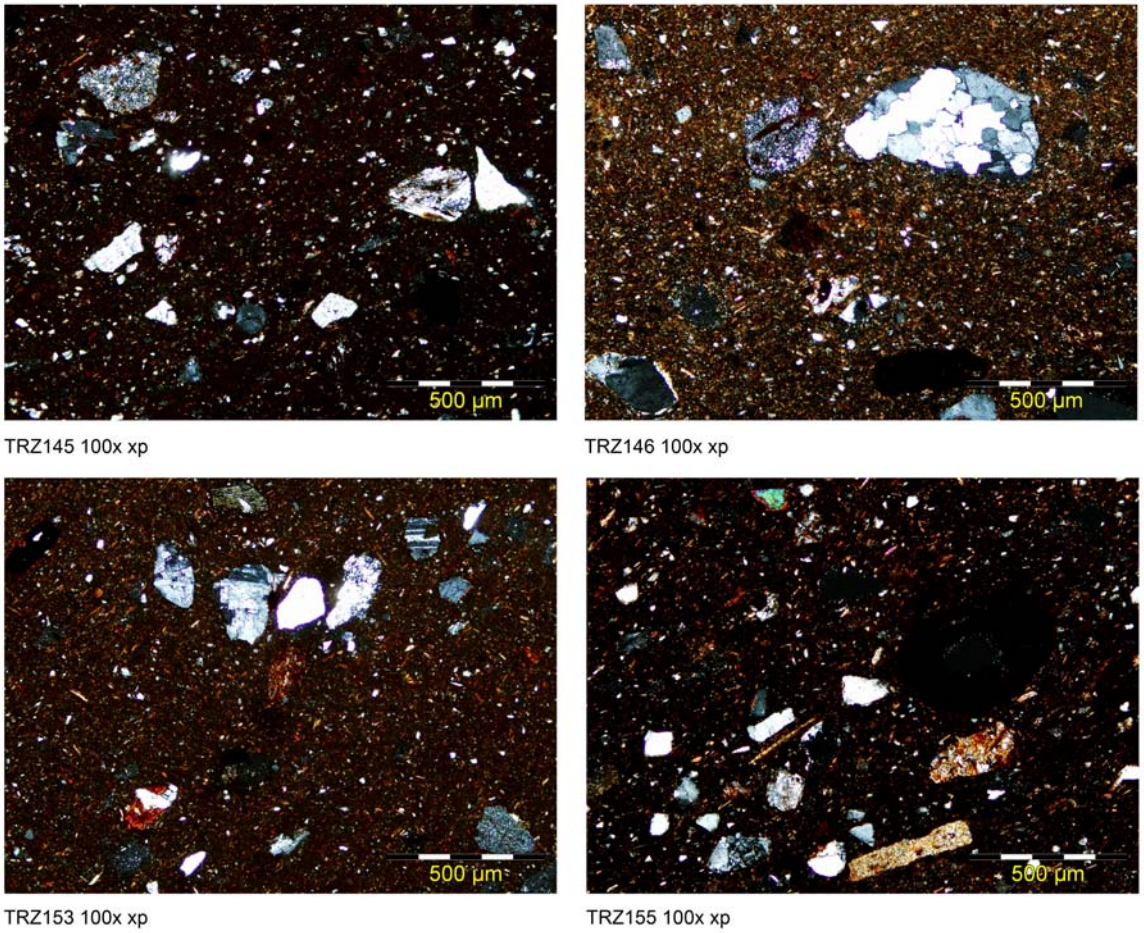


***Figure 9:*** Microphotographs by crossed polars (xp)
of the ceramics TRZ145, TRZ146, TRZ153 and TRZ155 belonging to fabric **F-AC1-B**

**TRZ152**

Clay matrix: Ca-rich (vitrified). Groundmass (scarce): quartz and muscovite. Coarser inclusions (≤ 0.3 mm): moderately abundant, sub-angular to sub-rounded, well sorted, single-spaced, unimodal grain-size distribution. Predominant to dominant: quartz, k-feldspar and plagioclase; Dominant to frequent: quartz-mica schist; Common to few: amphibole, garnet, muscovite; Few to occasional: pyroxene, serpentinite, basalt (Figure 10a).

**TRZ156**.

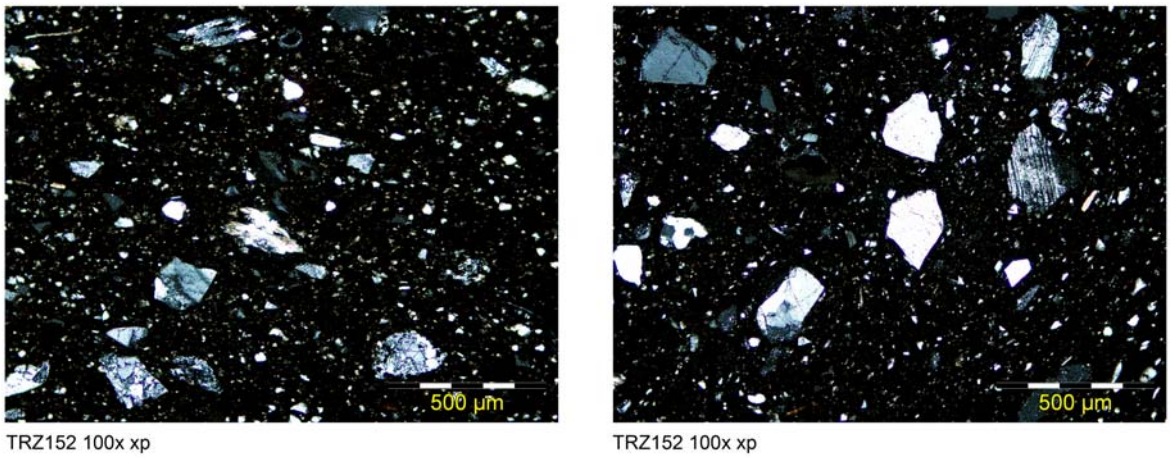


***Figure 10a:*** Microphotographs by crossed polars (xp) of the ceramic outlier TRZ152 from **AC1**

Clay matrix: Ca-rich (poorly vitrified). Groundmass (moderately abundant): quartz, muscovite, micritic calcite (dominant). Coarser inclusions (≤ 3.5 mm): moderately abundant, rounded to sub-rounded, elongated, poorly-sorted and single-spaced, bimodal grain-size distribution. Predominant to dominant: shell fragments; Dominant to frequent: sandstones and siltstones, opaques; Common to few: micritic calcite; Few to occasional: quartz, biotite and muscovite (Figure 10b).

***5.1.3. Mineralogical composition (XRD analysis)***

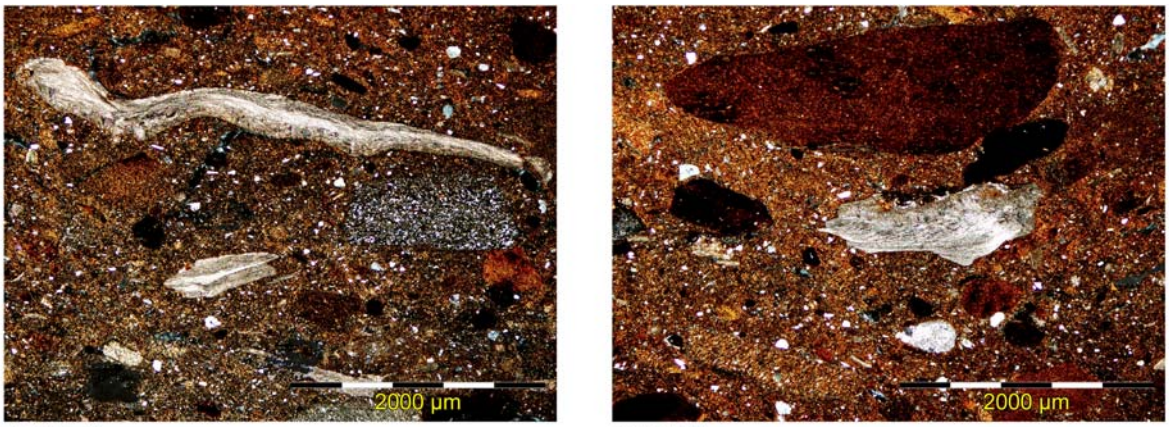


***Figure 10b:*** Microphotographs by crossed polars (xp) of the ceramic outlier TRZ156 from **AC1**

The nine individuals that identified into **AC1** represent three different EFT and mineralogical categories. The lowest fired ceramic is TRZ151 of **AC1-B**. In the diffractogram of Figure 11a, the presence of clear primary mineral phases (quartz, calcite, illite-muscovite, k-feldspars and plagioclase that according to petrography is primary) but not clear firing phases (gehlenite or pyroxene) indicates a firing temperature between 800°C and 850°C. On the other hand, TRZ147 of **AC1-A** and TRZ155 of **AC1-B** are both characterised by the simultaneous presence of primary (illite-muscovite) and firing phases (pyroxene and gehlenite), which indicates relatively high firing temperature (Figure 11b). The obvious presence of gehlenite and mostly pyroxene, as this last one is a crystalline phase which develops visibly under high temperatures in the ceramic paste, indicates a EFT around 950/1000°C. The decomposition of illite-muscovite still can not be observed in the diffractograms because the illite-muscovite peaks in this case correspond mostly to the picks of muscovite. Finally two individuals of **AC1-A** (TRZ145 and TRZ146) and four ceramics of **AC1-B** (TRZ148, TRZ150, TRZ153 and TRZ154) correspond to over fired ceramics (Figure 11c). The almost total decomposition of the illites-muscovites and the intense peaks of pyroxene with the additional absence of gehlenite, that has already decomposed, situate the EFT of these individuals over 1000°C, possibly between 1050°C and 1100°C.

The two ceramics from the chemical subgroup **AC2-A** (TRZ352 and TRZ353) are well fired because of the presence of clear primary mineral phases (quartz, illite-muscovite, k-feldspars, plagioclase, calcite and hematite) and incipient firing phases (gehlenite and pyroxene). Because of that, is deduced an EFT around 850/900-950ºC (Figure 12a). The five ceramics from **AC2-C** were fired at high temperature. However, the EFT at TRZ354, TRZ360 and TRZ363 can be estimated around 900/950-1000ºC (Figure 12b) whereas TRZ335 and TRZ343 are over fired (1000-1050ºC) (Figure 12c).

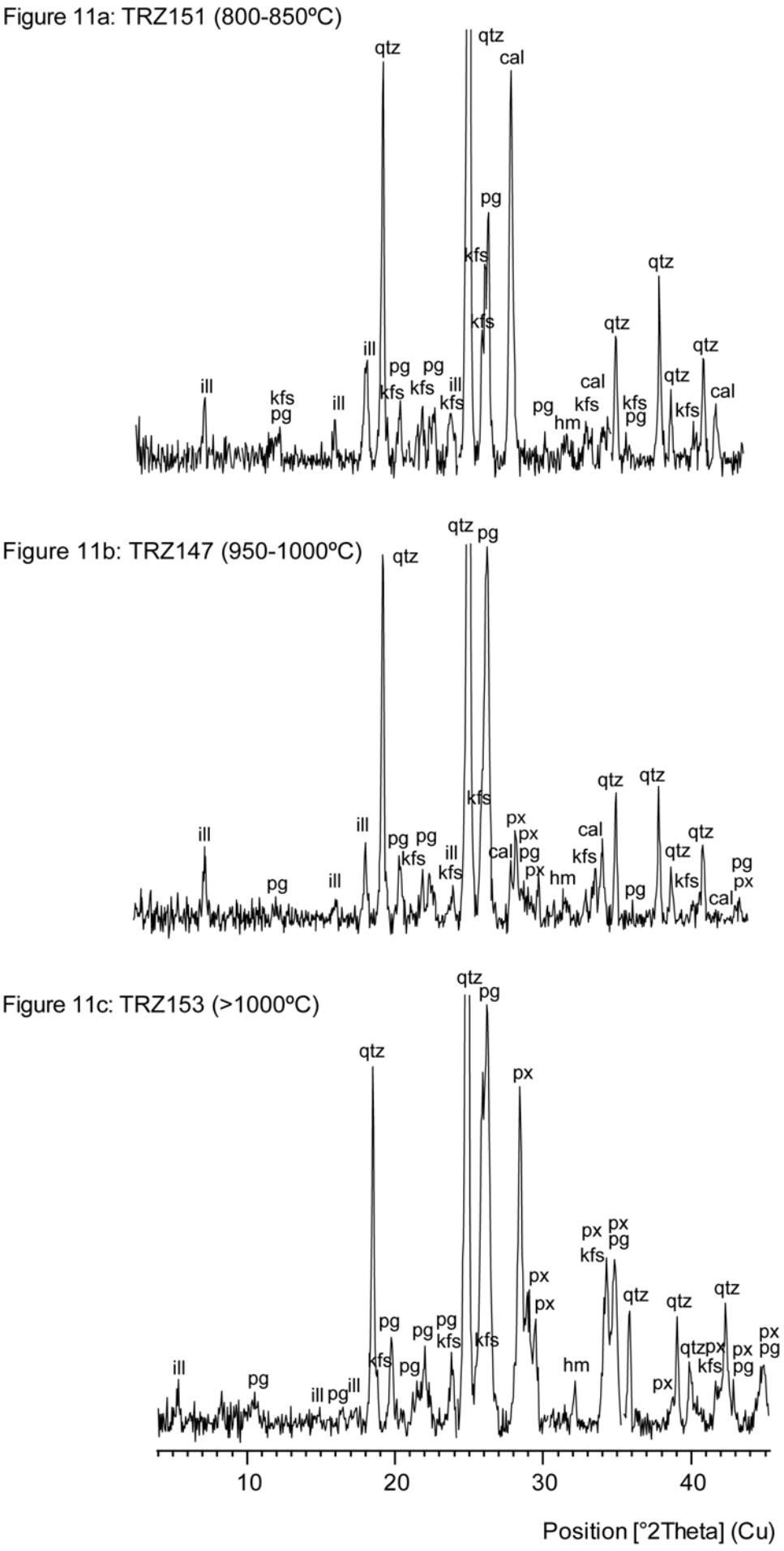


***Figure 11:*** Diffractograms of the individuals TRZ151, TRZ147 and TRZ153 representing the chemical group **AC1**; cal: calcite, hm: hematite, ill: illite-muscovite, kfs: k-feldspar, pg: plagioclase, px: pyroxene, qtz: quartz